

Innovative High Temperature Fuel Cell Systems

Siu Fai Au

Innovative High Temperature Fuel Cell Systems

Proefschrift

ter verkrijging van de graad van doctor
aan de Technische Universiteit Delft,
op gezag van de Rector Magnificus Prof. dr. ir. J.T. Fokkema,
voorzitter van het College van Promoties,
in het openbaar te verdediging

op dinsdag 7 januari 2003 te 16:00 uur

door
Siu Fai AU,
materiaalkundig ingenieur
geboren te Hong Kong

Dit proefschrift is goedgekeurd door de promotoren:

Prof. dr. J.H.W. de Wit

Prof. ir. R.W.J. Kouffeld

Toegevoegd promotor:

Dr. K. Hemmes

Samenstelling promotiecommissieleden:

Rector Magnificus

voorzitter

Prof. dr. J.H.W. de Wit

Technische Universiteit Delft, promotor

Prof. ir. R.W.J. Kouffeld

Technische Universiteit Delft, promotor

Dr. K. Hemmes

Technische Universiteit Delft, toegevoegd promotor

Prof. dr. G.G Hirs

Universiteit Twente

Prof. ir. L. Katgerman

Technische Universiteit Delft

Prof. dr. J.R. Selman

Illinois Institute of Technology, USA

Prof. dr. -ing H. Spliethoff

Technische Universiteit Delft

ir. N. Woudstra heeft als begeleider in belangrijke mate aan de totstandkoming van het proefschrift bijgedragen.

Published and distributed by: DUP Science

DUP Science is an imprint of

Delft University Press

P.O. Box 98

2600 MG Delft

The Netherlands

Telephone: +31 15 27 85 678

Telefax: +31 15 27 85 706

E-mail: Info@Library.TUDELFT.NL

ISBN 90-407-2375-3

Keywords: Fuel cells, modeling, flowsheet calculations

Copyright © 2002 by S.F. Au

All rights reserved. No part of the material protected by this copyright notice may be reproduced or utilized in any form or by any means, electronic or mechanical, including photocopying, recording or by any information storage and retrieval system, without written permission from the publisher: Delft University Press.

Printed in The Netherlands

Contents

1. Introduction

General	1
1.1. Fuel Cells	2
1.1.1. Types and principle	2
1.1.2. Advantages and disadvantages	4
1.2. This thesis	6
References	8

2. Fuel Cell modeling (Part I)

Analytical models and verification of models

Abstract	9
2.1. Introduction	10
2.2. Theory	11
2.2.1. Basic Fuel Cell Model.	11
2.2.2. Simple Model and Extended Model.	13
2.2.3. Reversible Cell Voltage V_{rev}	14
2.2.4. Irreversible Voltage Loss V_{irrev}	16
2.2.5. Quasi-Ohmic resistance r and the macroscopic resistance R	18
2.3. Experimental	19
2.4. Results	19
2.5. Comparing experimental results with calculated results of the analytical models	23
2.6. Conclusions	27
References	27

3. Fuel Cell modeling (Part II)

Numerical models in flowsheeting program and verification of models

Abstract	29
3.1. Introduction	30
3.2. Theory	31
3.3. Experiments and Calculations	34
3.4. Results and Discussions	37

3.5. Conclusions	42
Reference.....	43

4. Fuel Cell system optimization (part I)

Theoretical optimization of cell temperature of hydrogen fuel cell systems

Abstract	45
4.1. Introduction	46
4.2. Theory.....	46
4.3. Fuel cells combined with recovery Power Cycle.....	49
4.3.1. Ideal reversible fuel cell–bottoming cycle systems.....	49
4.3.2. Fuel utilization and Nernst loss	50
4.3.3. Non-ideal reversible fuel cell–bottoming cycle systems	53
4.4. MCFC system efficiency in practice.....	58
4.4.1. MCFC in practice.....	58
4.4.2. MCFC in practice combined with a bottoming power cycle.....	61
4.5. Conclusions	63
Reference.....	63

5. Fuel Cell system optimization (part II)

Influence of cell temperature on the efficiency of a MCFC CHP plant

Abstract	65
5.1. Introduction	66
5.2. System Configuration.....	67
5.2.1. Fuel Cell	68
5.2.2. Anode gas recirculation and Moisture Separation	70
5.2.3. Heat Exchange Steam Reformer and Fuel Preheat.....	71
5.2.4. Cathode gas recirculation.....	72
5.2.5. Expander and Waste Heat Boiler	72
5.3. Input Data and Calculations.....	72
5.4. Results and Discussions	74
5.5. Conclusions	81
References.....	82

6. Fuel Cell system optimization (part III)

Multistage Oxidation by serial connection of stacks.

<i>Abstract</i>	85
<i>6.1. Introduction</i>	86
<i>6.2. System calculations</i>	88
<i>6.3. Results and Discussions</i>	93
6.3.1. Net power efficiencies	93
6.3.2. Improvements by Multistage Oxidation	95
6.3.3. Overall CHP efficiencies	97
6.3.4. Comparison with previous works and discussions.....	97
<i>6.4. Conclusions</i>	100
<i>References</i>	101

7. Innovative Fuel Cell Concepts (part I)

The MCFC with a separate CO₂ channel

<i>Abstract</i>	103
<i>7.1. Introduction</i>	104
<i>7.2. Theory</i>	105
7.2.1. Principles.....	105
7.2.2. Advantages and disadvantages of the i-MCFC.....	107
7.2.3. Modeling the i-MCFC	108
<i>7.3. System calculations</i>	113
7.3.1. Reference system and adjustment to match the i-MCFC	113
7.3.2. Input parameters for the i-MCFC	116
<i>7.4. Results and discussions</i>	117
<i>7.5. Conclusions</i>	119
<i>References</i>	120

8. Innovative Fuel Cell Concepts (part II)

Electrochemical conversion of solid fuel

<i>Abstract</i>	123
<i>8.1. Introduction</i>	124
<i>8.2. Theory</i>	124
8.2.1. Fuel cell processes with zero reversible heat production.....	126
8.2.2. Fuel cell concepts with reversible heat absorption.....	128

8.3. Exergy balances of idealized power generation and gasification processes.....	129
8.3.1. Standard exergy values for several species.....	129
8.3.2. Combustion process for power generation.....	130
8.3.3. Hydrogen Fuel Cell for power generation.....	131
8.3.4. Gasification by Partial Oxidation	133
8.3.5. Direct Carbon Fuel Cell for power generation and gasification.....	135
8.3.6. Internal Direct-Oxidation Carbon Fuel Cell.....	139
8.4. Conclusions	142
References.....	143
9. Conclusions and Discussions	145
9.1. Simplified approaches.....	145
9.2. Detailed flowsheet calculations.....	146
Appendix A	
Exergy and the calculations of chemical exergy.....	149
Appendix B	
Performance measurements on a MCFC bench-cell.....	153
Summary	157
Samenvatting	161
Acknowledgement.....	165
Curriculum Vitae	167
List of Publications.....	169
List of symbols	171

Chapter 1

Introduction

The world's energy consumption has grown rapidly during the previous century and it is still growing fast. Especially the need for electricity has grown extremely rapidly. To satisfy this need, huge giga-watts thermal power plants are built in urban areas to convert world's fossil energy resources into electricity. Simultaneously, the world community starts to realize that changes are needed for mainly two reasons:

1. World's fossil energy resources are limited and we will approach the end of these resources sooner or later.
2. Discharge of gasses associated with the use of fossil fuel may threaten the environment and health of people.

Therefore, new alternatives in the field of electric power supply are needed that make less use of the world's fossil energy resources and produce electricity in a cleaner way.

Fuel cell systems are currently of interest by researchers and industry as a more efficient alternative for the conventional thermal power systems. The principle of fuel cell conversion does not involve thermal combustion. This is a great advantage over conventional thermal power systems and a major improvement in efficiency is theoretically possible. Pilot projects were executed in order to show the advantages of the fuel cell systems, and to obtain hands-on experience in building and operating fuel cell systems. These pilot plants were of relatively small size (ranging from 100 kW to 2 MW) and their efficiencies are indeed higher than their thermal power counterparts. Nevertheless, conventional technology has made progress as well and the advanced combined cycle power plants used in urban area are now approaching efficiencies of

50 %¹⁾ [1]. Fuel cell technology is facing serious competition of the established technology and additional improvements in fuel cell technology are vital. In order to make further improvements, a thorough understanding of the fuel cell process and the interaction between the fuel cell and the rest of the system is required.

1.1. Fuel cells

1.1.1. Types and principle

Fuel cells are electrochemical devices that convert the chemical energy of fuel directly into electricity. Sir William Robert Grove (1811 - 1896) is generally considered to be the inventor of fuel cells but Professor Christian Friedrich Schoenbein (1799 – 1868) was also working on the same principle at the same time. In a fuel cell (see Figure 1.1), a gaseous fuel is fed to the anode (negative electrode) and an oxidant is fed to the cathode (positive electrode). The electrochemical reactions that take place at both electrodes produce an electrical potential difference that can deliver work through an external circuit. The fuel cell is therefore in several aspects similar to a battery but with one major difference: a battery will cease to produce electricity when the chemicals, that are stored inside the battery, are fully consumed, while in theory the fuel cell continues producing electricity for as long as chemicals (mostly gaseous) are supplied.

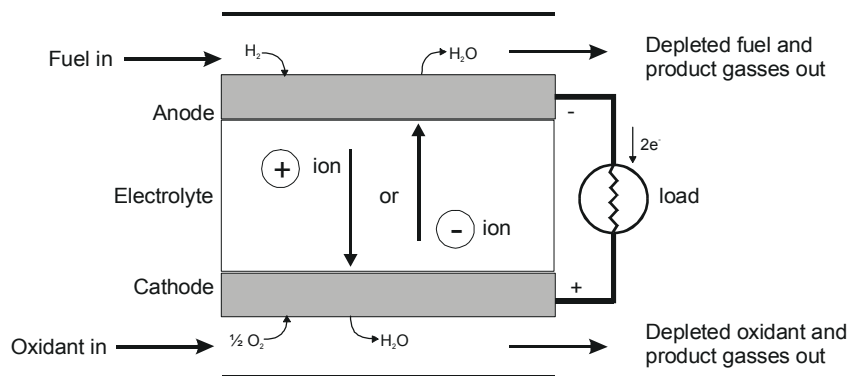


Figure 1.1. Schematic representation of a Fuel Cell.

¹⁾ This is the efficiency based on the higher heating value (HHV) of the fuel.

Several types of fuel cells are in various stages of development. These fuel cells are usually classified by the electrolyte that is used in the cells. In general these types are:

- Proton Exchange Membrane Fuel Cell (PEMFC), operating at ~80 °C
- Alkaline Fuel Cell (AFC), ~100 °C
- Phosphoric Acid Fuel Cell (PAFC), ~200 °C
- Molten Carbonate Fuel Cell (MCFC), ~650 °C
- Solid Oxide Fuel Cell (SOFC), ~800 °C to 1000 °C

The fuel cell electrochemical reactions that take place at the electrodes are given in Table 1.1.

Table 1.1. Fuel cell electrochemical reactions

Fuel Cell type	Anode reaction	Cathode reaction
PEMFC AFC PAFC	$H_2 \Rightarrow 2H^+ + 2e^-$	$\frac{1}{2}O_2 + 2H^+ + 2e^- \Rightarrow H_2O$
MCFC	$H_2 + CO_3^{2-} \Rightarrow H_2O + CO_2 + 2e^-$	$\frac{1}{2}O_2 + CO_2 + 2e^- \Rightarrow CO_3^{2-}$
SOFC	$H_2 + O^{2-} \Rightarrow H_2O + 2e^-$	$\frac{1}{2}O_2 + 2e^- \Rightarrow O^{2-}$

In general both the MCFC and the SOFC are categorized as high temperature fuel cells while the rest are low temperature fuel cells. In general, low temperature fuel cells are solely capable of using H_2 ²⁾ as fuel while high temperature fuel cells can also use CO and CH_4 as fuel using internal conversion by respectively the shift (1.1) and reform reactions (1.2)



²⁾ The recently presented Direct Methanol Fuel Cell (DMFC) is an exception. This low temperature fuel cell electrochemically converts methanol in a direct way.



Low temperature fuel cells are considered most suitable for small-scale applications up to 100 kW (i.e. portable, automotive, and decentralized power generation), while high temperature fuel cells are more suitable for mid- and large-scale applications (i.e. centralized power generation).

1.1.2. Advantages and disadvantages

In a conventional thermal power system, fuel is combusted thermally. This is followed by the conversion of heat to motion of pistons or turbines, which in turn drive a generator that produces electricity. This process consists of three conversion processes, as shown by Figure 1.2:

1. Enthalpy to heat: $\Delta H \rightarrow Q$
2. Heat to mechanical energy: $Q \rightarrow E_{mech}$
3. Mechanical energy to power: $E_{mech} \rightarrow P$

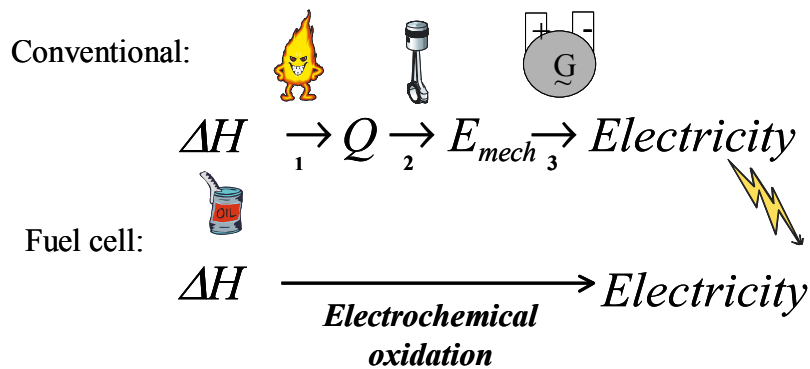


Figure 1.2. Conventional thermal power process vs. Fuel Cell process.

Each process introduces losses that adversely affect the overall conversion efficiency. Especially the combustion process introduces severe losses in work-potential or exergy of the fuel (see Appendix A) and this process should preferably be avoided.

The fuel cell process itself does not involve combustion of fuel into heat (see Figure 1.2). Instead it directly converts the Gibbs energy of the fuel into electricity and it does not suffer from the drawbacks of conventional power systems. The process that takes place is

the electrochemical oxidation, and this direct process enables higher efficiencies than conventional thermal power processes. Improving conversion efficiency leads to the reduced use of fossil fuels and CO₂ greenhouse gas emissions. Next to this fundamental advantage, the fuel cell process itself does not involve moving parts, and therefore can be designed to meet strict noise requirements and requires less or no operational maintenance. The operating temperatures of fuel cells are relatively low, which leads to virtually zero toxic NO_x emissions.

The major drawback that fuel cell systems are facing is cost. At the moment, the initial number of fuel cells produced for pilot plants and other test facilities is limited. The limited production numbers make each unit very expensive. Eventually when fuel cells are becoming commercially available, the costs of fuel cell units will drop and the operating costs of fuel cell system will go down. Moreover, fuel cell systems are very complex. The fuel cell itself is just the core of the system and it needs a complete and costly auxiliary system to support it. As an example, Figure 1.3 gives the schematic process flow diagram of the 1MW MCFC pilot plant in Kawagoe, Japan, that was in operation in 1999. Even in this simplified process flowsheet, the fuel cell is just one part of the complete system, although it is the most important and often the most expensive part! The complexity of fuel cell systems is the subject of this thesis.

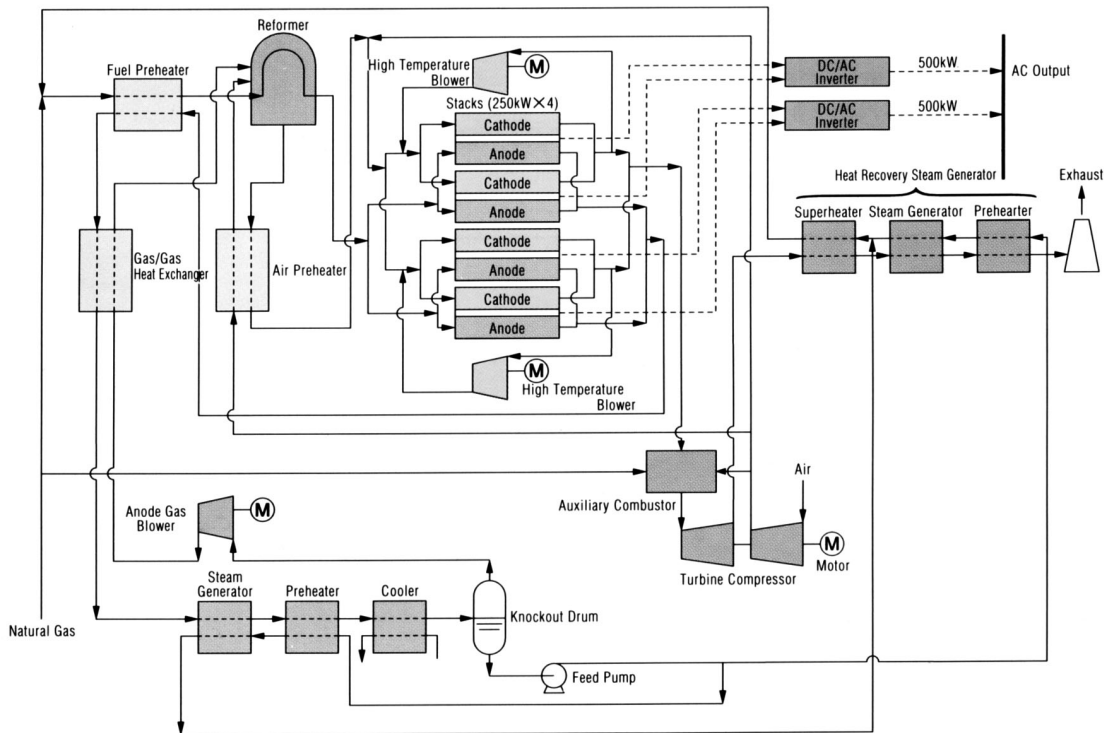


Figure 1.3. Process flow diagram of the 1 MW MCFC pilot plant of Kawagoe, Japan (figure taken from reference [2]).

1.2. This thesis

The example in Figure 1.3 illustrates the complexity of fuel cell systems. Auxiliary equipments are needed to support the fuel cell process, and the combination of auxiliary equipments is called the Balance of Plant (BOP). Each component of the BOP and the fuel cell itself has its own operating characteristics. Due to the large number of components, it is hard to understand the complex interactions between the fuel cell and the BOP. Without understanding these interactions, designing and improving fuel cell systems become an inefficient random process.

This thesis presents the results of studies to understand the complex interactions in a fuel cell system. Additionally, this thesis provides insight into fundamental aspects of the fuel cell conversion processes. This involves combined efforts in the fields of electrochemistry (for understanding the fuel cell process) and mechanical engineering (for understanding the

energy flows and hardware). These studies resulted in innovative ideas that help improve the fuel cell conversion processes in general. Chapter 2 starts with the operating characteristics of fuel cells by introducing Standaert's analytical fuel cell models (see reference [3]) and the verification of these models with experimental measurements. A similar fuel cell model has been worked out numerically and has been implemented in the flow-sheeting program Cycle-Tempo [4]. Chapter 3 presents the introduction and the verification of this model with the same experimental results as described in Chapter 2. By verifying both models a solid foundation is created for two different directions of studies:

1. *Electrochemical conversion by using a simple analytical fuel cell model.*

Chapter 4 presents a theoretical study of combining fuel cells with conventional power cycle systems. The effects of fuel cell operating temperature and irreversible losses on the overall efficiency are investigated and the results are analyzed.

2. *Detailed analysis of fuel cells systems by flowsheet calculations.*

Flowsheet calculations are used to analyze operating parameter and configuration changes of complex fuel cell system. The analyses show the interactions between the fuel cell and the BOP. Chapter 5 presents the study on changes in fuel cell operating temperature in a detailed MCFC system. Chapter 6 presents the study on parallel and serial configurations of fuel cell for the same detailed system. Chapter 7 presents the system study of a conceptual MCFC with a separate CO₂ supply (i-MCFC).

Finally, with a look at future developments, Chapter 8 presents a theoretical study on electrochemical production methods that combine the production of power and chemical products.

References

- [1] *Advanced Combined Cycle; Kawagoe Thermal Power Station Group No. 4 & 5*, Chubu Electric Power Co., Inc., Japan (1998)
- [2] *Molten Carbonate Fuel Cell*, MCFC Research Association, Tokyo, Japan (1999)
- [3] F. Standaert, *Analytical Fuel Cell Modelling and Exergy Analysis of Fuel Cells*, PhD Thesis, ISBN 90.9012330-X, Delft University of Technology (1998).
- [4] Cycle-Tempo version 4.42, Delft University of Technology, Section Thermal Power Engineering; TNO Environment, Energy and Process Innovation, (2000).
<http://www-pe.wbmt.tudelft.nl/ev/cycle/cycle.html>

Chapter 2: Fuel Cell modeling (Part I)

Analytical models and verification of models

This chapter is published in the Journal of Electrochemical Society 148(10), pp. A1051-A1057, titled: VERIFICATION OF ANALYTICAL FUEL CELL MODELS BY PERFORMANCE TESTING AT A 110 cm² MOLTEN CARBONATE FUEL CELL, by S.F Au, W.H.A. Peelen, F.R.A.M. Standaert, K. Hemmes and I. Uchida, (2001).

Abstract

This chapter presents a performance test of a 110 cm² Molten Carbonate Fuel Cell bench cell as a function of output current and gas utilization. These results are compared with the predictions of cell performance of two analytical models, the Simple Model and the Extended Model, for which a revised derivation is given. A comparison of measurements and models results in a value for the quasi-Ohmic resistance r , of 1.02 Ωcm^2 and 1.07 Ωcm^2 , respectively for the Simple Model and the Extended Model. Using this as the only fitted parameter and other theoretical parameters, the Simple Model and the Extended Model describe the cell performance with a relative error of at most 5 % and 1 %, respectively, for fuel utilization above 10 %. Both models have therefore shown their reliability.

2.1. Introduction

Successful industrial applications of Molten Carbonate Fuel Cells (MCFCs) need accurate prediction of unit-cell performance and operation characteristic. This unit-cell characteristic is the basis for accurate mathematical models of fuel cell systems, which facilitates the integration and optimization of the MCFC in existing industrial processes by enabling the systematic study of the total system's benefits, efficiency and costs. In other words, applications of MCFCs can only be explored when accurate unit-cell models are available. Such models are derived from descriptions of the physical processes inside the unit-cell using both thermodynamic parameters and kinetic parameters. Therefore, both types of parameters determine the cell's efficiency and performance. Although thermodynamic parameters can be calculated using available thermodynamic properties, kinetic parameters can only be obtained experimentally. Therefore, reliable experimental results are essential for accurate performance prediction and thus for the application of fuel cells. Furthermore, in these mathematical models, assumptions are made regarding physical processes in order to simplify the models. To justify these assumptions experimental data is needed to verify the reliability of the models.

This chapter presents the verification of the operation characteristics predicted by the Analytical Fuel Cell Models for a unit-cell proposed by Standaert et al. [1, 2]. The predicted operation characteristics are compared with measurements on a 110 cm² MCFC bench cell using only one experimental parameter. This experimental parameter is the internal resistance of the MCFC.

In previous derivations of the Analytical Fuel Cell Models, little attention was paid to distinguish the difference between theoretical parameters and measurable quantities hence compromising the practical use of these models. Therefore, we first give a revised derivation to models containing only operational parameters that can be measured or calculated.

2.2. Theory

2.2.1. Basic Fuel Cell Model.

In a fuel cell under load, gaseous reactants are converted into product species, heat and electric power. The objective of the fuel cell model is to determine which fraction of chemical energy stored in the reactant is converted into electric power and which fraction of it is converted into heat by using parameters that are controlled by fuel cell operators. These control parameters are in practice the total fuel utilization, u_f , which is the degree of conversion of the reactant that is fed into the cell, and the current density, i . Therefore, the goal of the fuel cell model is to determine the cell voltage V_{cell} as function of u_f and i .

Previously the Basic Fuel Cell Model is introduced by describing a fuel cell by an equivalent electrical circuit (see Figure 2.1).

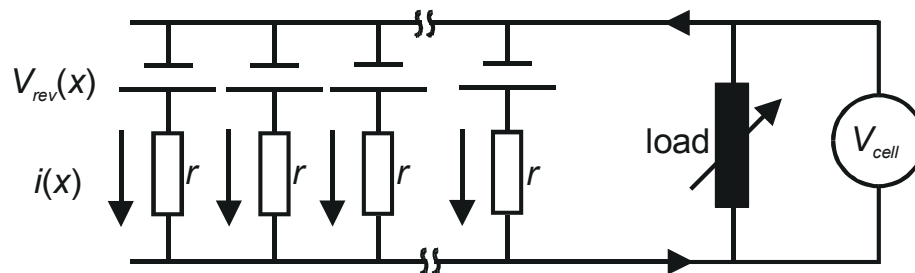


Figure 2.1. Fuel cell represented as an equivalent electrical circuit, taken from Standaert et.al. [1, 2].

Conversion of gaseous reactant inside the cell causes a gas composition gradient between the fuel cell gas inlet and outlet. Since the local gas composition determines the local cell voltage, $V_{eq}(x)$, given by the Nernst equation, a similar gradient in the $V_{eq}(x)$ exists between the gas inlet and outlet. In this model, the overall cell voltage V_{cell} is assumed constant over the cell due to the good conductance of metallic current collectors. The difference between $V_{eq}(x)$ and V_{cell} is the force needed to overcome resistances inside the cell such as transport of species and reaction resistances. These resistances combined are called here the quasi-Ohmic resistance r , and throughout this thesis, it is assumed to be uniform as a function of x . Therefore the $V_{eq}(x)$ and the local current density $i(x)$ obey a quasi-Ohmic relation and that is:

$$i(x)r = V_{eq}(u) - V_{cell} \quad (2.1)$$

Here the theoretical Nernst potential $V_{eq}(u)$ is expressed as a function of the local cumulative gas utilization u , which is a function of the local conversion rate $i(x)$ of the total amount of reactant fed into the cell i_{in} [see reference [1], p.10]:

$$\frac{i(x)}{i_{in}} = \frac{du}{dx} \quad (2.2)$$

with $u=0$ at $x=0$.

Starting here, Standaert derived an integral expression for V_{cell} by first multiply equation (2.1) by $\frac{du}{dx}$ and integrating over the length of the cell. Using equation (2.2), the integral expression results in:

$$\frac{r}{i_{in}} \int_0^1 i^2(x) dx = \int_0^1 (V_{eq}(u) - V_{cell}) \frac{du}{dx} dx \quad (2.3)$$

Changing the integral variable of the integral on the right side from x to u results in:

$$\frac{r}{i_{in}} \int_0^1 i^2(x) dx = \int_0^{u_f} V_{eq}(u) du - V_{cell} u_f \quad (2.4)$$

with $u = u_f$ at $x = 1$, which can be written as:

$$\boxed{V_{cell} = \frac{1}{u_f} \int_0^{u_f} V_{eq}(u) du - \frac{r}{i_{cell}} \int_0^1 i^2(x) dx} \quad (2.5)$$

(see reference 1, p109)

Here we have arrived to the objective of the fuel cell model.

Note that this equation is exact within the model assumptions. Also, we have not solved the differential equation (2.2) but merely rewritten it in the form of an integral expression for V_{cell} . However, it appears that we do not need to solve equation (2.5) since the integrals for the exact function of $V_{eq}(u)$ and $i(x)$ on the right side have clear physical meanings. The first integral on the right side expresses the thermodynamic reversible part of V_{cell} and the second integral expresses the irreversible losses:

$$V_{cell} = V_{rev}(u) - V_{irrev}(i) \quad (2.6)$$

2.2.2. Simple Model and Extended Model

Using several realistic approximations, the integrals in equation (2.5) can be solved into explicit expressions of the total gas utilization u_f and the output current density i_{cell} . Standaert derived the following expression for the Simple Model in which $V_{eq}(u)$ is assumed linear and the current distribution is assumed homogenous (see reference [1], p.15):

$$V_{cell}^{SM} \approx V_{eq}^*(0) - \frac{1}{2} \alpha_f u_f - r i_{cell} \quad (2.7)$$

Hence, the Simple Model predicts that the cell voltage is linear on both u_f and i_{cell} .

The model is further refined to the Extended Model by introducing correction for oxidant utilization, “initial dip” of $V_{eq}(u)$ and a first-order approximation for the current distribution. Standaert derives the following expression for the Extended Model [reference [1], p16]:

$$V_{cell}^{EM} \approx V_{eq}^*(0) - \frac{1}{2} \alpha_{tot} u_f + \frac{0.003}{u_f} - \left[1 + \frac{1}{3} \left(\frac{\alpha_{tot} u_f}{2 r i_{cell}} \right)^2 \right] r i_{cell} \quad (2.8)$$

Next, we systematically introduce the three assumptions and explain the terms and symbols used in this expression, but before we do this, note that both analytical models are

derived for isothermal conditions (i.e. r is homogenous). However, non-isothermal conditions are inevitable in practice and the differences in results in the modeling of isothermal and non-isothermal conditions are discussed previously by Standaert et al. [3]. He showed that both expression (2.7) and (2.8) can be adapted for non-isothermal condition by using modified $V_{eq}^*(0)$, α_{tot} and r . Furthermore, he has shown that the differences in results are small (see reference [3]).

2.2.3. Reversible Cell Voltage V_{rev} .

The equilibrium potentials V_{eq} of both the anode and cathode are given by the Nernst equation, in which usually concentrations are used. However, we need an expression of the Nernst potential $V_{eq}(u)$ as function of the total fuel gas utilization u_f . This was calculated by Standaert (reference [1], p126, and reference [2]) using the assumption that gas composition changes only in the direction from the gas inlet to the gas outlet. Figure 2.2 shows this result as a solid line.

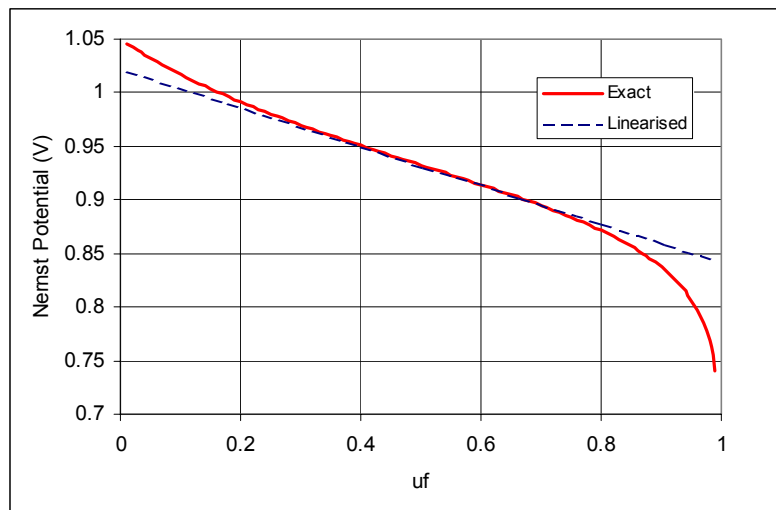


Figure 2.2. Exact and linearized Nernst potential under standard MCFC testing condition, taken from Standaert et.al. [1, 2].

This exact expression for $V_{eq}(u)$ turns out to be too elaborated and therefore unsuitable for analytical purposes. Standaert further proposed a simplification using a linear approximation for $V_{eq}(u)$ in order to find an analytical solution for V_{rev} (reference [1], p11, and [2]):

$$V_{eq}(u) \approx V_{eq}^*(u) \equiv V_{eq}^*(0) - \alpha_f u \quad (2.9)$$

with α_f the modulus of the slope of the linear approximation for $V_{eq}(u)$.

The result of this linearization is shown as a dotted line in Figure 2.2.

Using this linearized Nernst equation the integral for $V_{rev.}$ is solved as:

$$V_{rev.} = \frac{1}{u_f} \int_0^{u_f} V_{eq}(u) du \approx V_{eq}^*(0) - \frac{1}{2} \alpha_f u_f \quad (2.10)$$

The Simple Model (equation (2.7)) uses this expression for the reversible part.

Note that the parameter α_f depends slightly on the procedure by which the linear approximation is made. Nevertheless, α_f is essentially determined by the temperature and gas composition at the inlet only, and it can be calculated using the Nernst equation.

Figure 2.2 shows discrepancies between the $V_{eq}(u)$ and $V_{eq}^*(u)$ at both low and high fuel utilization under standard MCFC testing conditions. At low fuel utilization, Standaert called this discrepancy the “initial dip” and he proposed an additional correction term. This correction term is derived to be about 3mV/ u_f under standard MCFC testing condition (reference [1], p17, [2]):

$$V_{rev.} \approx V_{eq}^*(0) - \frac{1}{2} \alpha_f u_f + \frac{0.003}{u_f} \quad (2.11)$$

Generally, a correction at high fuel utilization is not needed since fuel cells are normally operated at a range of fuel utilization (i.e. $u_f < 0.8$) where this correction is not needed (see Figure 2.2).

Additionally, the effect of oxidant gas utilization can be added similarly by linearizing the Nernst equation for the oxidant utilization and then by using α_{tot} instead of α_f .

$$V_{rev.} \approx V_{eq}^*(0) - \frac{1}{2}\alpha_f u_f - \frac{1}{2}\alpha_{ox} u_{ox} + \frac{0.003}{u_f} \equiv V_{eq}^*(0) - \frac{1}{2}\alpha_{tot.} u_f + \frac{0.003}{u_f} \quad (2.12)$$

with α_{tot} is defined as (reference [1], p20):

$$\alpha_{tot} = \alpha_f + \alpha_{ox} \frac{u_{ox}}{u_f} \quad (2.13)$$

Both refinements of initial dip and oxidant utilization are introduced in the Extended Model (equation (2.8)).

The reversible cell voltage is now written solely in parameters, which can be calculated (α_f , α_{ox} , α_{tot} , $V_{eq}^*(0)$) or controlled (u_f).

2.2.4. Irreversible Voltage Loss $V_{irrev.}$

In order to solve the integral for the irreversible voltage loss, Standaert proposed two approximation for $i(x)$: a zero order approximation (reference [1], p15; [2]) and a first order approximation (reference [1], p15, [2]). The zero order approximation assumes a homogeneous current distribution, i.e. $i(x)$ is constant. This leads to a simple expression for the irreversible voltage loss:

$$V_{irrev.} = \frac{r}{i_{cell}} \int_0^1 i^2(x) dx \approx i_{cell} r \quad (2.14)$$

The Simple Model (equation (2.7)) uses this expression for the irreversible part.

This solution for the integral is very simple and it provides an upper limit for V_{cell} . Under loading condition, $V_{eq}(u)$ is clearly a function of x while r is assumed to be independent of x , hence $i(x)$ cannot be homogeneous. The zero order approximation results in an upper limit for V_{cell} since the average of the square of a variable is larger or equal to the square of the average. Standaert proposed later a better assumption, namely, a linear decreasing current density, i.e. a first order approximation (reference [1], p15). Under this assumption the second integral in equation (2.5) is solved as (reference [1], p15, [2]):

$$V_{irrev.} \approx \left[1 + \frac{1}{3} Z^2 \right] r i_{cell} \quad (2.15)$$

with Z as a dimensionless number defined by:

$$Z = \frac{\alpha_{tot}}{2r i_{in}^f} \quad (2.16)$$

Combining equation (2.14), (2.15) and the definition of u_f ($u_f = i_{cell} / i_{in}^f$) we get the following expression for the irreversible voltage loss:

$$V_{irrev.} \approx \left[1 + \frac{1}{3} \left(\frac{\alpha_{tot} u_f}{2r i_{cell}} \right)^2 \right] r i_{cell} \quad (2.17)$$

This refinement of the first order approximation is introduced in the Extended Model (equation (2.8)) and expression (2.17) is used for the irreversible voltage loss. Further refinements in the current density distribution yield only very small correction on the first order approximation (see reference [1], p25).

The irreversible cell voltage is now written in parameters, which all can be calculated (α_{tot}), measured (r) or controlled (u_f, i_{cell}). Both the Simple Model and the Extended Model provide a tool to fuel cell system designers to predict unit cell or stack operation and performance characteristics. By comparing the predicted operation characteristics of both the Simple Model and the Extended Model with experimental results, we can evaluate the accuracy of both models and distinguish the contributions of the refinements of the Extended Model (i.e. oxidant utilization, initial dip and inhomogeneous current distribution).

In both models, all parameters are known or can be calculated except for the quasi-Ohmic resistance r . This is therefore the only parameter, in both models, which needs to be obtained experimentally.

2.2.5. Quasi-Ohmic resistance r and the macroscopic resistance R

A method to determine this r is by measuring the macroscopic resistance R of the cell, which is defined as:

$$R = - \left(\frac{\partial V_{cell}}{\partial i_{cell}} \right)_{u_f, u_{ox}} \quad (2.18)$$

Assuming the Simple Model, the quasi-Ohmic resistance r is the same as this macroscopic resistance R and it can be determined with a polarization curve. However, we need here to be aware of the wrong assumption of a uniform current distribution. A better way to determine the r is by using the Extended Model. In this model the R is given by:

$$R^{EM} = - \left(\frac{\partial V_{cell}^{EM}}{\partial i_{cell}} \right) = r - \frac{\alpha_f^2 u_f^2 + 2\alpha_f u_f \alpha_{ox} u_{ox} + \alpha_{ox}^2 u_{ox}^2}{12r i_{cell}^2} \quad (2.19)$$

The difference between the Simple Model and the Extended Model is the second term in equation (2.19), which relates R with the total gas utilization, gas composition at the inlet (by α_f and α_{ox}) and current load. Therefore, the Extended Model predicts a non-Ohmic behavior of the unit-cell and r needs to be fitted from experimental results.

In practice, in a MCFC both α_{ox} and u_{ox} are small which results in:

$$R^{EM}_{u_{ox}=0} \approx r - \frac{\alpha_f^2 u_f^2}{12r i_{cell}^2} \quad (2.20)$$

A typical operational condition for a MCFC is $\alpha_f = 0.18$ V, $u_f = 80$ % and $i_{cell} = 150$ mA/cm² (see experimental section for the typical temperature and testing gas composition). Using these values, we can calculate R for the Extended model and estimate the differences in R between the Simple Model and the Extended model:

$$R^{EM}_{u_{ox}=0} \approx r - \frac{0.0768}{r} \quad (2.21)$$

For a 110cm² bench cell we have experimentally determined an Ohmic resistance of about 1 Ωcm^2 . This result shows that r is in the order of 1 for both models and that the difference in r for both models is in the order of 8 % with a higher r for the Extended Model.

2.3. Experimental

Measurements were performed on a 110 cm² Li/Na MCFC single cell at Tohoku University in Sendai, Japan. This cell was manufactured, installed and tested by Ishikawajima-Harima Heavy Industry Co. (IHI) and has been successfully operated for 3330 hours before the measurements described in this work were performed. The MCFC was operating at 650 °C. The anode was fed with 80 % H₂ and 20 % CO₂ humidified at 60°C. The cathode was fed with 70 % air and 30 % CO₂. Measurements were performed under atmospheric conditions. The flow rate of both anode and cathode gasses were set according to the current load and required utilization. Additional information about this experimental setup is given in Appendix B.

Steady state polarization and current interrupt were used to determine the macroscopic resistance R at different fuel utilization and gas flow. Results of both methods were compared. In addition to this, steady-state polarization was performed at a current load of 0, 30, 50, 80, 100, 110, 120, 130, 140, 150, and 180 mA/cm² for the characterization of the cell and for the evaluation of the fuel cell model. The steady-state polarization measurements were carried out using a potentiostat/galvanostat (Toho Technical Research 2012). Current interruption measurements were carried out by cutting the current load of 100 mA/cm², supplied by a current source (Hokuto Denko HC-113), using a mercury switch, and the following potential relaxation was recorded using a digital oscilloscope (Lecroy 9304A).

2.4. Results

First, the macroscopic resistance R of the cell was determined using both steady-state polarization method and current interrupt method. Using steady-state polarization method we determined R at constant fuel and oxidant utilization, while using current interrupt method we determined R at constant current load. The results of the steady-state

polarization of the cell with gas flows according to a fuel utilization (u_f) of 60 % and oxidant utilization (u_{ox}) of 40 % are given in Figure 2.3.

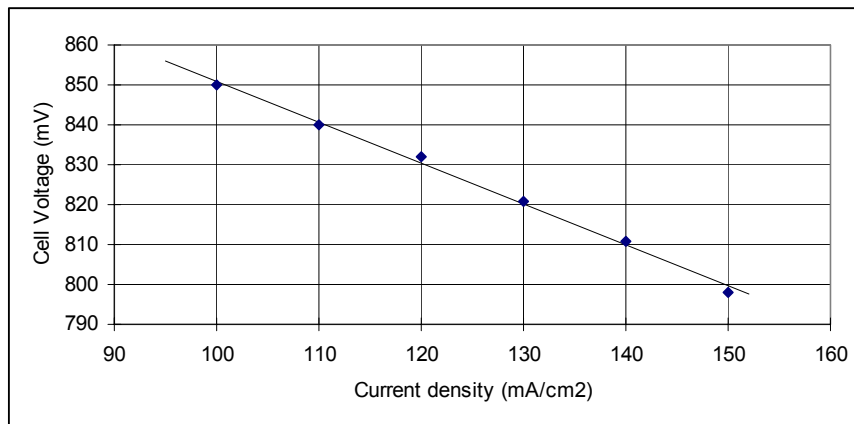


Figure 2.3. Steady state polarization at $u_f / u_{ox} = 60 \% / 40 \%$

Figure 2.3 shows that the cell voltage decreases linearly with the output current and thus the bench cell behaves Ohmically in this range of current density. Using the least-square method, a macroscopic resistance R of $1.02 \pm 0.03 \Omega\text{cm}^2$ was obtained. This result was verified with current-interrupt method shown in Figure 2.4.

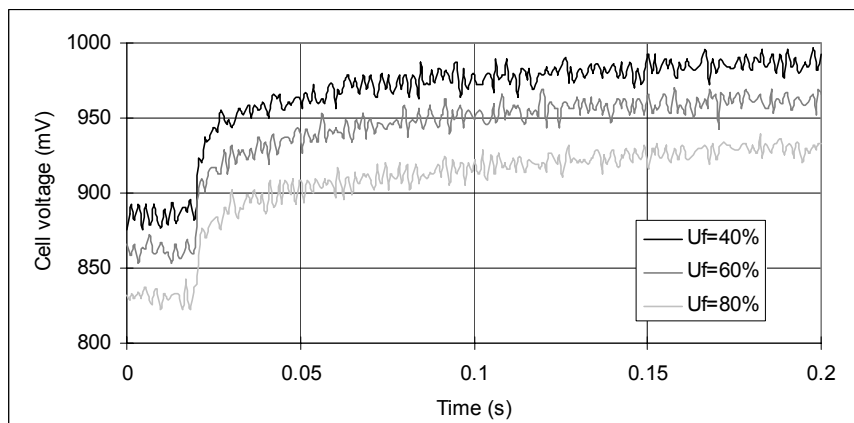


Figure 2.4. Transient response after a current load of 100 mA/cm^2 and $u_{ox} = 40\%$

It shows the potential relaxation of the cell voltage after a current interrupt of 100 mA/cm^2 at different initial fuel utilization and at a constant 40 % initial oxidant utilization (i.e., utilization during load). Here we see an almost instantaneous (within $5 \mu\text{s}$) initial potential drop of the cell voltage, which levels off relatively quickly to a seemingly constant polarization. It took about 0.2 s before this seemingly constant potential was reached. Lee et al [4] ascribe the process with the shortest time constant to the real Ohmic drop, and the

second process to charge- and mass-transfer resistances. The effect of Ohmic drop and charge/mass-transfer processes combined is accounted in both the Simple Model and the Extended Model by a single quasi-Ohmic resistance r . Therefore, 0.2 s is about the time constant we need to determine the quasi-Ohmic resistance.

Using Ohm's law, (i.e., determining the potential relaxation after 0.175 s divided by the current load of 100 mA/cm²), a value for R of about $1.01 \pm 0.02 \text{ } \Omega\text{cm}^2$ was determined for the three fuel utilization. This result corresponds very well with the result obtained by steady-state polarization.

For the comparison of fuel cell models, we will use the results obtained by steady-state polarization. These results yield an $r = 1.02 \text{ } \Omega \text{ cm}^2$ for the Simple Model, while an $r = 1.07 \text{ } \Omega\text{cm}^2$ for the Extended Model was obtained by fitting.

In previous work at ECN the Netherlands, Machielse [5] experimentally determined the R of a 1000 cm² MCFC. The R of their cell was $1.195 \text{ } \Omega\text{cm}^2$. The MCFC tested here has a significantly smaller R and thus better performance. Since the result of Machielse was published in 1991, the difference in performance is probably due to improvement in cell technology over the last years.

Next, we give the operation characteristics of the unit cell using galvanostatic steady-state polarization. The results of the measurements at several fuel gas flow settings are given in Table 2.1.

Table 2.1. Cell potential as function of current load for several fuel gas flow rates.

		V_{cell} (mV)			
		i_{in}^f (mA/cm ²)			
		750	375	250	188
i_{cell} (mA/cm ²)	0	1056	1055	1056	1051
	30	1019	1010	1001	989
	50	993	979	966	955
	80	956	937	918	902
	100	927	909	885	868
	110	916	894	869	850
	120	901	879	852	830
	130	888	865	843	811
	140	876	848	820	794
	150	860	833	803	767
180	801	769	729	---	

All measurements were performed with a cathode gas flow rate equals to a current equivalent of $i_{in}^{ox} = 375 \text{ mA/cm}^2$. Figure 2.5 shows the same results as a function of the fuel utilization u_f after recalculation.

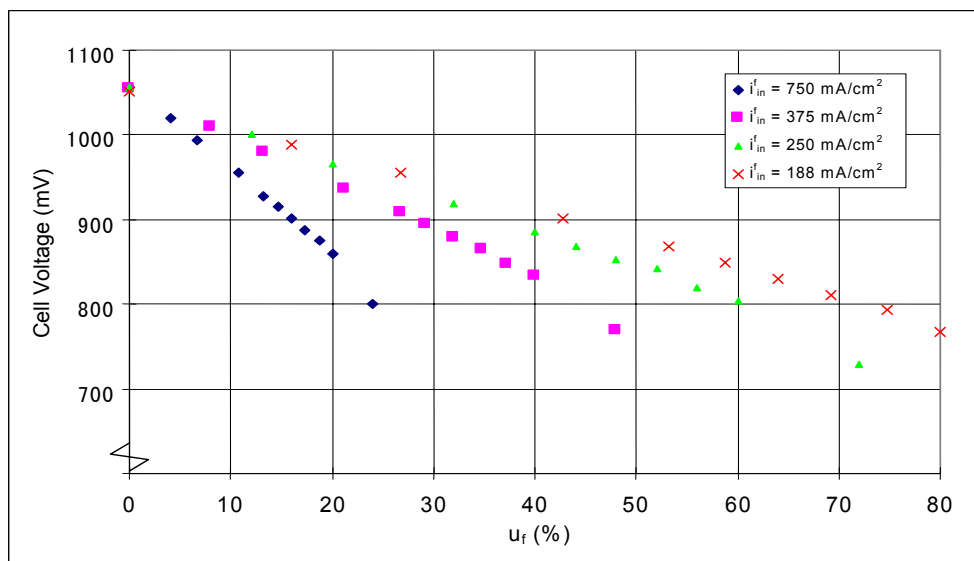


Figure 2.5. Steady state polarization at different gas flow settings.

The current equivalent of the applied fuel gas is given at the legend. Note the oxidant gas flow is kept constant; therefore the abscissa in Figure 2.5 represents changes in u_f , i_{cell} and u_{ox} .

For all four different fuel gas settings, Figure 2.5 shows that the cell voltage decreased linearly with the fuel utilization. Note that for the fuel gas setting of 750, 375, and 250 mA/cm², the points with the highest fuel utilization deviate slightly from the linearity. These points are obtained at a current density of 180 mA/cm². Following to Hirschenhofer [6], a performance decrease at high current density is expected due to diffusion limitations, an effect not included in the model. These points are therefore omitted in the fitting and analysis given next.

2.5. Comparing experimental results with calculated results of the analytical models

Figure 2.6 gives two 3D representations of the same experimental results given by Table 2.1. In this figure, a plane that intersects the measurements is plotted showing that bench cell is behaving linearly for both u_f and i_{cell} . The encircled points are those obtained at a current density of 180 mA/cm².

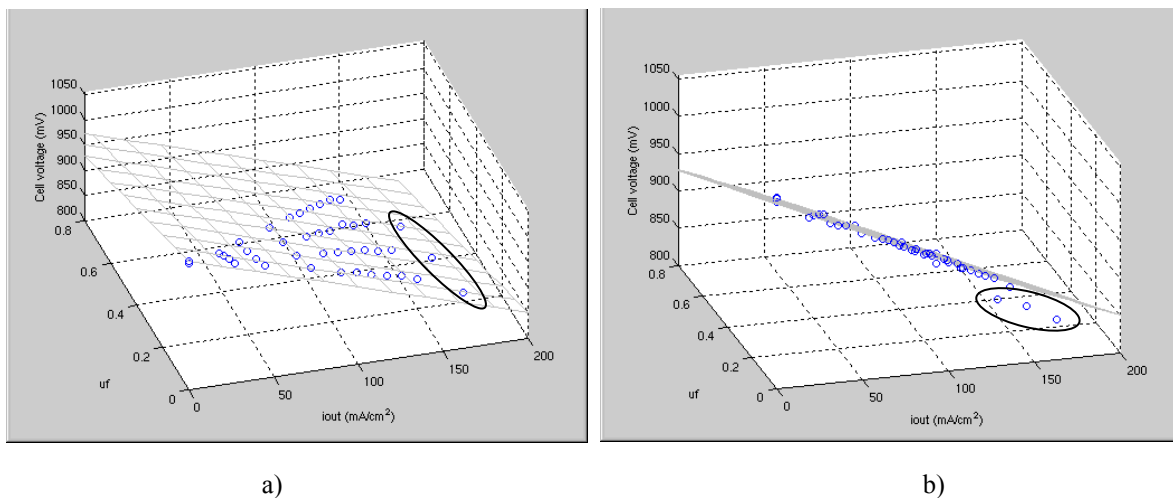


Figure 2.6. 3D plots of the results of steady-state polarization (o) with the fitted plane seen from two different viewing angles. Three deviating points with $i_{out} = 180 \text{ mA/cm}^2$ are circled.

Apparently the cell performance is well described by the bilinear Simple Model using $V_{eq}^*(0) = 1.051 \text{ V}$ (i.e., the measured Open Cell Voltage of the cell), and $r = 1.02 \text{ } \Omega\text{cm}^2$ determined with the steady state polarization measurements given by Figure 2.3. Using this r , the α_f fitted to our experimental data is determined to be $\alpha_f = 0.316 \text{ V}$. The plane given

by the Simple Model using these parameters is plotted in Figure 2.6. However the theoretical values for the linearized Nernst potential are: $V_{eq}^*(0) = 1.03$ V and $\alpha_f = 0.18$ V (reference [2]), which shows that the Simple Model is incorrect in the reversible heat production since the fitted α_f is much larger than the theoretical α_f . Figure 2.7 shows the experimental results and the plane described by the Simple Model using the theoretical values for the linearized Nernst potential.

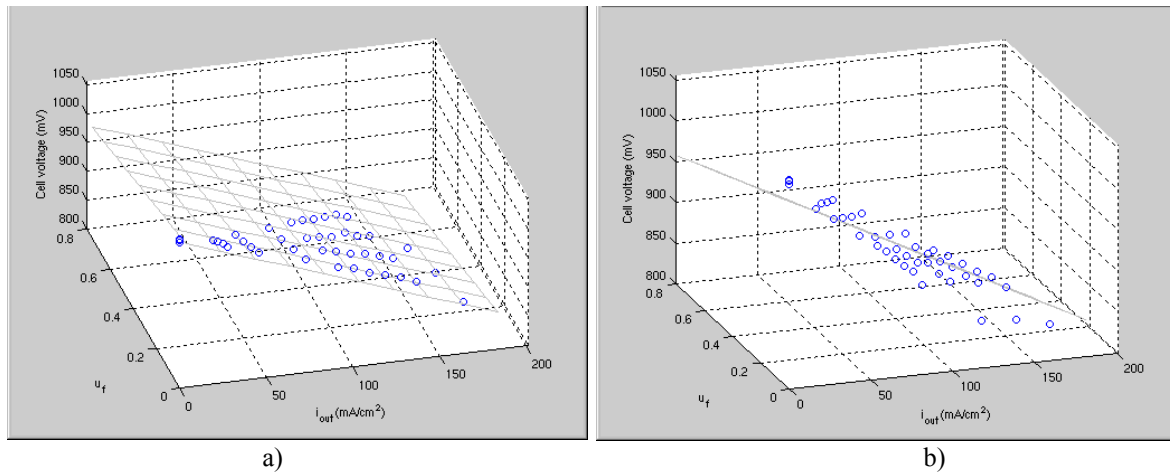


Figure 2.7. Comparison of the experimental results (o) and the plane described by the Simple Model, seen from 2 different viewing angles.

This figure shows clearly the discrepancy between the experimental result and the Simple Model where only r is fitted. The discrepancy between the fitted value for $V_{eq}^*(0)$ and α_f , and their theoretical values are caused by the assumptions and shortcomings made in the Simple Model. In the Extended Model, we include the initial dip, the oxidant utilization and the non-homogenous current distribution. Next we will show that with these refinements, the theoretical values for $V_{eq}^*(0)$ and α_f can be used and yield a perfect fit.

The cell performance is compared with the predicted performance by the Extended Model. As for the parameters, we use the above given theoretical values for $V_{eq}^*(0) = 1.03$ V and $\alpha_f = 0.18$ V, and $\alpha_{ox} = 0.041$ V (reference [1], p20). Only the quasi-Ohmic resistance is obtained by fitting the Extended Model to the experimental results given in Table 2.1. The fitted result is $r = 1.07 \Omega\text{cm}^2$. Figure 2.8 and Figure 2.9 show the same experimental results with the plane described by the Extended Model.

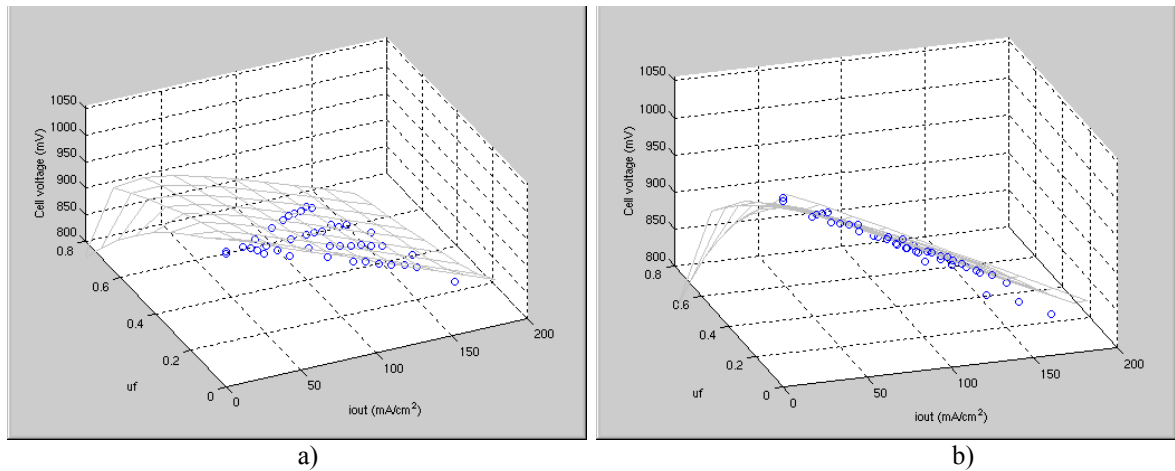


Figure 2.8. Comparison of the experimental results (o) and the plane described by the Extended Model, seen from two different viewing angles.

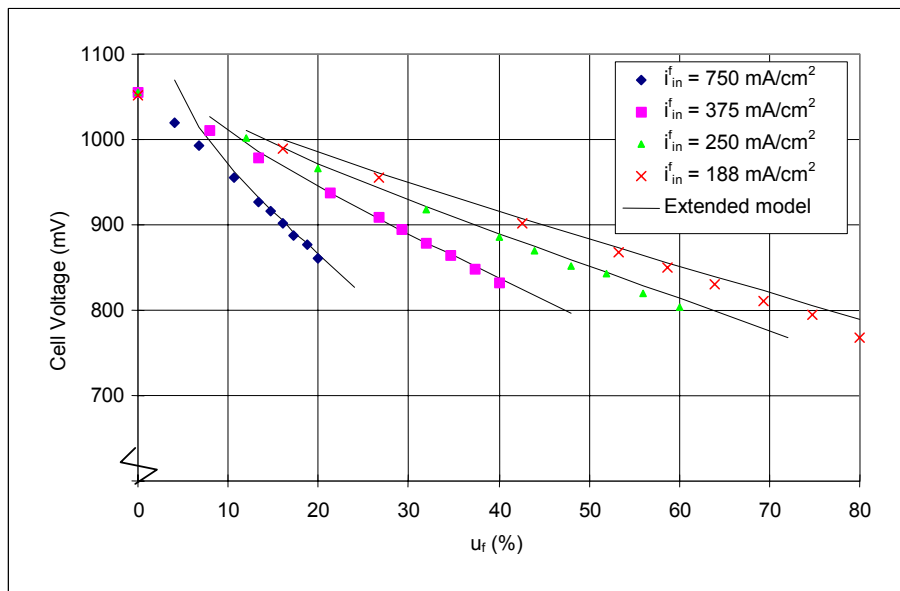


Figure 2.9. 2D plot of the experimental results and the cell voltage described by the Extended Model.

Figure 2.8 and Figure 2.9 show the way the Extended Model describes nearly all the data points, except for those obtained at low fuel utilization, which are clearly shown in Figure 2.9. The discrepancy becomes important at $u_f < 10\%$. However, compared to the Simple Model, the Extended Model gives a better performance prediction. For comparison of both models, a set of data at gas flows of $i_{in}^f = i_{in}^{ox} = 250 \text{ mA/cm}^2$ is taken, and the mismatch between the measured and predicted performance ΔV is plotted in Figure 2.10 as a function

of i_{cell} . Note again that for both models, we only fit r and use the same theoretical values for the linearized Nernst potential (i.e., $V_{eq}^*(0) = 1.03$ V and $\alpha_f = 0.18$ V).

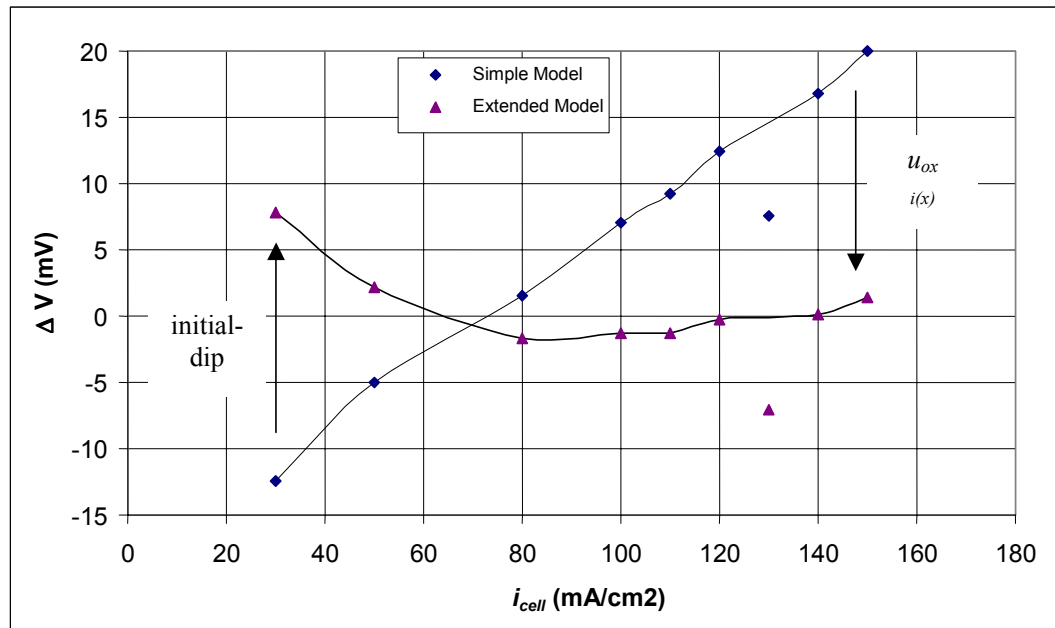


Figure 2.10. Performance mismatch for the Simple Model and the Extended Model.

Figure 2.10 shows that the points corresponding with the measurement at 130 mA/cm² deviate significantly from the rest of the measurement, and therefore they are considered as an artifact. From this figure, we can see that ΔV for both models are within 20 mV range, which translate into a relative accuracy of more than 95 %. Therefore, both models are capable of describing the cell performance. More importantly, Figure 2.10 shows that ΔV for the Simple Model is increasing linearly with the current load, whereas ΔV for the Extended Model is about zero, except for low i_{cell} . Clearly, a significant better agreement is obtained by the Extended Model (ΔV between -2 to +8 mV) than by the Simple Model (ΔV between -12 to 20 mV). For the Extended Model, these numbers translate into a relative accuracy of more than 99 %. This is an almost perfect fit, especially considering the fact that only r is fitted. The improvement in accuracy is obtained by three differences in these models that can be clearly identified. At low current density, the correction for the initial dip causes a better agreement, even though it may be a bit overcorrected. At high current density, the corrections for oxidant utilization and for the inhomogeneous current distribution become important.

2.6. Conclusions

Both the Simple Model and the Extended Model are capable of describing the cell voltage with the quasi-Ohmic resistance r as the only fitted parameter. For the 110 cm² MCFC bench cell it is determined as 1.02 Ωcm² and 1.07 Ωcm² using the Simple and Extended Model respectively. Using this result, the Extended Model describes the cell performance for fuel utilization higher than about 10 % within -5 to +10 mV, which is at the most a relative error of 1 %. Only for very low fuel utilization, the Extended Model gives an over correction for the initial dip (e.g., at $u_f = 4\%$) The absolute error for the Simple Model is between -24 to +40 mV, which is at most a relative error of 5 %.

In conclusion, although being not bilinear, the performance prediction of the Extended Model is better than the performance prediction by the Simple Model for the bilinear cell performance. The Simple Model is a very simple expression but less accurate at fuel utilization higher than 10 %. The Extended Model is very accurate but consists of a more elaborated nonlinear expression.

Acknowledgments

The Netherlands Organization for Science Research (NWO), the Dutch Stichting VSB Fonds and Japanese New Energy and Industrial Development Organisation (NEDO) are acknowledged for partly supporting this work. Ishikawajima-Harima Heavy Industry Co. (IHI) is acknowledged for the 100 cm² -class Molten Carbonate Fuel Cell (MCFC). Dr. C. G. Lee and H. Nakano are acknowledged for their help during the experimental work at Tohoku University.

References

- [1] F. Standaert, *Analytical Fuel Cell Modelling and Exergy Analysis of Fuel Cells*, PhD Thesis, ISBN 90.9012330-X, Delft University of Technology (1998).
- [2] F. Standaert, K. Hemmes, N. Woudstra, *Analytical fuel cell modeling*, J. Power Sources, **63**, p.221-234, Elsevier (1996).
- [3] F. Standaert, K. Hemmes and N. Woudstra, *Analytical fuel cell modelling; non-isothermal fuel cells*, J. Power Sources, **70**, p.181-199, Elsevier (1998).
- [4] C.G. Lee, H. Nakano, T. Nishina, I. Uchida, Y. Izaki and S. Kudoe, *Characterization of a 100 cm² class molten carbonate fuel cell with current*

interruption, J. Electrochem. Soc. **145** (8), p.2747-2751, Pennington NJ (1996)

- [5] L.A.H. Machielse, *Simple model for the estimation of isothermal fuel cell performance*, **PV 91-10**, The Electrochemical Society Proceeding Series, p.166-174, Pennington NJ (1991)
- [6] J.H. Hirschenhofer, D.B. Stauffer and R.R. Engleman, *Fuel Cells, A Handbook*, US Department of Energy (1994).

Chapter 3: Fuel Cell modeling (Part II)

Numerical models in a flowsheeting program and verification of models

This chapter is accepted for publication by the Energy Conversion and Management, titled: VERIFICATION OF A SIMPLE NUMERICAL FUEL CELL MODEL IN A FLOWSHEETING PROGRAM BY PERFORMANCE TESTING AT A 110cm² MOLTEN CARBONATE FUEL CELL, by S.F Au, N. Woudstra and K. Hemmes, (2002).

Abstract

This chapter presents a verification of a simple numerical model that uses the cell resistance as the only experimental parameter. Two methods for determining this experimental parameter are evaluated by comparing the actual measured cell voltages with the calculated cell voltages at various gas utilizations and current loads. Furthermore, the results of the model are compared with the analytical fuel cell model that is previously developed at Delft University. Both the simple numerical model and the analytical fuel cell model use isothermal electrochemical relations for the determination of performances. In order to assess this numerical model for application to non-isothermal molten carbonate fuel cell stacks found in practice, the discrepancy between the results from isothermal model and non-isothermal model is discussed. The maximum relative discrepancy between the measured and calculated cell voltage by the numerical model was 3 %. This discrepancy was reduced to 1.7 % when using a fitted value for the cell resistance. Comparison of isothermal and non-isothermal models shows that the differences in results can in general be neglected.

3.1. Introduction

Fuel cells and in particular high temperature fuel cells need a wide variety of auxiliary equipments in order to operate both efficiently and reliably, all together called a fuel cell system. A previous study [1] from our group has shown that the efficiency of the total fuel cell system depends strongly on the design of the complete system and the performance of the fuel cell. It is therefore crucial to have reliable system studies made of the complete fuel cell system in order to optimize the system configuration and operating parameters. For conventional energy conversion systems, there are several flowsheeting software packages commercially available, and they have proven their practical value [2]. Some of these packages provide the option of modeling fuel cell systems. In most cases, the fuel cell is characterized by a fixed design point, i.e. power output at given gas utilizations and mass flows. These data are sufficient when calculation of the efficiency at the design condition is required. The possibilities for part load off-design calculations are often very limited in spite of the fact that these calculations are very important. In general, fuel cells have superior part load performances with respect to conventional heat conversion systems, and in order to use this advantage, part load off-design calculations of fuel cell systems are obligatory and flowsheeting software should facilitate these calculations as much as possible. An accurate fuel cell model that describes the fuel cell performance as a function of the operating parameters is hence required. Calculations of system performances at design and off-design conditions then become possible and open new possibilities for designers to refine and optimize fuel cell system lay-outs. An additional advantage of integrating a fuel cell model into a flowsheeting program is that the energy and mass flows of the fuel cell stack and the balance of plant are then linked. The interaction between the stack and the balance of plant is simultaneously considered. This can significantly reduce the effort in designing and optimizing fuel cell systems.

A flowsheeting program has been developed by Delft University of Technology, and this program contains a standard fuel cell apparatus with a fuel cell performance model built-in. This fuel cell apparatus has the desired features of calculating the stack power output at various operating conditions, and it is of general importance to have the accuracy of the fuel cell performance verified, since the reliability of the flowsheet calculations depends on the accuracy of the model. This article presents a verification of the fuel cell performance

model by comparing the calculated results with experimental results obtained from a 110 cm² molten carbonate fuel cell (MCFC) bench cell.

3.2. Theory

In a fuel cell under load, gaseous reactants are converted into product species, heat and electric power. This feature can be integrated into a system flowsheet when these features are translated into mass and energy flows. See Figure 3.1 for an example of a data processing routine that is implemented in a flowsheeting program.

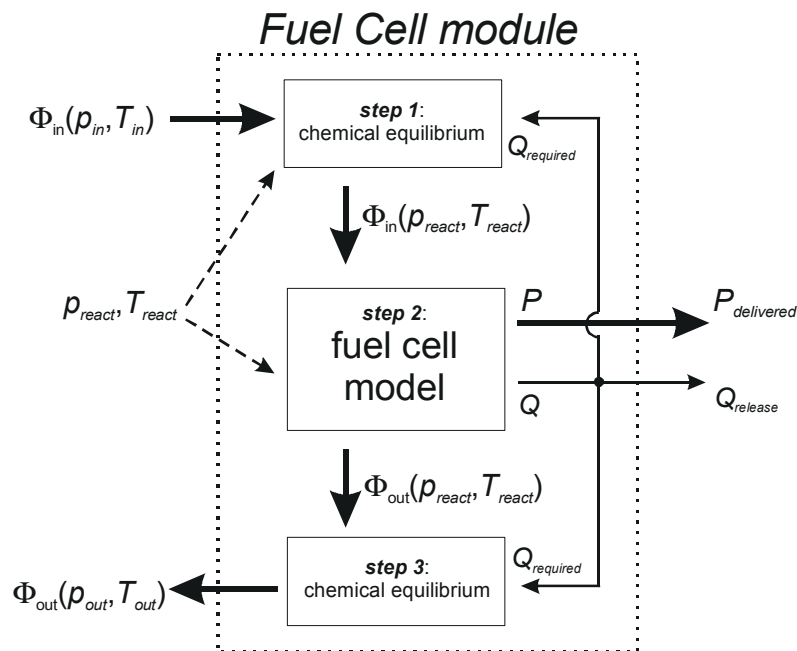


Figure 3.1. Data processing routine of the fuel cell module in a flowsheeting program.

Common practice in flowsheet calculations is to define the mass flows $\Phi_{in,i}$ and $\Phi_{out,i}$ for the anode and cathode and the amount of electrical power $P_{delivered}$ that is delivered at a specified pressure p_{react} and temperature T_{react} . The amount of heat Q that is produced results from the energy balance. Off-design conditions are modeled by defining new mass flows $\Phi_{in,i}$ and $\Phi_{out,i}$ together with a new $P_{delivered}$, which must all be according to the manufacturer's specifications. Experimental data of each off-design condition from the fuel cell manufacturer is compulsory, and the number of off-design conditions that can be modeled is limited by the number of this experimental data.

The objective of the fuel cell model is to determine the performance of the fuel cell (i.e. $P_{delivered}$) as a function of the parameters that are controlled by the fuel cell operators. These control parameters are, in practice, the total fuel utilization u_f , which is the degree of conversion of fuel that is fed into the cell, and the current density i_{cell} . Therefore, the goal of the fuel cell model is to determine the cell voltage V_{cell} as a function of u_f and i_{cell} . The flowsheeting program Cycle-Tempo [3] that the group has been developing contains a fuel cell model that does exactly this: calculating $V_{cell}(u_f, i_{cell})$. The physics of this model can be described by an equivalent circuit shown by Figure 2.1.

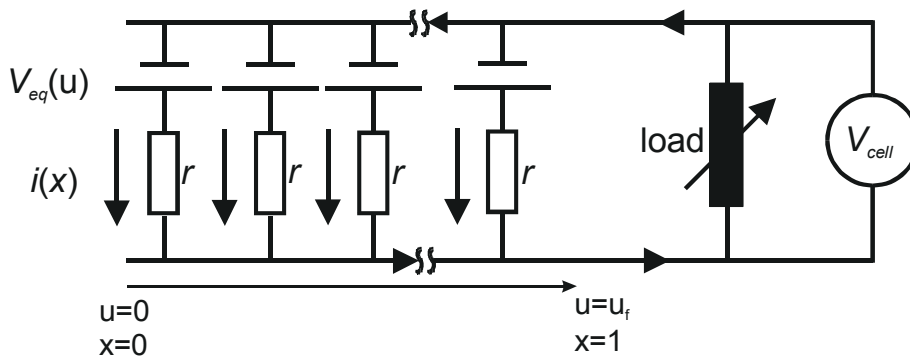


Figure 2.1. Fuel cell represented as an equivalent electrical circuit.

This one dimensional model is applied for analytical analysis by Standaert et al. [4], and it is described in more detail in the Chapter 2. In summary, this model assumes an Ohmic relation for the local irreversible losses. These losses are due to the ionic/electronic conductance but also due to activation and diffusion polarization, although the latter are, in theory, not Ohmic or linear. Nevertheless, linear i_{cell} - V_{cell} relations are obtained for MCFCs in practice (see references [5] and [6]), and diffusion limitation is observed only at high current densities beyond standard operating conditions (see Figure 2.5 and Figure 2.6).

The result of this assumption is that V_{cell} can be determined at any operating condition by solving two integrals given by equation (2.5).

$$V_{cell} = \frac{1}{u_f} \int_0^{u_f} V_{eq}(u) du - \frac{r}{i_{cell}} \int_0^1 i^2(x) dx \quad (2.5)$$

V_{eq} is here the Nernst Voltage expressed as function of the cumulative local fuel utilization u , $i(x)$ is the local current density and r is the quasi-Ohmic resistance that accounts for all

irreversible losses. Therefore, the first integral represents the reversible cell voltage as function of total fuel utilization u_f and the second integral represents the irreversible losses as function of mean current density i_{cell} . This equation can be used to calculate the cell voltage at any operating condition (including off-design) by using solely r as the experimental parameter. Note here that although the irreversible losses of each sub cell in Figure 2.1 is assumed to be Ohmic, a linear i_{cell} - V_{cell} behavior is only obtained when the local current density $i(x)$ is constant.

By assuming a quasi-Ohmic behavior for the local irreversible losses, the diffusion limitation as discussed in reference [8] is not taken into consideration. In contrast to other two dimensional models (e.g., references [7-10]) or three dimensional models (e.g., references [10-12]), this one dimensional model is very simple and can be solved analytically allowing further analytical analysis of results, which is done in another paper (reference [13]). Unlike elaborate two or three dimensional models, this simple one dimensional model is solved very quickly, which is a great advantage for integrating into flowsheet calculations that, in general, already require frequent use of iterative solving routines. A simple model helps in reducing computational time and converging mass and energy balances. Optimization of the operating parameters and system configuration then becomes much less time consuming.

A numerical routine is implemented in the flowsheeting program to solve the integrals given by equation (2.5). This is done by using a user defined mean cell temperature T_{cell} and pressure p_{cell} . Both T_{cell} and p_{cell} are used for the calculation of $V_{eq}(u)$, and therefore, the cell performance is calculated at isothermal condition. Gas compositions of the fuel cell's inlets must be given or they should be determined by the flowsheet via a previous apparatus. Both the fuel utilization u_f and the cell area A_{cell} ¹⁾ should be given as design criteria. Solving the integrals numerically offers the flexibility of choosing either i_{cell} or V_{cell} as the input parameter, and the numerical routine is capable of calculating the other. Both co-flow and counter-flow configurations are implemented. For the high temperature fuel cells, the model also includes shift and methane reforming reactions. Chemical equilibrium for the shift reaction is assumed during the calculation of $V_{eq}(u)$. As an option, methane gas can be used as fuel by either direct or indirect internal reforming. Direct

¹⁾ It is possible to calculate A_{cell} , as desired in a design case, but then $P_{delivered}$, i_{cell} and r_{cell} must be given

internal reforming is done by assuming chemical equilibrium for the reforming reaction during each calculation of $V_{eq}(u)$ while for the indirect internal reforming, this equilibrium is calculated only once before entering the fuel cell.

After the cell performance calculations, the program determines the power density of the cell, which determines the heat dissipation per unit area. The given gas inlet composition, i_{cell} , u_f , and A_{cell} predetermine the outlet gas composition and mass flow of the anode. To fulfill the energy balance, the user can either decide to let the program iteratively determine the amount of cathode mass flow at a given outlet temperature, or the user can decide to calculate the outlet temperature of both the anode and cathode at a given cathode mass flow. This outlet temperature is here independent of T_{cell} that is defined by the user.

3.3. Experiments and Calculations

Experimental measurements were performed on a 110 cm² Li/Na MCFC bench cell at 650 °C. Because of the small size of this cell, it is assumed that this cell is operating at isothermal conditions. This cell was manufactured, installed and tested by Ishikawajima-Harima Heavy Industry Co. (IHI), at Tohoku University (Japan). Using standard testing gas composition (see Paragraph 2.3), the cell voltage is measured at various current loads at four fixed anode and cathode mass flows. The equivalent current input²⁾ i_{in}^f of anode mass flows are 750, 375, 250 and 188 mA/cm². A stoichiometric mixture of O₂ and CO₂ is used for the cathode gas composition. The cathode gas mass flow is fixed for all measurements at an equivalent i_{in}^{ox} of 375 mA/cm². The current load is varied between 30 to 150 mA/cm² and the cell voltage V_{cell} at various loads is measured. The results are four sets of cell voltages denoted by the i_{in}^f used, each voltage being a function of current density, fuel utilization and oxidant utilization. The range of operating and testing conditions in terms of the operating parameters i_{cell} , u_f and u_{ox} are summarized in Table 3.1. The measurement method and results are described in detail in Paragraph 2.3 and 2.4 respectively. Additional information about this experimental setup is given in Appendix B.

²⁾ This means that (theoretically) at respectively 750 to 188 mA/cm² the fuel gas would be fully converted.

Table 3.1. Operating and testing conditions.

Cell temperature (T_{cell})	650 °C
Operating pressure (p_{cell})	1 bar
Fuel utilization (u_f)	0.04 – 0.80
Oxidant utilization (u_{ox})	0.08 - 0.40
Current density (i_{cell})	30 – 150 mA/cm ²

The only experimental parameter in the fuel cell model that needs to be determined experimentally is the fuel cell quasi-Ohmic resistance r . In Paragraph 2.2, two methods for determining this parameter are distinguished: (1) measure the macroscopic resistance R ($R = dV_{cell} / di_{cell}$) by determining the polarization resistance, or (2) fit the current-voltage characteristics to the analytical Extended Model and determine the quasi-Ohmic resistance r . From the same bench cell and experimental results, the values obtained for r and R can be different due to non-homogenous current distribution inside the cell. From experimental results obtained from this IHI bench cell, we previously have measured $R = 1.02 \Omega\text{cm}^2$ for the macroscopic resistance, and we have determined $r = 1.07 \Omega\text{cm}^2$ for the quasi-Ohmic resistance by fitting (see paragraph 2.2 for details). Both r and R will be used for the cell resistance in the next analysis, and differences in the calculated results will be examined.

The operating conditions of the experiments are applied on a small MCFC system model, which is shown in Figure 3.2A. This model is used to calculate the cell voltage using Cycle-Tempo version 4.13 [3]. Note that this figure consists of process schemes produced by the program, and it uses different nomenclatures as explained by the included legend.

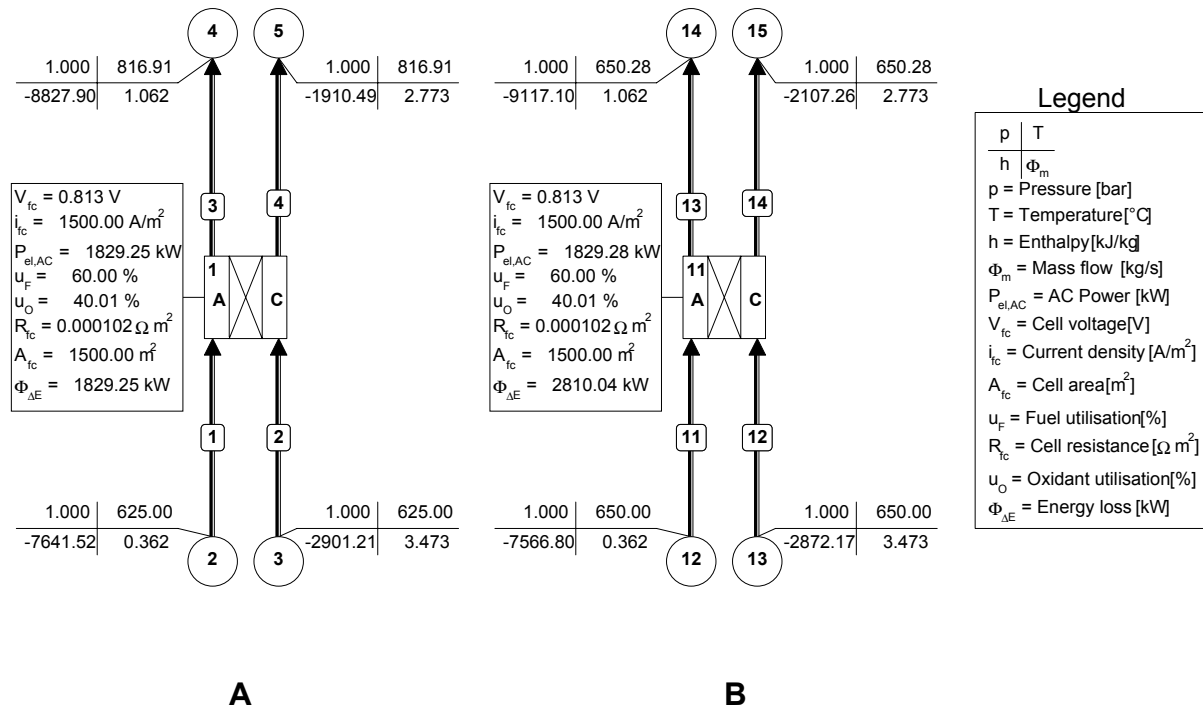


Figure 3.2. Two example of model calculation.

In order to simulate the operating conditions of the experimental set-up fully, the gas flows, gas compositions and fuel utilizations are set equal to the experimental conditions. The gas compositions of the anode and cathode inlets are set at, respectively, pipe number 1 and 2. An arbitrary value of 1500 m² is chosen for the cell area, which input is needed since this program calculates in absolute mass flows in units of [kg/s]. This value does not influence the calculation of the cell voltage since both anode and cathode massflows are set according to this arbitrary cell area and to the equivalent current input that was used during the measurements. The anode and cathode mass flows are set at the gas sources (respectively apparatus 2 and 3). The experimentally determined cell resistance (R or r) and fuel utilization u_f are set at the fuel cell (apparatus 1). The anode mass flow, cell area and fuel utilization together correspond to the current density i_{cell} of the measurement.

The data processing routine of the Cycle-Tempo fuel cell module is schematically given in Figure 3.1. The data processing routine goes as follows:

Step 1: the gas is heated up to the fuel cell operating temperature T_{cell} .

Step 2: calculations by the one-dimensional fuel cell model in which the power output and heat release of the fuel cell is calculated.

Step 3: adjust cathode mass-flow or gas outlet temperature to fulfill the energy balance.

The fuel cell model used by the flowsheeting program is isothermal for its chemical and electrochemical calculations (Step 2 in Figure 3.1), and the temperature T_{cell} and pressure p of the experiment are set accordingly at the fuel cell. Energy conservation is obtained by a temperature rise of both the anode and cathode gas flows (Steps 1 and 3). Note that this temperature rise varies with each calculation, and it is used for the energy balances only. This temperature rise is not taken into account in the performance calculation of the fuel cell model due to the fact that the chemical and electrochemical calculations (and thus, the whole performance modeling part) are done under isothermal conditions at the user defined mean temperature T_{cell} . To prove this, Figure 3.2B shows the result at full isothermal conditions by adding an additional cooling of 960.76 kW³⁾, represented in Figure 3.2 by the difference in the energy loss $\Phi_{\Delta E}$ between A and B. Both results for the cell voltage are the same, but the temperatures of the inlets and outlets are different. The difference in last digit of the power output is solely caused by numerical errors. It is clear that the temperature determined for the outlets by Step 3 of the process scheme do not alter the result of the fuel cell model (Step 2 in Figure 3.1).

3.4. Results and Discussions

Using the simple numerical model, we have calculated the cell voltages under identical operating conditions (i.e. $V_{cell}(u_f, u_{ox}, i_{cell})$ using R or r as the only externally determined experimental parameter). Figure 3.3 and Figure 3.4 show the results of the calculations with $R = 1.02 \Omega\text{cm}^2$ and respectively $r = 1.07 \Omega\text{cm}^2$. For each operating condition, we have plot the calculated cell voltage against the measured cell voltage. The solid line should have been the results for the case of full agreement. The example of calculation shown by Figure 3.2A is encircled. Before discussing the results, we should note that the data in both figures comprises calculations and measurements done under a wide range of

³⁾ This is exactly the amount of heat that is produced by the cell that needs to be dissipated. This value is determined with another calculation.

operating conditions. The fuel utilization is varied between 0.04 and 0.8 and the current density is varied between 0.03 and 0.15 A/cm² (see Table 3.1). For example, Figure 3.5 shows the results of measurement with $i_{in}^f = 250$ mA/cm² where the input gas flows for the anode and cathode are held constant while i_{cell} is varied. Hence, the result is proportioned to i_{cell} , u_f and u_{ox} , as indicated in this figure on the x-axis. Only R and r are externally measured, respectively, fitted. All other parameters (gas compositions, T_{cell} , p , i_{cell} , u_f and u_{ox}) are all experimental parameters, which, for all calculations, are set according to the experimental conditions.

Figures 3.3 and 3.4 show that a slightly better agreement will be achieved when using the quasi-Ohmic r as fitted with the analytical Extended Model rather than the measured macroscopic resistance R . Nevertheless, using $R = 1.02$ Ωcm², the discrepancy between measured and calculated data is small with an average relative error of about 0.5 %. The calculated cell voltages deviate more from the measurement in the lower left corner of the graph. This part represents operating conditions at high gas utilization and current density. Even then, the maximum observed discrepancy is just 3 % at the lowest point on the left, operating at $i_{cell} = 150$ mA/cm², $u_f = 0.8$ and $u_{ox} = 0.4$ (i.e. full load condition). The discrepancy reduces significantly when the fitted $r = 1.07$ Ωcm² is used, as shown by Figure 3.4. The difference in using 1.02 or 1.07 Ωcm² is most significant when operating at high utilization and high current density (i.e., the lower left corner of both figures). These conditions are most used in practice due to economical reasons. The maximum observed discrepancy is just 1.7 %, again at the same operating point of $i_{cell} = 150$ mA/cm², $u_f = 0.8$ and $u_{ox} = 0.4$. A better fit can therefore be obtained by using the fitted value r rather than the measured value R .

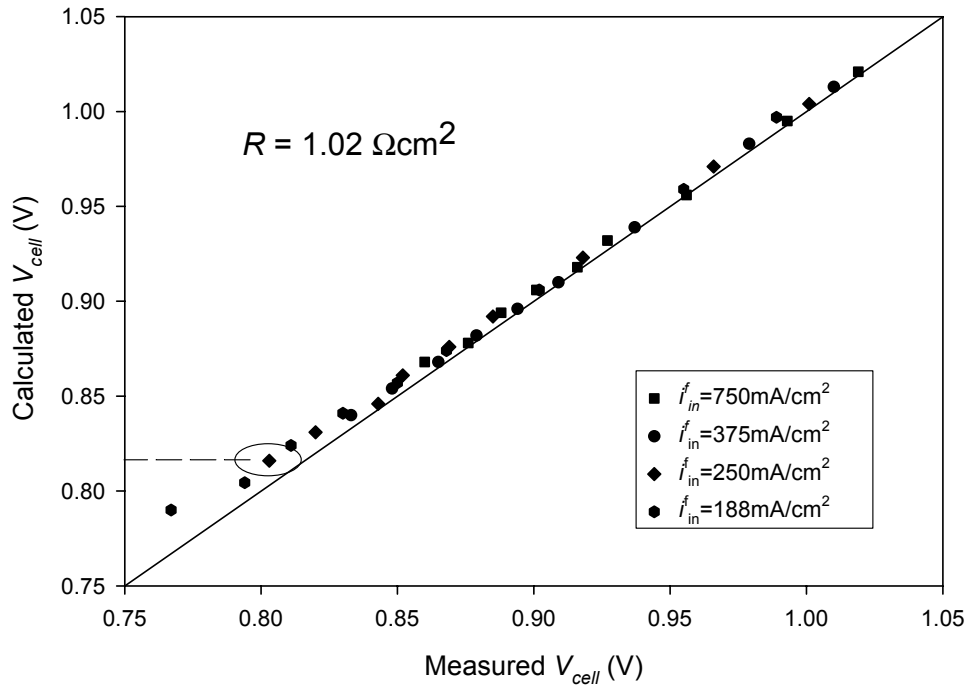


Figure 3.3. Comparison of calculations with the measurements using the measured $R = 1.02 \Omega\text{cm}^2$.

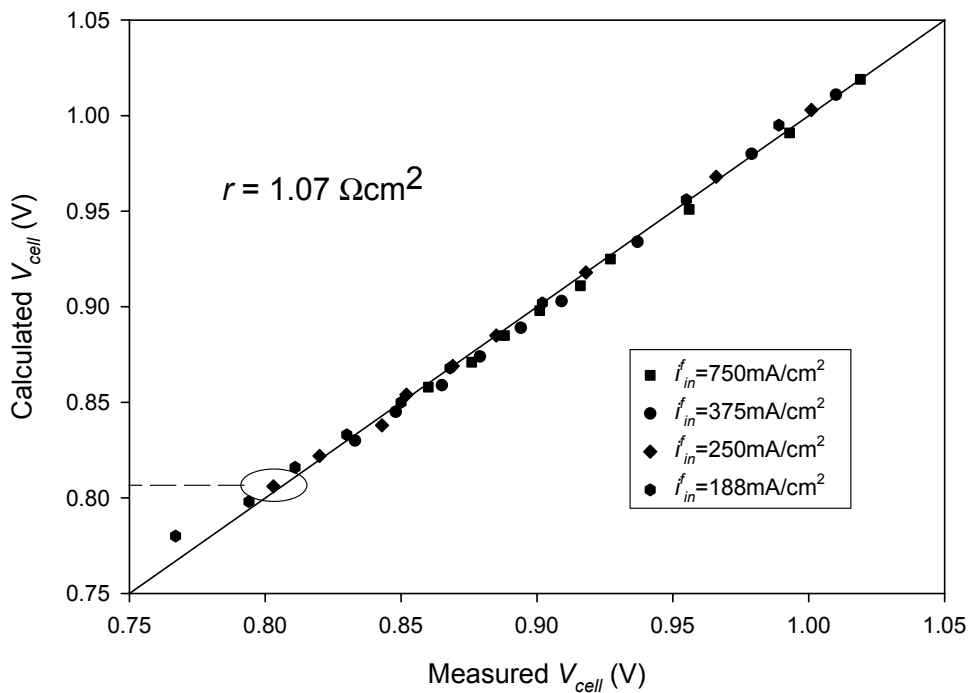


Figure 3.4. Comparison of calculations with measurements using the fitted $r = 1.07 \Omega\text{cm}^2$.

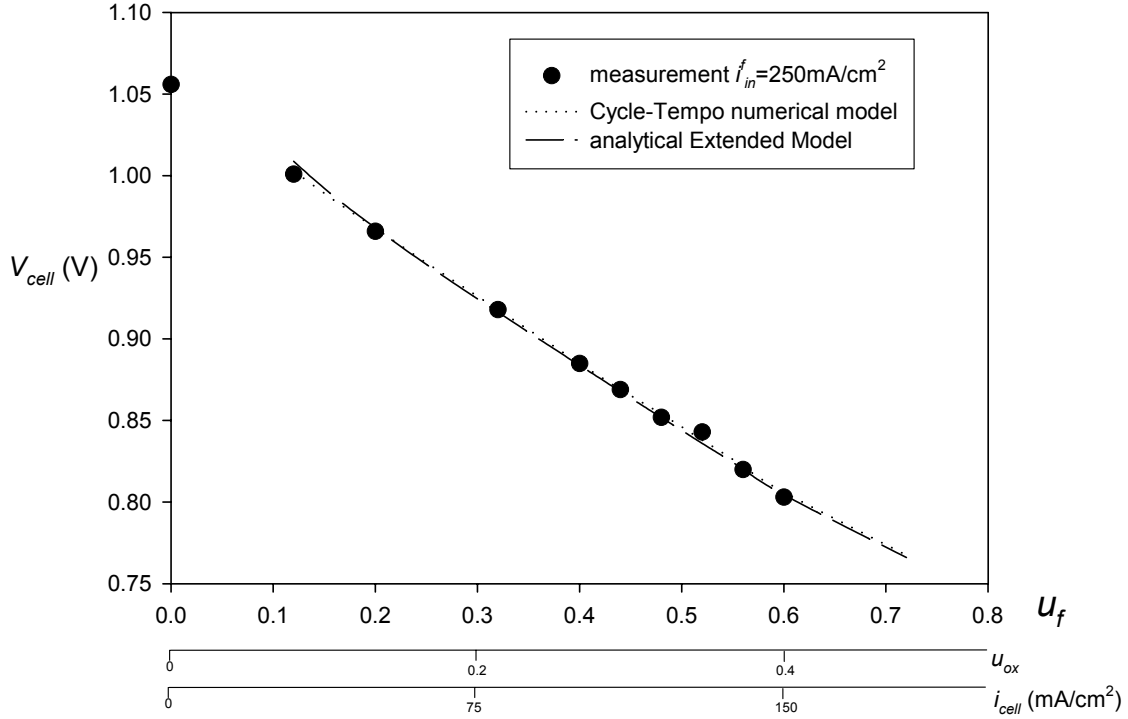


Figure 3.5. Comparison of the Cycle-Tempo Model with the analytical Extended Model and experimental results, using $r = 1.07 \Omega\text{cm}^2$.

By assuming the bench cell to operate isothermally, we so far have assessed the use of the simple numerical fuel cell model under isothermal condition. The main objective of a flowsheeting program is to facilitate the evaluation of fuel cell plant designs. The fuel cell stacks that are used in these plants are highly non-isothermal, and hence, we need to estimate the discrepancy for using isothermal results on non-isothermal conditions expected in practice. For this, we will use the analytical isothermal Extended Model (see paragraph 2.2.2) and its non-isothermal derivative (see reference [15]) that we have developed earlier. The Extended Model (equation (2.8)) is the analytical solution of equation (2.5) by linearizing the Nernst equation, added a correction of the initial dip and by assuming a linear decreasing current distribution in the cell (see Paragraph 2.2 for details).

$$V_{cell}^{EM} \approx V_{eq}^*(0) - \frac{1}{2} \alpha_{tot} u_f + \frac{0.003}{u_f} - \left[1 + \frac{1}{3} \left(\frac{\alpha_{tot} u_f}{2r i_{cell}} \right)^2 \right] r i_{cell} \quad (2.8)$$

V_{eq}^* is the linear fit for the Nernst equation as function of u and α_{tot} is the slope of the linear part of V_{eq} calculated for both fuel and oxidant utilization.

For the estimation, the results from the simple numerical model are compared with the results from the Extended Model. Figure 3.5 shows the results of Cycle-Tempo simple numerical model and the analytical Extended Model together (both using $r = 1.07 \Omega\text{cm}^2$) with the experimental measurements at $i_{in}^f = 250 \text{ mA/cm}^2$ (see abscissa of Figure 3.5 for operating conditions). It shows that the calculated cell voltages by the program's numerical model and by the Extended Model are about the same. This confirms the accuracy of the linearizations and corrections made in the Extended Model (i.e. linearized Nernst equation, linear approximation for the current distribution and correction for "initial dip").

A comparison of this analytical isothermal Extended Model, its non-isothermal derivative and two more elaborate numerical fuel cell models developed by de Groot [16] have been previously presented by Standaert et al. [15]. Figure 3.6 is the comparison taken from reference [15], and here, the analytical models are the Extended Models and the numerical models are de Groot's models. This figure shows the comparison of results and, in particular, the range of fuel utilization where discrepancy is expected. The lines in Figure 3.6 show that the differences in the calculated cell voltages are small (about 3mV). Furthermore, it shows that the difference between the isothermal and non-isothermal results is about constant over the range of fuel utilization. This small difference between isothermal and non-isothermal results suggests that we may use this simple numerical fuel cell model in situations where the fuel cell is operated under non-isothermal conditions. With this, we should be aware of the discrepancy that may influence the calculation of the complete fuel cell system. Generally, this 3mV discrepancy translates to a relative error of tenths of percent points for the fuel cell power output. It is for the user of the software package to decide whether a compensation of the result is required.

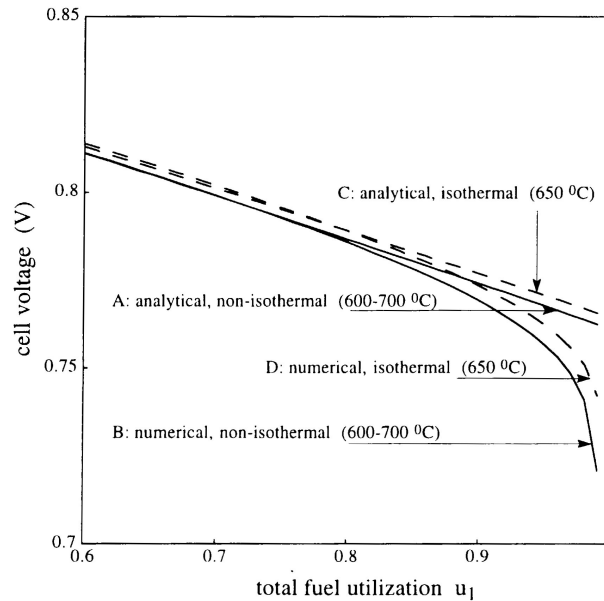


Figure 3.6. Comparison of isothermal and non-isothermal results of fuel cell models, (figure taken from Standeart et al. [15]).

3.5. Conclusions

The results of a simple numerical fuel cell model of a flow-sheeting program are compared with experimental results of an isothermal MCFC bench cell. Two values were used for the cell resistance that describes the irreversible losses (i.e. transport resistance and kinetics) of the cell: the macroscopic resistance R , which is the measured polarization resistance, and the fitted quasi-Ohmic resistance r that is obtained by fitting. Both comparisons show that the results of the model are in accordance with the experimental results. Using the macroscopic resistance R , the average relative discrepancy is within 0.5 % with a maximum of 3 % at full load condition. Additional improvement in the accuracy is obtained by using the fitted quasi-Ohmic resistance r , and the maximum relative discrepancy reduces to 1.7 % at full load condition. Another comparison of the results with other theoretical models suggests that the fuel cell model of the flowsheeting program, based on isothermal calculation of the electrochemical process, can be used with high accuracy for non-isothermal conditions.

These results are very promising, since this model is very simple but accurate. Unlike other detailed models (e.g., references [8-11]), this model is solved very quickly and is

incorporated in a flowsheeting program. The use of a single experimental parameter in modeling high temperature fuel cell performance has proven to be accurate. It is shown that the design and off-design performances of the MCFC are still fully described and, thus, can be used for flowsheet simulations of MCFC systems. The flowsheeting tool can facilitate the design and optimization of fuel cell systems at both design and off-design conditions. With this tool, standard flowsheeting analysis methods, like exergy and pinch-point analysis, become available for fuel cell systems.

Acknowledgement

Ishikawajima-Harima Heavy Industry Co. (IHI) is acknowledged for the 100 cm² –class Molten Carbonate Fuel Cell (MCFC).

Reference

- [1] A. de Groot and N. Woudstra, *Exergy Analysis of a Fuel-Cell system*. p. 32-39, Journal of the Institute of Energy **68**, (1995)
- [2] I. Giglmayr, M. Nixdorf and M. Pogoreutz, *Comparison of Software for Thermodynamic Process Calculation*, VGB PowerTech 2/2001 (2001)
- [3] Cycle-Tempo version 4.13, Delft University of Technology, Section Thermal Power Engineering; TNO Environment, Energy and Process Innovation, (1999). <http://www-pe.wbmt.tudelft.nl/ev/cycle/cycle.html>
- [4] F.R.A.M. Standaert, K. Hemmes and N. Woudstra, *Analytical fuel cell modeling*, p221-234, Journal of Power Source **63**, (1996).
- [5] S.F. Au, W.H.A. Peelen, F.R.A.M. Standaert, K. Hemmes and I. Uchida, *Verification of Analytical Fuel Cell Models by Performance Testing at a 110 cm² Molten Carbonate Fuel Cell*. p. A1051-A1057, Journal of Electrochemical Society **148** (10), Pennington NJ, USA, (2000).
- [6] L.A.H. Machielse, *Simple model for the estimation of isothermal fuel cell performance*. **PV 91-10**, The Electrochemical Society Proceeding Series, p.166-174, Pennington NJ (1991)
- [7] T.L. Wolf and G. Wilemski, *Molten Carbonate Fuel Cell Model*, p.48-55, Journal of the Electrochemical Society, Pennington, **130** (1), NJ, USA, (1983)

- [8] E. Arato, B. Bosio, P. Costa and F. Parodi, *Preliminary experimental and theoretical analysis of limit performance of molten carbonate fuel cells*. p74-81, Journal of Power Sources **102**, (2001).
- [9] D. Singh, D.M. Lu and N. Djilali, *A two-dimensional analysis of mass transport in proton exchange membrane fuel cells*, p.431-452, International Journal of Engineering Science **37**, (1999).
- [10] M. Iwata, T. Hikosaka, M. Morita, T. Iwanari, K. Ito, K. Onda, Y. Esaki, Y. Sakaki and S. Nagata, *Performance analysis of planar-type unit SOFC considering current and temperature distributions*. p.297-308, Solid State Ionics **137**, (2000).
- [11] W. He and Q. Chen, *Three-dimensional simulation of a molten carbonate fuel cell stack using computational fluid dynamics technique*, p.25-32, Journal of Power Sources **55**, (1995)
- [12] W. He and Q. Chen, *Three-dimensional simulation of a molten carbonate fuel cell under transient conditions*, p.182-192, Journal of Power Sources **73**, (1998)
- [13] S.F.Au, K. Hemmes and N. Woudstra, *The influence of operating temperature on the efficiency of combined fuel cell and power cycle system*. p.A879-A885, Journal of The Electrochemical Society **149** (7), (2002).
- [14] S.F. Au, W.H.A. Peelen, F.R.A.M. Standaert, K. Hemmes and I. Uchida, *Assesment of Two Analytical Fuel Cell Models by Performance Testing at a 110 cm² Molten Carbonate Fuel Cell*. p. 90-98, Electrochemical Society Conference Proceeding **PV 99-20**, The Electrochemical Society, Pennington, NJ, USA (1999), ISBN 1-56677-243-5.
- [15] F.R.A.M. Standaert, K. Hemmes and N. Woudstra, *Analytical fuel cell modeling; non-isothermal fuel cells*, p181-199, Journal of Power Sources **70**, (1998).
- [16] A. de Groot, *Exergy analysis of high temperature fuel cell systems*, PhD-thesis, Delft University of Technology, The Netherlands (to be published in 2003).

Chapter 4: Fuel Cell system optimization (part I)

Theoretical optimization of cell temperature of hydrogen fuel cell systems

This chapter is published in the Journal of Electrochemical Society 149(7) pp. A879-A885, titled: THE INFLUENCE OF OPERATING TEMPERATURE ON THE EFFICIENCY OF COMBINED FUEL CELL AND POWER CYCLE SYSTEM, by S.F Au, K. Hemmes and N. Woudstra, (2000).

Abstract:

This chapter presents an investigation of fuel cell systems consisting of a hydrogen fuel cell and a bottoming power cycle in which the exergy of waste heat is recovered. Starting from thermodynamics and the reversible limit, the conversion efficiency of fuel cell systems is examined as function of fuel cell operating temperature. Practical fuel cell systems are examined here first by using simple assumptions for the loss functions. These functions are later refined by using experimentally determined performance equations for a molten carbonate fuel cell (MCFC) stack. The temperature dependence of the efficiency of the total MCFC systems is predicted and analyzed. Within practical limits, the operating temperature of the fuel cell has only minor impact on the overall system efficiency. This provides a degree of freedom in the optimization of other performance parameters such as endurance and cost.

4.1. Introduction

Fuel cell technology is about to become available as an alternative for the theoretically less efficient thermal combustion technology. Especially the molten carbonate fuel cell (MCFC) and solid oxide fuel cell (SOFC) are interesting technologies for the stationary power supply due to their high operation temperature. The exergy of the waste heat is high enough to make further conversion into electricity possible. These relatively new fuel cell technologies have to compete with conventional combustion technology, which already has a century to mature. In order to be competitive, recent fuel cell research is focused on reduction of costs and extension of lifetime. Although these developments are essential in order to make fuel cells economically attractive, loss of efficiency might be the price to be paid to achieve those goals. However, high efficiency is the main advantage of fuel cell technology. It is therefore now necessary to change our focus back on the main advantage of fuel cell technology, that is, to convert chemical energy into electricity as efficiently as possible.

This chapter presents an investigation on the influence of the operating temperature on the conversion efficiency of combined fuel cell and power cycle hybrid system. Our objective is to find the optimum operating temperature of these systems by starting with basic thermodynamic and finishing by adding the more complex temperature behavior of irreversible losses of a MCFC that is found in practice.

4.2. Theory

Fuel cells are energy conversion devices in which generally hydrogen is oxidized electrochemically.



When the fuel cell is operated reversibly, part of the enthalpy Δh is converted into power, namely the Gibbs free energy Δg . This reversible process has to fulfill the requirement of zero entropy production, imposed by the second law of thermodynamics. The decrease in the amount of gas molecules, and the entropy changes associated with that, must be

compensated by an equal amount of entropy production. This is accomplished by the dissipation of heat with an amount equal to $T\Delta s$ and hence lowering the maximum electric efficiency η_{fc} of a fuel cell given by

$$\eta_{fc} = \frac{\Delta g}{\Delta h} = \frac{\Delta h - T\Delta s}{\Delta h} = 1 - T \left(\frac{\Delta s}{\Delta h} \right) \quad (4.2)$$

This expression can be further simplified by considering the condition at which reaction (4.1) occurs spontaneously. The temperature at which this process takes place is the spontaneous combustion temperature $T_{\Delta G=0}$ at which the change of Gibbs energy is zero (see reference [1])

$$0 = \Delta h_{T_{\Delta G=0}} - T_{\Delta G=0} \Delta s_{T_{\Delta G=0}} \Rightarrow T_{\Delta G=0} = \frac{\Delta h_{T_{\Delta G=0}}}{\Delta s_{T_{\Delta G=0}}} \quad (4.3)$$

Assuming that the ratio of enthalpy and entropy is about constant as function of temperature, we can substitute this ratio in equation (4.2) and we get this expression for the conversion efficiency

$$\eta_{fc} = 1 - \frac{T}{T_{\Delta G=0}} \quad (4.4)$$

Hence the fuel cell efficiency is decreasing linearly¹⁾ with temperature, and it behaves oppositely to conventional combustion. With conventional combustion, the exergy of heat of combustion is determined by the Carnot efficiency η_c , which increases with temperature and approaches 100 % efficiency asymptotically

$$\eta_c = 1 - \frac{T_0}{T} \quad (4.5)$$

¹⁾ Δh , Δs and their ratio depend slightly on temperature, and the fuel cell efficiency is therefore not exactly linear with temperature. We will neglect this effect at the moment in order to keep this evaluation transparent.

Both η_{fc} and η_c are plotted in Figure 4.1 as function of temperature.

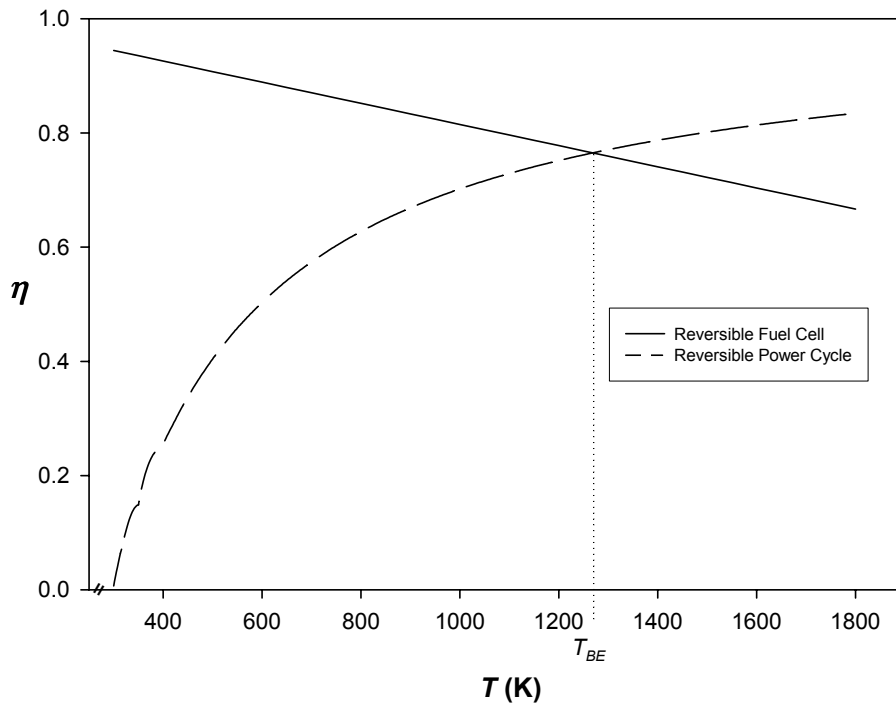


Figure 4.1. Reversible efficiencies of H₂/O₂ Fuel Cells and Power Cycles as function of T .

It shows a break-even temperature T_{BE} where both efficiencies are the same

$$1 - \frac{T_0}{T_{BE}} = 1 - \frac{T_{BE}}{T_{\Delta G=0}} \Rightarrow T_{BE} = \sqrt{T_0 T_{\Delta G=0}} \quad (4.6)$$

In the temperature range below T_{BE} , a fuel cell can indeed in principle obtain a higher efficiency than a power cycle. However, for the temperature range above T_{BE} , the opposite holds and an ideal power cycle is more favorable. Note that we can simply estimate T_{BE} . Using $T_0 = 298$ K and $T_{\Delta G=0} = 5400$ K²⁾, T_{BE} is found to be about 1300 K, which falls within the range of operating temperatures of a SOFC. Therefore, although it is frequently

²⁾ This is approximately the value for $T_{\Delta G=0}$ using the Δh_0 and Δs_0 at 298 K.

mentioned that fuel cells are not limited by Carnot limitation and hence they are more efficient, Figure 4.1 simply shows that this is only true for a limited temperature range.

An interesting aspect is that the decreasing efficiency of fuel cell simply means that the amount of released heat is increasing while simultaneously the exergy of this heat is increasing. The opposite temperature behavior of the efficiencies of fuel cells and power cycles suggests that these two are complementary processes. It is therefore of interest to study the combination of these two and its temperature dependency.

4.3. Fuel cells combined with recovery Power Cycle

“If you can’t beat them join them”, this certainly holds for fuel cells and power cycles. Obviously, the efficiency of a reversible system in which the dissipated heat from a fuel cell is used in a bottoming power cycle will be higher than that of a fuel cell solely. The temperature dependency of the efficiency of this combination is analyzed next. First, we analyze the reversible systems followed by the analysis in which irreversibility is taken into account.

4.3.1. Ideal reversible fuel cell–bottoming cycle systems

The reversible fuel cell generates power with an efficiency of η_{fc} meaning that the fraction of dissipated heat is equal to $(1 - \eta_{fc})$, which exergy is here reversibly converted by the reversible bottoming power cycle at the Carnot efficiency η_c . Hence, the total system efficiency η_s of this combination shown in Figure 4.1 given by

$$\eta_s = \eta_{fc} + (1 - \eta_{fc})\eta_c \quad (4.7)$$

Substituting equations (4.4) and (4.5) into this, we conclude that the system efficiency is a constant and independent on operating temperature. The system efficiency is simply given by

$$\eta_s = 1 - \frac{T}{T_{\Delta G=0}} + \left(1 - \left(1 - \frac{T}{T_{\Delta G=0}}\right)\right) \left(1 - \frac{T_0}{T}\right) = 1 - \frac{T_0}{T_{\Delta G=0}} \quad (4.8)$$

The efficiency of this system is very high since the spontaneous combustion temperature $T_{\Delta G=0}$ is in general much higher than the temperature T_0 of the environment. Using $T_0 = 298$ K and $T_{\Delta G=0} = 5400$ K, the efficiency of this system is found to be about 0.94. This is exactly the efficiency of a reversible fuel cell at room temperature, in which the exergy of the release heat is zero. Moreover, it is also equal to the Carnot efficiency at exactly the spontaneous combustion temperature $T_{\Delta G=0}$ at which a (hypothetical) hydrogen fuel cell does not deliver any work, but instead works as a combustion chamber. The fuel cell produces only heat, which exergy is fully converted by the bottoming cycle. In the temperature range below T_0 , a higher efficiency is obtained by a stand-alone reversible fuel cell while in the temperature range above $T_{\Delta G=0}$ a stand-alone reversible power cycle has a higher efficiency. In the intermediate temperature range, the decreasing fuel cell efficiency with temperature is compensated by the increase in the exergy of heat yielding a temperature independent system efficiency given by equation (4.8). Hence, fuel cell and power cycle are two complementary processes and together they form an ideal couple, which has a reversible limit that is very high and temperature independent. Here lays the principle for the high efficiency of recently proposed combination systems consisting of a SOFC or MCFC and a gas turbine (e.g., see reference [2]).

4.3.2. Fuel utilization and Nernst loss

Losses in systems are generally determined by irreversibility, which reduces the system's efficiency. However, most fuel cells suffer from a phenomenon called Nernst loss. The Nernst loss is caused by a decrease in local driving forces as fuel and oxidant gasses are being utilized (see reference [3]). As the fuel and oxidant gasses are being utilized, the amount of gas molecules are further reduced and the entropy changes associated with that is equally compensated by an additional reversible heat production. This is analogous to what is described in the previous section. Strictly speaking, Nernst loss is not a loss but a reduction in efficiency imposed by thermodynamics.

Standaert et al. [4] has derived a Simple Fuel Cell Model in which the effect of Nernst loss is taken into account. He found that in the first order Nernst loss is proportional to the fuel utilization u_f (see paragraph 2.2.3)

$$3,4) \quad V_{cell}^{SM,r=0}(u_f) = V_{eq}^*(0) - \frac{1}{2}\alpha_f u_f \quad (4.9)$$

Here α_f is the slope of the linearized Nernst equation as function of the fuel utilization and therefore α_f , and the Nernst loss ($\frac{1}{2}\alpha_f u_f$) are proportional to RT/nF . Introducing the dimensionless proportionality factor β , we have

$$\alpha_f = \frac{RT}{nF} \beta \quad (4.10)$$

Next, we will look more closely to the influence of Nernst loss on the electric efficiency of the fuel cell. For this we will use the definition of the thermal neutral voltage V_m , which is the ideal cell voltage where zero heat is released and therefore all enthalpy is transferred into electric work [5]:

$$V_m \equiv \frac{-\Delta H}{nF} \quad (4.11)$$

Using equation (4.9), (4.10) and (4.11), the electric efficiency η_{fc} is given by

$$\eta_{fc}(u_f) = \frac{V_{cell}^{SM,r=0}(u_f)}{V_m} = \eta_{fc}(0) + \frac{RT\beta}{2\Delta h} u_f \quad (4.12)$$

Note that we can express the fuel cell efficiency in a similar way as equation (4.4)

³⁾ This is the Simple Fuel Cell Model (equation (2.7)) in the reversible limit where the quasi Ohmic internal resistance r is zero.

⁴⁾ The effect of the oxidant utilization is neglected in the Simple Fuel Cell Model, but it can be incorporated analogously.

$$\begin{aligned} \eta_s(u_f) &= 1 - \frac{T}{T_{\Delta G=0}} - \frac{T}{\left(\frac{2\Delta h}{R\beta u_f}\right)} = 1 - \frac{T}{\left(\frac{2T_{\Delta G=0}\Delta h}{2\Delta h - T_{\Delta G=0}R\beta u_f}\right)} \\ &= 1 - \frac{T}{T_{\Delta G=0}^{u_f}} \end{aligned} \quad (4.13)$$

with

$$T_{\Delta G=0}^{u_f} = \frac{2T_{\Delta G=0}\Delta h}{2\Delta H - T_{\Delta G=0}R\beta u_f} \quad (4.14)$$

We have used the MCFC as an example to illustrate the effect of Nernst loss on the fuel cell efficiency. The MCFC is chosen here since the cell voltage of this type of cell suffers most severely from Nernst loss. Operating with standard testing gas composition (see paragraph 4.4.1 Table 4.3 for the exact gas composition) at 923 K, α_f has the value of 0.180 V, from which we can calculate that β is about 4.5. Operating at $u_f = 0.8$, the spontaneous combustion temperature is lowered from 5500 K to about 4100 K, and together the break-even temperature T_{BE} is lowered from 1300 K to about 1100 K (see Figure 4.2).

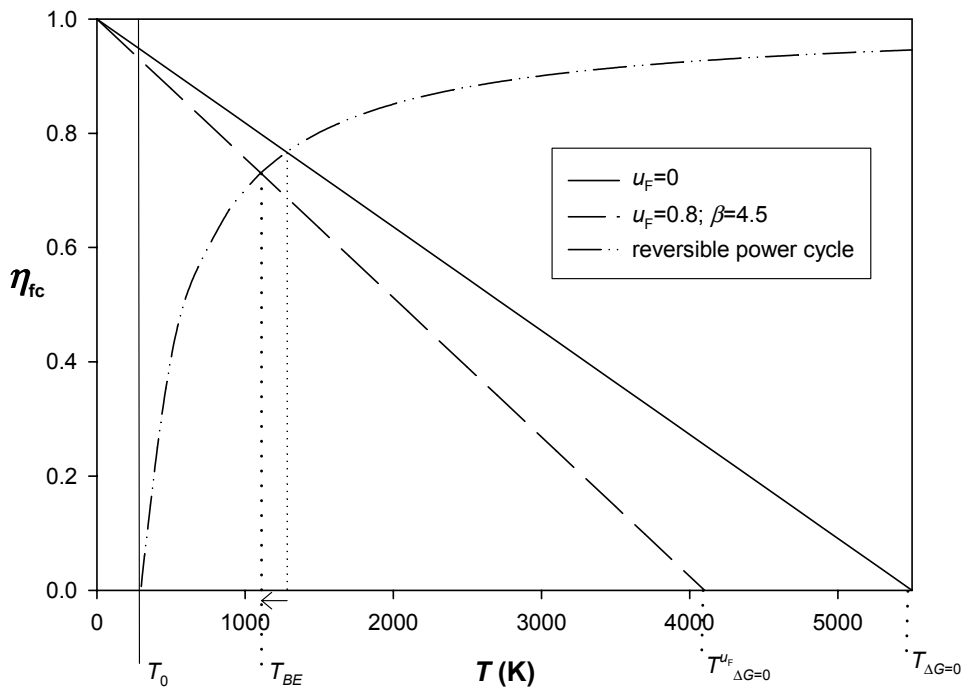


Figure 4.2. The influence of fuel utilization on the fuel cell efficiency.

As for the overall efficiency of the combined fuel cell power cycle system, we can analyze the influence of Nernst loss by filling equation (4.12) in equation (4.7)

$$\begin{aligned}\eta_s(u_f) &= \eta_{fc}(u_f) + (1 - \eta_{fc}(u_f))\eta_c \\ &= \eta_{fc}(u_f) + (1 - \eta_{fc}(u_f))\left(1 - \frac{T_0}{T}\right) \\ &= \eta_{fc}(0) + \frac{RT\beta u_f}{2\Delta H} + \left(1 - \eta_{fc}(0) + \frac{RT\beta u_f}{2\Delta H}\right)\left(1 - \frac{T_0}{T}\right)\end{aligned}$$

After some rearranging, we get

$$\eta_s(u_f) = \eta_s(0) + \frac{RT_0\beta}{2\Delta h}u_f \quad (4.15)$$

It shows that including the Nernst loss, the calculation for the system efficiency does not principally change, at least not its T dependence. However, the overall system efficiency becomes lower, and to show its effect we use here again the MCFC as an example. With $\beta = 4.5$ and $u_f = 0.8$, we can calculate that the reversible theoretical limit drops from 94 % to 92 %. This two percent loss of total electrical efficiency is caused by the loss of the exergy represented by the heat of the Nernst loss. This reversible heat is here partly (68 % at 923 K to be exact) recovered by the bottoming power cycle and therefore the total electrical efficiency does not decrease significantly. With the introduction of Nernst loss, the total electrical efficiency of the combination stays independent of temperature

4.3.3. Non-ideal reversible fuel cell–bottoming cycle systems

In the previous section, we have seen that the electrical efficiency of the fuel cell-power cycle combination does not depend on the operating temperature when both are operated reversibly. In practice, however, irreversible losses always occur and in this section we analyze their influence on the electrical efficiency. First, we use a simple approach with

which irreversibility is considered temperature independent. Then, we introduce the more complex temperature dependent behavior of irreversibility found in practice.

We have seen in the previous section that fuel cell and power cycle are complementary devices. At low temperature, the fuel cell is efficiently producing most of the electricity while at high temperature the power cycle is efficiently recovering the reversibly produced heat from the fuel cell. Starting here, we can expect that in the situation when polarization losses in the fuel cell are taken into account and simultaneously assuming the power cycle to operating ideally, the optimum temperature for the system will be found at high temperature. In this case, the reversible power cycle is efficiently producing most of the power. Vice versa, when the fuel cell is considered ideal and losses occur in the power cycle, the optimum temperature will be found at low temperature. If both the fuel cell and the power cycle are considered non-ideal as in all practical situations, we expect the optimum temperature will lie in the intermediate temperature range. We can simply estimate this temperature behavior by introducing simple approaches for the irreversibility for both the fuel cell and power cycle.

In first approximation, the losses of a power cycle can be incorporated by a temperature independent intrinsic efficiency η_i . The efficiency of this power cycle is then:

$$\eta_c^* = \eta_i \left(1 - \frac{T_0}{T} \right) \quad \text{with } 0 < \eta_i < 1 \quad (4.16)$$

The intrinsic efficiency η_i accounts for both losses in the power cycle and for the losses that occur during heat transport from the fuel cell to the power cycle. In practice, this factor depends on system size and temperature but for typical fuel cell applications, we may assume it to be between 0.8 and 0.9.

Combined with a reversible fuel cell we find an overall system efficiency linear decreasing with T

$$\begin{aligned} \eta_s^* &= \eta_{fc} + (1 - \eta_{fc}) \eta_c^* \\ &= 1 - \eta_i \frac{T_0}{T_{\Delta G=0}} - (1 - \eta_i) \frac{T}{T_{\Delta G=0}} \end{aligned} \quad (4.17)$$

This is shown by Figure 4.3.

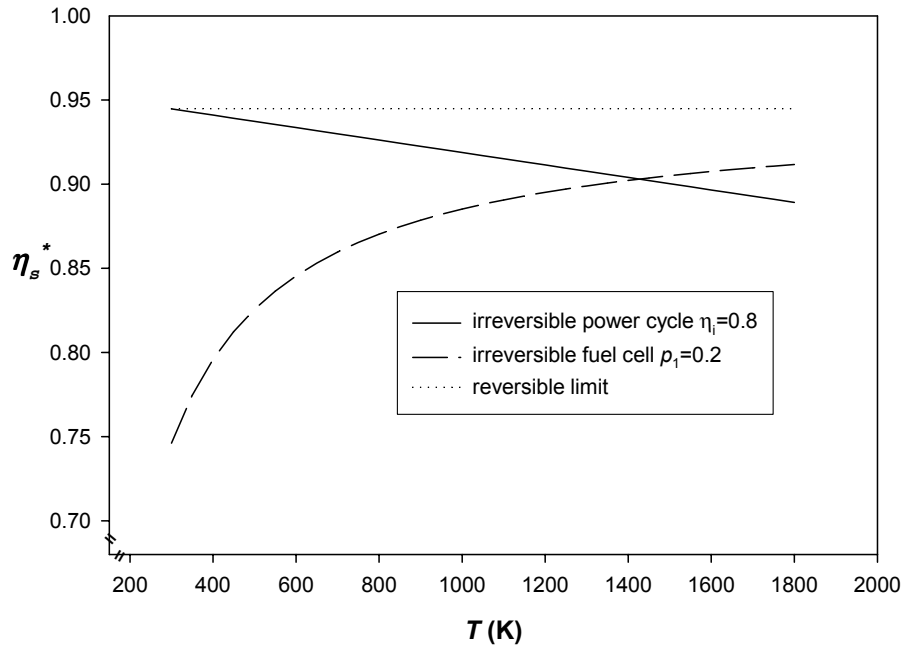


Figure 4.3. System efficiencies of fuel cell-power cycle combination with an irreversible fuel cell (solid) or irreversible power cycle (dashed), and the reversible limit (dotted).

As for the irreversibility of the fuel cell, for the purpose of these general calculations we can first assume that the reversible efficiency is lowered by a constant fraction p_1 ⁵⁾:

$$\eta_{fc}^* = 1 - \frac{T}{T_{\Delta G=0}} - p_1 \quad (4.18)$$

Combined with the reversible power cycle we find this expression for the total electrical efficiency

$$\eta_s^* = 1 - p_1 \frac{T_0}{T} - \frac{T_0}{T_{\Delta G=0}} \quad (4.19)$$

⁵⁾ In practice, this fraction is a constant exergy loss and by approximation, a temperature independent voltage drop caused by the cell's irreversibility. In the Simple Fuel Cell Model as introduced in paragraph 2.2.2 (see also reference [4]), this means a constant ri_{cell} .

As expected, the system efficiency increases with temperature due to the more efficient power cycle as shown by Figure 4.3. However, if both fuel cell and power cycle operate irreversibly than the combination of equation (4.11) and (4.18) yields:

$$\eta_s^{**} = 1 - p_1 - \frac{T}{T_{\Delta G=0}} + \eta_i \left(p_1 + \frac{T_0}{T_{\Delta G=0}} \right) \left(1 - \frac{T_0}{T} \right) \quad (4.20)$$

Here a true maximum can be found at a temperature T_{\max} of

$$T_{\max} = \sqrt{\frac{T_0 T_{\Delta G=0} p_1 \eta_i}{1 - \eta_i}} \quad (4.21)$$

The maximum efficiency is given by:

$$\eta_s^{**}(T_{\max}) = 1 - p_1 (1 - \eta_i) - \frac{\eta_i T_0}{T_{\Delta G=0}} - \frac{2(1 - \eta_i)}{T_{\Delta G=0}} \sqrt{\frac{p_1 T_0 T_{\Delta G=0} \eta_i}{1 - \eta_i}} \quad (4.22)$$

Here we use $\eta_i = 0.8$ and $p_1 = 0.2$ as an example and Figure 4.4 shows the efficiencies of the two separate systems as well as the combined systems together with their reversible limits. In this example T_{\max} is found at 1125 K and $\eta_s^{\max} = 0.833$. At the same temperature, both the stand alone fuel cell and power cycle are delivering power at an efficiency of 59 % and therefore the combination of fuel cell and power cycle are again performing significantly better than each of them separately. Furthermore, the maximum efficiency of this combination is very flat as shown by Figure 4.4. So, despite the fact that in principle there is an optimum temperature, we have the freedom to deviate from this optimum temperature for other, more practical reasons of necessary without having to sacrifice severely on efficiency.

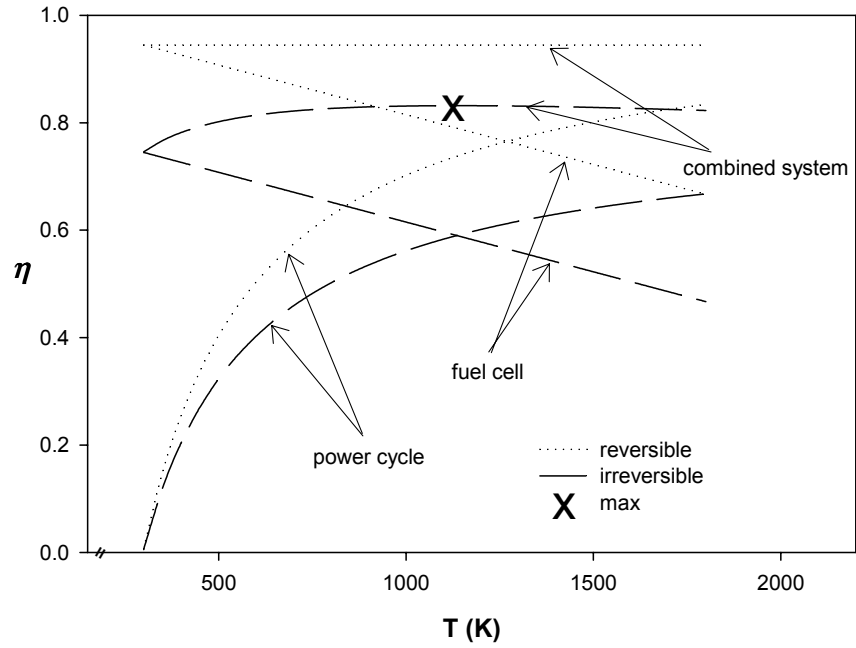


Figure 4.4. Efficiencies of fuel cell, power cycle and combined system operating reversibly and irreversibly.

It is interesting to see that the optimum temperature of this combination lies in the same range where MCFCs and SOFCs are presently operating, i.e. 900 to 1300 K. This is further illustrated by Figure 4.5 and Table 4.1. Only for very high fuel cell efficiency and low power cycle efficiency T_{max} is lower than the operating range of present high-temperature fuel cells. We now further refine this evaluation by introducing temperature-dependent relations for the irreversible losses of a MCFC that is found in practice.

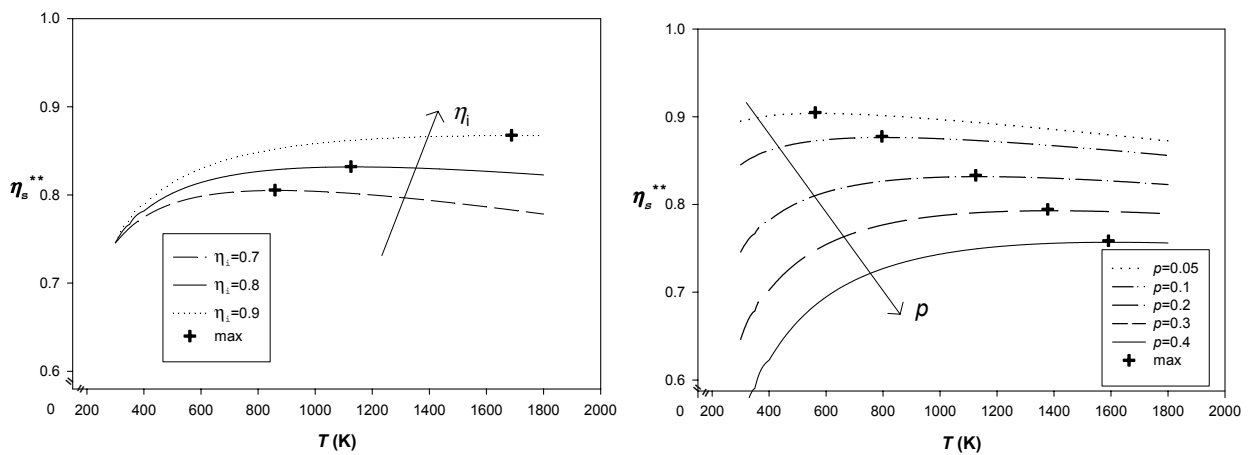


Figure 4.5. η_s^{**} as function of losses η_i and p_1 .

Table 4.1: Optimum temperature T_{\max} (in K) for several η_i and p_1 .

η_i	p_1 :	0.05	0.1	0.2	0.3	0.4
0.7		430	608	859	1052	1215
0.8		562	796	1125	1378	1591
0.9		844	1193	1688	2067	2387

4.4. MCFC system efficiency in practice

In the previous section, we have assumed a simple constant irreversible loss for the fuel cell. In practice, this loss consists of polarization losses caused by transport and reaction kinetics and these phenomena are highly temperature dependent. In this section, we will use current experimental data from state-of-the-art MCFC stacks in order to have a more realistic representation of the fuel cell system efficiency.

Additionally, in the first order analysis above we have assumed that both the Δh and Δs are temperature independent. In order to make the following analysis as complete as possible, we include the small temperature dependency of these thermodynamic quantities following the data in the *Handbook of Chemistry and Physics* [6]. The influence of Nernst loss is also incorporated.

4.4.1. MCFC in practice

The irreversible losses of the fuel cell are often assumed to increase linearly with the average current density [7,8]. The corresponding factor is therefore called the quasi-Ohmic resistance r , which consists of series of contributions by the anode, electrolyte and cathode, which are all assumed to behave Ohmically, i.e., independent of the current density. This is also used in the Simple Fuel Cell Model of Standaert (see paragraph 2.2.2 and reference [4]):

$$V_{cell}^{SM}(u_f, i) = V_{eq}^*(0) - \frac{1}{2}\alpha_f u_f - r i_{cell} \quad (4.23)$$

$$r = r_a + r_{\Omega} + r_c \quad (4.24)$$

In paragraph 2.5, it is shown that this is a fairly accurate way of describing the fuel cell's operating characteristics under a wide range of operating conditions. For the MCFC stack, CRIEPI⁶⁾ has recently published empirical relations for the quasi-ohmic resistance as function of a number of parameters [9,10]:

$$\begin{aligned}
 r_a &= C_a T \exp\left(\frac{\Delta h_a}{RT}\right) \frac{1}{\sqrt{p_{a,H_2}}} \\
 r_\Omega &= \frac{d}{d_b} C_\Omega \exp\left(\frac{\Delta h_\Omega}{RT}\right) \\
 r_c &= C_{c1} \exp\left(\frac{\Delta h_{c1}}{RT}\right) \frac{T \sqrt{p_{CO_2}}}{p_{c,O_2}^{0.75}} + \frac{C_{c2} \exp\left(\frac{\Delta h_{c2}}{RT}\right) T}{m_{c,CO_2} + C_{c3} \exp\left(\frac{\Delta h_{c3}}{RT}\right) m_{c,H_2O}}
 \end{aligned} \tag{4.25}$$

with the following fitting values:

Table 4.2: Values for the fitting parameters for the cell resistance [9,10]:

Parameter	Value
C_a	$9.50 \cdot 10^{-7} \text{ } \Omega\text{cm}^2$
C_{c1}	$6.91 \cdot 10^{-15} \text{ } \Omega\text{cm}^2$
C_{c2}	$3.75 \cdot 10^{-9} \text{ } \Omega\text{cm}^2$
C_{c3}	$1.07 \cdot 10^{-6} \text{ } \Omega\text{cm}^2$
C_Ω	$9.48 \cdot 10^{-3} \text{ } \Omega\text{cm}^2$
Δh_a	27.9 kJ/mol
Δh_{c1}	179.2 kJ/mol
Δh_{c2}	67.2 kJ/mol
Δh_{c3}	95.2 kJ/mol
Δh_Ω	23.8 kJ/mol
d_b	0.916 mm

Most importantly here, these relations give the irreversible losses of the MCFC as function of temperature. Figure 4.6 shows the three contributions and the overall quasi-Ohmic-resistance as function of temperature within the practical limits of 600 to 700°C. It shows that in this temperature range the overall quasi-Ohmic resistance r of the MCFC decreases

⁶⁾ Central Research Institute of Electric Power Industry, Japan

rapidly with temperature, and that the temperature behavior of r is dominated by the cathode.

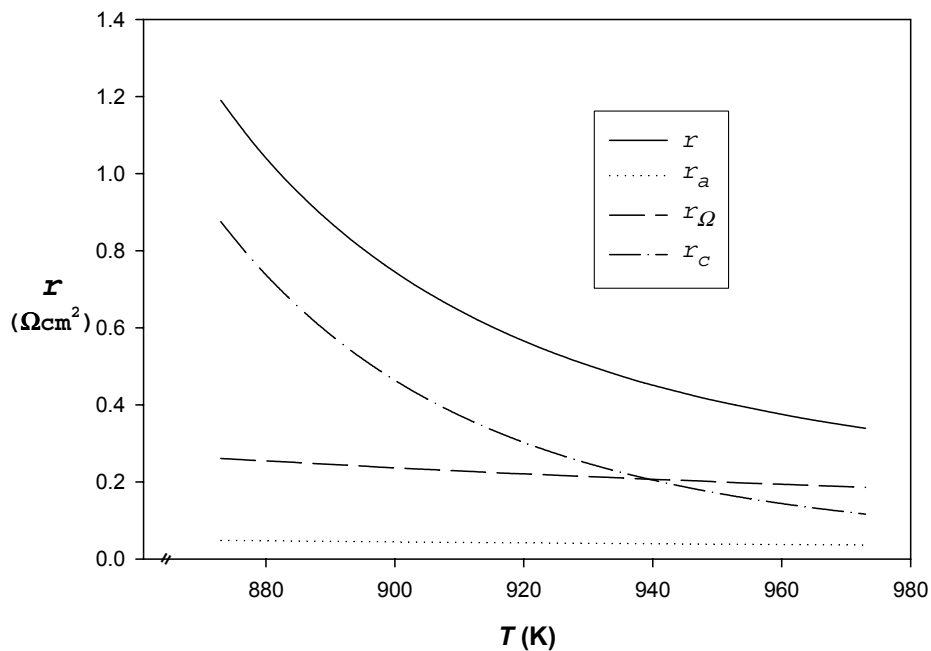


Figure 4.6. MCFC quasi-ohmic resistances as function of temperature with standard testing gas.

For the following analysis, we use as the gas compositions the commonly used standard testing gas. Furthermore, the fuel utilization and current density are set to the values commonly used for benchmarking. The exact numbers are given by Table 4.3.

Table 4.3: Used gas composition and operating condition

p_{a,H_2}	0.64
p_{a,H_2O}	0.20
p_{c,O_2}	0.14
p_{a,CO_2}	0.16
p_{c,CO_2}	0.30
u_f	0.80
i_{cell}	150 mA/cm ²

Figure 4.7 shows the distribution of power and heat of a stand-alone MCFC operating under standard testing gas and load. The irreversible losses decrease as the temperature

risers, but still large part of the energy is released as reversible heat (i.e., $T\Delta S$ reversible heat and Nernst loss). The electrical efficiency of the fuel cell is low, even here when neglecting power consumption by auxiliary devices. We clearly see that the stand-alone MCFC fed with hydrogen suffers strongly from the inevitable laws of thermodynamics in the sense that a lot of (reversible) heat is inevitably produced.

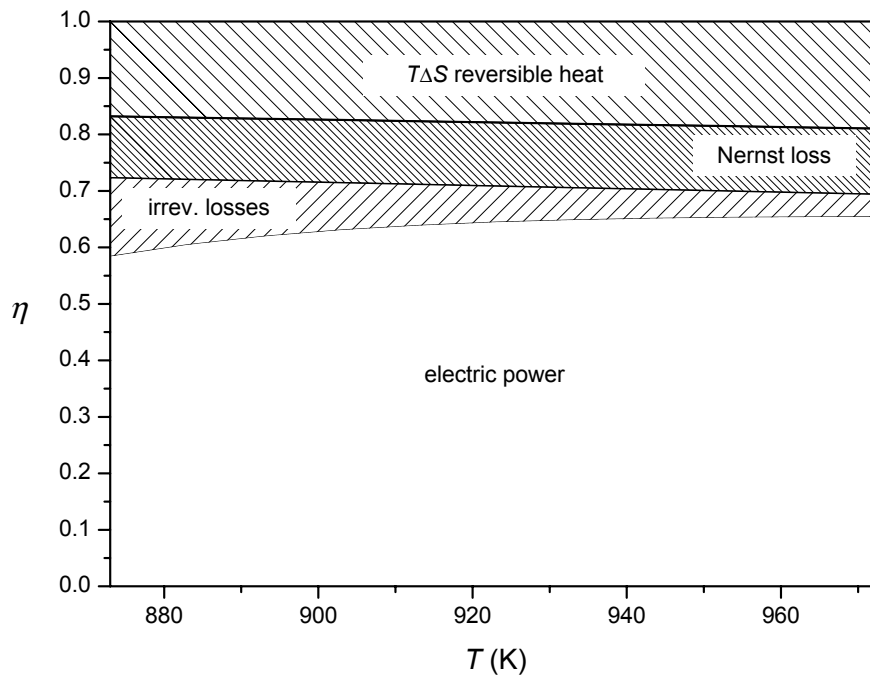


Figure 4.7. Heat and power distribution of an MCFC in practical situation.

4.4.2. MCFC in practice combined with a bottoming power cycle

To complete this evaluation, a bottoming power cycle is incorporated to the MCFC. Note here that the empirical relations for the quasi-Ohmic resistances are determined from measurements performed at temperatures between 873 K and 973 K, and therefore these relations are only valid in this region. Nevertheless, for the evaluation of system efficiency we extrapolate these equations of irreversible losses beyond the temperature range of the measurements. As for the irreversible loss for the power cycle, we have the difficulty of not knowing the exact value for the intrinsic efficiency. This efficiency is not only temperature and size depended but it is also determined by economics since it's often possible to increase the power cycle efficiency at the expense of higher costs. To overcome all the inadequacies, we have considered the η_i again as a temperature independent variable

and calculate the overall conversion efficiency of the combined system for various values for η_i starting from 0.7 for the worst case until 1 for a reversible power cycle. Figure 4.8 shows the results of these calculations.

It's clear that the exponential increase of the irreversibility of the MCFC for low temperature causes the system efficiency to collapse for temperatures below about 900 K. With $\eta_i = 0$, the system efficiency reduces to the stand-alone efficiency of the MCFC indicated by the solid line (see Figure 4.8). For a typical intrinsic efficiency η_i between about 0.7 and 0.9, the total combined system efficiency is again fairly constant similar to the results we had with the simple temperature independent losses. The combined fuel cell and power cycle system is therefore in general very flexible in its operating temperature. Obviously, the total system efficiency increases with increasing bottoming cycle efficiency. In practice, the flexibility in operating temperature means that we can match the operating temperature for both endurance of the MCFC and the efficiency of the bottoming cycle.

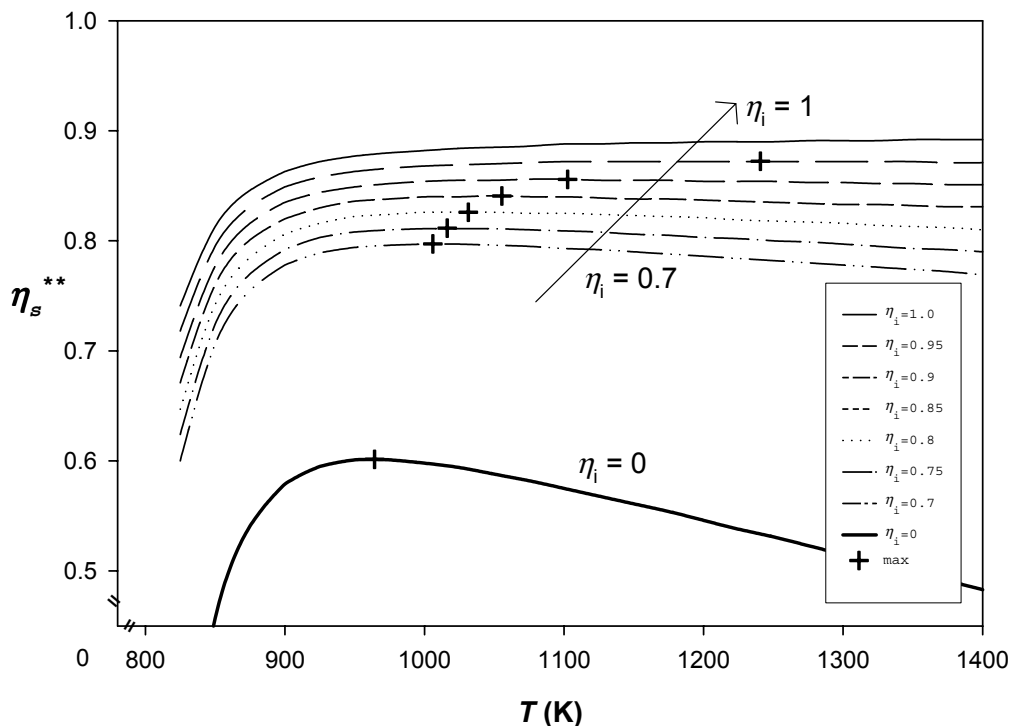


Figure 4.8. Efficiencies of combined systems under realistic conditions.

4.5. Conclusions

The hydrogen-based high-temperature fuel cell technology is becoming even more interesting when it is combined with a recovery power cycle. The laws of thermodynamics impose this since otherwise part of energy is released as heat and this is not favorable for the conversion efficiency when electricity is desired. The choice of operating temperature of the fuel cell is of minor importance. This is shown generally by using simple assumptions for irreversibility. Further refinement of the complex temperature behavior of irreversibility of the MCFC does not change this general conclusion. In practice, it means that fuel cell system designers have the freedom to choose the operation temperature to meet other important requirements. Especially the endurance of the fuel cell is essential in reducing costs. What remains is that the total conversion efficiency can be improved by optimizing the efficiency of the recovery power cycle. This means that fuel cell and thermal power technologies should cooperate closely in order to make a big step ahead in the energy conversion technology.

References

- [1] A.J. Appleby, *Fuel Cell Systems*, p. 157, L.J.M. Blomen, M. N. Mugerwa, Editors, Prentice Hall, (1993)
- [2] Abstract 2000 Fuel Cell Seminar, Portland, Oregon, (USA), (2000)
- [3] F. Standaert, K. Hemmes and N. Woudstra, *Nernst Loss and Multistage Oxidation in Fuel Cells*, p. 92, 1998 Fuel Cell Seminar Abstracts, Palm Springs, California, (USA), (1998).
- [4] F. Standaert, K. Hemmes, N. Woudstra, *Analytical fuel cell modeling*, J. Power Sources, **63**, p.221-234, Elsevier (1996).
- [5] J.R. Selman, *Fuel Cell Systems*, p. 345, L.J.M. Blomen, M. N. Mugerwa, Editors, Prentice Hall, (1993)
- [6] R. David, *Handbook of Chemistry and Physics*, 72nd edition, CRC Press, (1992).
- [7] L.A.H. Machielsen, in *Modeling of Batteries and Fuel Cells*, R.E. White, M.W. Verbrugge, J.F. Stockel, Editors, **PV 91-10**, p. 166, The Electrochemical Society Proceedings Series, Pennington, NJ (1991).
- [8] K. Hemmes, F. Standaert, N. Woudstra and J.H.W. de Wit, *Fundamentals*

of Fuel Cells and Fuel Cells Modeling, Proceedings of the 2nd IFCC, Kobe, (JP) (1996).

- [9] F. Yoshiba, N. Ono, Y. Izaki, T. Watanabe and T. Abe, *Numerical analyses of the internal condition of a molten carbonate fuel cell stack: comparison of stack performances for various gas flow types*, p328-336, *Journal of Power Sources* **71**. (1998).
- [10] Y. Mugikura, H. Morita, M. Yoshikawa and T. Watanabe, *Modification of cathode performance equation and reaction mechanism of MCFC*, Proceeding of the 7th FCDIC Fuel Cell Symposium, Tokyo (JP) (2000).

Chapter 5: MCFC system optimization (part II)

Influence of cell temperature on the efficiency of a MCFC CHP plant

This chapter is submitted for publication to the Journal of Power Sources as: THE INFLUENCE OF OPERATING TEMPERATURE ON THE EFFICIENCY OF A COMBINED HEAT AND POWER FUEL CELL PLANT, by S.F. Au, S.J. McPhail, N. Woudstra, and K. Hemmes, (2002).

Abstract

It is generally accepted that the ideal operating temperature of a Molten Carbonate Fuel Cell (MCFC) is 650 °C. Nevertheless, when waste heat utilization in the form of an expander and steam production cycle is introduced in the system, different temperature level might prove more productive. This chapter presents a first attempt to optimize the MCFC operating temperatures of a practical MCFC system by presenting a case study in which the efficiency of a combined-heat-and-power (CHP) plant is analyzed. The fuel cell plant under investigation is designed around a 250 kW-class MCFC fuelled by natural gas, which is externally reformed by a Heat Exchange Reformer (HER). The operating temperature of the MCFC is varied over a temperature range between 600 and 700 °C while keeping the rest of the system the same as far as possible. Changes in energetic efficiency are given and the causes of these changes are further analyzed. Furthermore, the exergetic efficiencies of the system and the distribution of exergy losses in the system are given. Flowsheet calculations show that there is little dependency on the temperature in the first order. Both the net electrical performance and the overall exergetic performance show a maximum at approximately 675 °C, with an electrical efficiency of 51.9 % (LHV), and an overall exergy efficiency of 58.7 %. The overall thermal efficiency of this CHP plant

increases from 87.1 % at 600 °C to 88.9 % at 700 °C. Overall, the change in performance in this typical range of MCFC operating temperatures is small.

5.1. Introduction

Fuel cells play an important role in the continuing effort to increase the efficiency of electricity production and to reduce atmospheric pollution. High net power efficiency can be achieved thanks to the principle of direct conversion of chemical energy to electrical energy, and thereby avoiding the extra steps of combustion, heat transfer, expansion and generation as in a conventional plant. Furthermore, when high-temperature cells like the Molten Carbonate Fuel Cell (MCFC) are used, additional increase in the overall efficiency can be obtained by proficient residual heat utilization. Then, in order for the total efficiency to be as high as possible, it is possible that the ideal fuel cell operating conditions will not coincide with the optimal total system performance.

It is generally accepted that the ideal operating temperature of an MCFC is 650 °C. For current state-of-the-art fuel cells, this temperature is the best compromise between performance and endurance [1-3]. Optimization studies of MCFC system efficiencies are therefore done in the fields of cell and stack configurations [4-6] and system configurations [7,8]. However, when waste heat utilization in the form of an expander and steam generation is introduced into the system, another temperature level might prove to be more productive.

In Chapter 4, we have performed a theoretical study to the efficiencies of fuel cell systems using simple assumptions for the irreversible losses (see references [9, 10]). The results were obtained by assuming temperature-independent losses for the recovery of the exergy of the residual heat. In practice, the efficiency of waste heat recovery depends on the temperature of the system. Furthermore, the interactions between the fuel cell stack, auxiliary equipments and waste heat recovery system were previously neglected. Here, we present detailed flowsheet calculations of a typical external reformed MCFC combined-heat-and-power plant (CHP) with which we investigate the influence of the fuel cell operating temperature on the system performance. This system has been modeled and implemented in the program Cycle-Tempo [11], which Delft University has developed for flowsheet calculations. The effects of varying the cell temperature upon various system

aspects have been investigated, and based on these results, the optimal operating temperature for maximum efficiency will be presented.

5.2. System configuration

The system selected for this study is similar to a system-design considered for a 250 kW natural gas MCFC-system as jointly defined in the past by the Delft University of Technology and ECN (Netherlands Energy Research Foundation) [12]. It has the following main features:

- 250 kW class combined-heat-and-power system
- natural gas as primary fuel
- fuel gas is externally reformed
- pressurized system operating at 4 bar

The initially proposed system has an intricate connection between the anode cycle and the cathode cycle (via the pre-heating stages and mixing). This connection is here removed mainly as regards to stability, constructive simplicity and controllability. Separating the two flows should bring about a better system. Figure 5.1 shows the flowsheet of the modified system that is taken directly¹⁾ from the flowsheeting program. The system layout shows that apart from the fuel cell we can distinguish five subsystems. Next, the fuel cell and the subsystems will be introduced by explaining their functions. Furthermore, the input data used for the different components will be presented. These inputs characterize performances of state-of-the-art equipments.

¹⁾ Components that are needed solely for starting values of mathematical iterations are removed here.

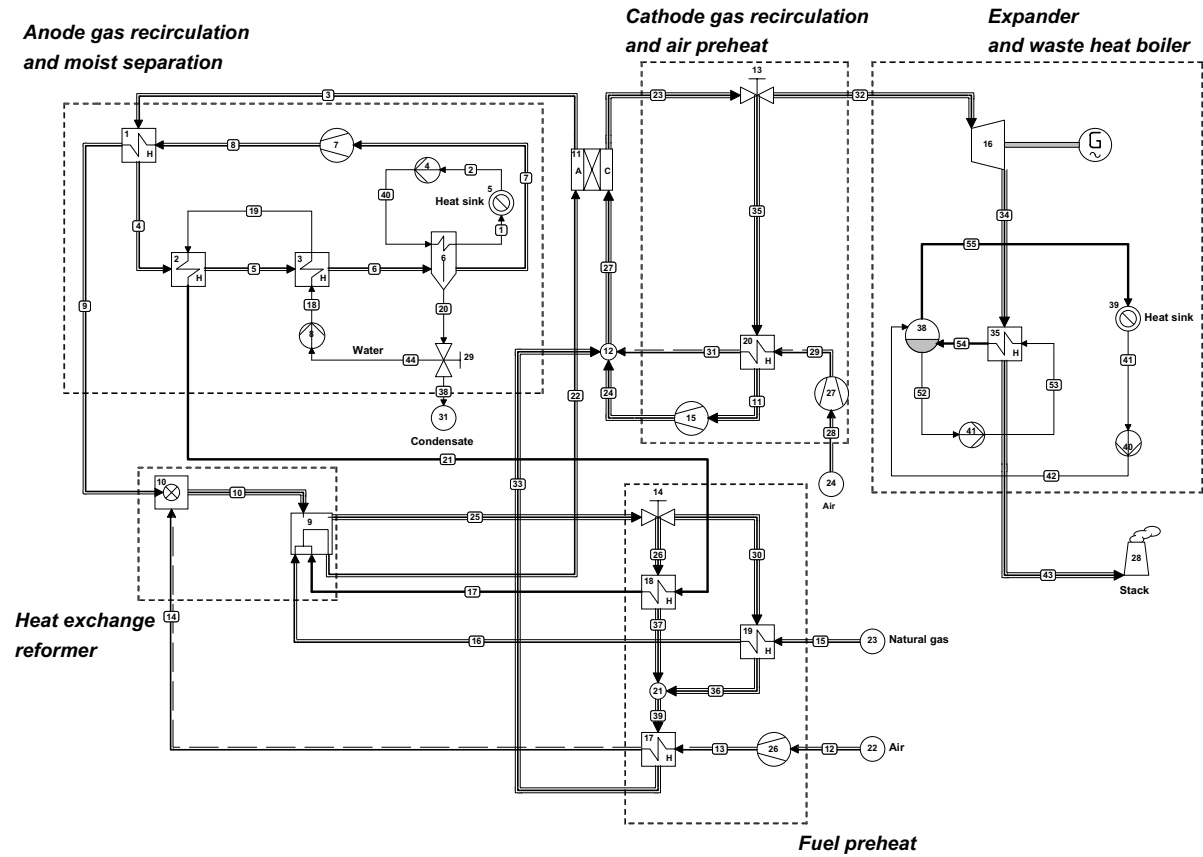


Figure 5.1. Flowsheet of the 250kW-class MCFC CHP plant.

5.2.1. Fuel Cell

A unique feature of the fuel cell model in the flowsheeting program is its capability of calculating design and off-design performances by using the quasi-Ohmic resistance r of the cell as performance specification. In Chapter 3, a description of this model is given and the accuracy of the model is checked by comparing the calculated cell performance with experimental results. We have found an average relative discrepancy of 0.5 % over a wide range of operating conditions, and a maximum discrepancy of 3 % at full load (see Paragraph 3.4). Hence, it can safely be assumed that the model is correct and its accuracy is sufficient to be used for flowsheeting purposes. This fuel cell model enables the use of empirical relations for the temperature dependency of the internal resistance measured by CRIEPI²⁾ (see references [6, 14]). They obtained the following empiric relations for the

²⁾ Central Research Institute of Electric Power Industry (Japan)

internal resistances r , which can be separated in an anode contribution r_a , an electrolyte resistance r_Ω and a cathode contribution r_c

$$r = r_a + r_\Omega + r_c \quad (4.24)$$

with

$$\begin{aligned} r_a &= C_a T \exp\left(\frac{\Delta h_a}{RT}\right) \frac{1}{\sqrt{p_{a,H_2}}} \\ r_\Omega &= \frac{d}{d_b} C_\Omega \exp\left(\frac{\Delta h_\Omega}{RT}\right) \\ r_c &= C_{c1} \exp\left(\frac{\Delta h_{c1}}{RT}\right) \frac{T \sqrt{p_{CO_2}}}{p_{c,O_2}^{0.75}} + \frac{C_{c2} \exp\left(\frac{\Delta h_{c2}}{RT}\right) T}{m_{c,CO_2} + C_{c3} \exp\left(\frac{\Delta h_{c3}}{RT}\right) m_{c,H_2O}} \end{aligned} \quad (4.25)$$

The symbols C_i and Δh_i represent fitting parameters and activation enthalpies respectively. d_b is the normalization parameter for the electrolyte matrix thickness with the thickness $d = 0.916$ mm. The fitting parameters and activation enthalpy are obtained by fitting the above empirical relations to experimental measurements performed in a temperature range of 600 – 700 °C, and in a pressure range of 1 to 5 bar. The resulting values are given in Table 4.2 in paragraph 4.4.1.

The empirical relations are used to calculate the quasi-ohmic resistance as function of cell temperature, pressure and average gas composition (by means of average partial pressures p_i and mol fractions m_i). The overall quasi-Ohmic resistance r determines the irreversible losses and thus the performance of the cell. Note that the symbols p and T are here used for partial pressure [bar] and absolute temperature [K] respectively.

In this study, both the cell area A_{cell} and the current density i_{cell} are kept constant and they are given in Table 5.1. The power delivered by the fuel cell is a function of the quasi-Ohmic resistance, fuel utilization and gas inlet compositions³⁾. Losses due to the DC to AC conversion are introduced by the inverter efficiency η_{DC-AC} . Fuel utilization is fixed at 70

³⁾See paragraph 2.2.1 for more details on fuel cell modeling.

%, which is 5 % lower than described in reference [12]. The reason for the lower fuel utilization lays solely on the separation of anode and cathode cycles. Due to this separation, extra enthalpy is required to heat the fuel, and to provide enough heat for the heat exchange reformer (HER) without subtracting this from the cathode cycle. By reducing the fuel utilization, the fuel input has increased and more heat is available from the anode off-gas. Friction losses are introduced by imposing pressure drops of 0.05 and 0.1 bar for the anode and cathode respectively. Co-flow design is assumed and the temperature difference between the inlets and the outlets of both anode and cathode are set at 100 K.

The system is implemented in such a way that the fuel cell is the dominant apparatus and that both fuel and air consumptions are mainly⁴⁾ determined by it. Fuel consumption is determined by i_{cell} , A_{cell} and u_f . The cathode mass flow, and the related air consumption, is determined by the heat to be discharged from the fuel cell.

5.2.2. Anode gas recirculation and Moisture Separation

Fuel that is not converted by the fuel cell is combusted in the reformer (HER). However, the anode off-gas contains large amount of moisture that will adversely influence the performance of the HER. The anode off-gas is therefore cooled in several stages to separate most of the moisture. The transferred heat is used for heating up and evaporating water that is needed for the reforming reaction. Heat released in the moisture separator is utilized by external consumers (e.g. a district heating system) represented here by a heat sink. The moisture separator produces hot water at 80 °C. After utilization, this water is cooled to a temperature of 60 °C and is recirculated back to the moisture separator. The anode off-gas is circulated by a blower, reheated and transferred to the HER. This dried anode recycle gas leaves the anode gas recirculation and moisture separation subsystem at a fixed temperature of 460 °C in order to keep the inlet temperature of the heat exchange reformer constant throughout this study.

The efficiency of the heat transfer processes depends strongly on the choice of flow configuration and the final temperature differences between primary and secondary flows.

⁴⁾ The other consumer of air is the combustion chamber of the heat exchange reformer. This amount of air is relatively small.

Here, all heat exchangers are operated in counter flow mode. Only the low-end temperature difference (ΔT_{low}) of the steam evaporator (app. #2) is fixed at 20 K. Others temperatures are calculated using the fixed inlet temperature of the HER and the boiling temperature of water at the exchanger's outlet.

5.2.3. Heat Exchange Reformer and Fuel Preheat

The Heat Exchange Reformer (HER) is modeled here by a combustion chamber and a steam-reforming reactor. The combustion chamber is fuelled by the dried anode off-gas and the air factor λ of combustion is set at 1.1⁵⁾ with which flue-gas at a temperature of over 1250 °C is obtained. The heat that can be supplied from the flue-gas is sufficient for the reforming reaction (apparatus 9, Figure 5.1), superheating steam (apparatus 18) and pre-heating fuel (apparatus 19). The remaining heat is used for heating air (apparatus 17) that is supplied to the combustion chamber (apparatus 10). The temperature of the air leaving the heat exchanger is set at 440 °C and the temperature of both natural gas and steam that enter the HER are set at 480 °C. The natural gas heater (apparatus 19) and the steam heater (apparatus 18) are placed here in parallel since in practice both heat exchangers are combined in a single unit.

After passing the air preheater (apparatus 17), the CO₂ rich flue-gas is mixed with the recycled cathode gas and preheated fresh air to provide the MCFC cathode with O₂ and CO₂.

The reforming reaction is modeled by assuming chemical equilibrium at 800 °C and 4 bar. The ratio of steam to fuel is set to 2.59 kg/kg. Friction losses are introduced in the reformer by imposing pressure drops of 0.5 bar and 0.25 bar for the primary process flow (the product gas flow) and the secondary heat exchange flow (the flue-gas flow) respectively. Other friction losses are introduced by pressure drops of 0.05 bar for both primary and secondary sides of the fuel preheating line. The isentropic efficiency of the air compressor is assumed at 0.72.

⁵⁾ This means 10% more air than needed for stoichiometric combustion.

5.2.4. Cathode gas recirculation

The cathode gas not only provides O₂ and CO₂ for the electrochemical reaction, it also serves as the main coolant for the fuel cell, and therefore the mass flow of the cathode gas has to meet the cooling requirements. This mass flow of air necessary for cooling is far greater than required for the cathode reaction. Part of this air is recirculated and the amount of recirculation is set accordingly to assure the fixed cathode inlet temperature after mixing this recirculation flow with fresh air and flue-gas from the HER. Before mixing, this recycle flow is partly cooled by preheating the pressurized fresh air. The flue-gas from the HER is the main source of CO₂ required for the cathode reaction. In all considered situations, the concentration of CO₂ at the cathode inlet exceeds the commonly assumed minimum of 8 mol%.

5.2.5. Expander and Waste Heat Boiler

The hot pressurized gas that leaves the cathode recycle loop produces electricity through an expander attached to a generator. Losses are introduced by defining the isentropic efficiency η_i for the expander ($\eta_i = 75\%$) and conversion efficiency η for the electrical generator ($\eta = 95\%$). After expansion, the temperature of the flue-gas is sufficiently high to produce saturated steam. The pressure and temperature of this steam is set at 10 bar and about 180 °C. This steam can be applied for industrial heating purposes and the utilization of this heat is represented here by a heat sink. The returning condensate from this sink is used to feed the boiler. Finally, the residual flue-gas is discharged to the environment through a flue-gas stack.

5.3. Input Data and Calculations

The system performance strongly depends on the input data. In particular the isentropic efficiencies of rotating equipment, pressure drops and pinch points of heat exchangers determine the irreversible losses of the system and therefore also the calculated overall efficiency. For this study, we have used a combination of input data that characterize state-of-the-art equipments. Table 5.1 gives a summary of the main input parameters for the equipments in the system.

Table 5.1: Input parameters of the system.

Fuel Cell	
A_{cell}	250 m ²
i_{cell}	1500 A/m ²
u_f	70 %
η_{DC-AC}	96 %
p	4 bar
Δp_{anode}	0.05 bar
$\Delta p_{cathode}$	0.1 bar
$T_{out}-T_{in}$	100 °C
Anode gas recirculation and moisture separation.	
T_{out} anode recirculation gas	460 °C
$T_{hot\ water}$	80 °C
$T_{utilization}$	20 °C
ΔT_{low} Evaporator	20 °C
Δp Heat Exchangers	0.05 – 0.10 bar
Δp Moist Separator	primary side 0.15 bar; secondary side 0.1 bar
η_i for pump	0.70
η_i for blower	0.72
Heat Exchange Reformer and fuel preheat.	
λ (air factor) combustor	1.1
Steam to Fuel ratio reformer	2.59
T_{react} reformer	800 °C
p_{react} reformer	4 bar
Δp reformer	primary side 0.5 bar; secondary side 0.25 bar
T_{out} reformer	according to cell inlet temperature
Δp heat exchangers	0.05 bar for both primary and secondary sides
T_{feed} reformer	480 °C
T_{air} combustor	440 °C
η_i compressor	0.72
Cathode gas recirculation	
Δp heat exchanger	0.05 bar for both primary and secondary sides
η_i compressor	0.72
Expander and Waste Heat Boiler	
ΔT_{low} Evaporator	20 °C
Δp heat exchanger	primary side 0.1 bar; secondary side 0.01 bar
Δp utilization	0.2 bar
η_i expander	0.75
η generator	0.95
η_i pumps	0.75

The energy input to the system is determined by the size of the fuel cell, anode gas composition and fuel utilization. Since these parameters are fixed for all calculations, the energy input of the system is constant, and in all cases the energy input is 557.57 kW, based on the lower heating value (LHV), and exergy input is 580.82 kW, based on $T_0 = 25$ °C. The source for the energy and exergy input is natural gas, which is of Dutch “Slochteren” quality, with as main components about 81 mole% CH₄ and 14 mole% N₂, and with a LHV of 708.22 kJ/mol. Other mass input of this plant is air which is defined according to the ISO standard. The exact compositions used for both natural gas and air can be found in the handbook of the program (reference [11]).

The fuel cell system is analyzed at five different cell operating temperatures (600, 625, 650, 675 and 700 °C). Using 650 °C as a reference, the operating temperature of the fuel cell is adjusted by changing the cell temperature and the quasi-ohmic resistance of the cell together with the change in the cathode gas recirculation percentage. Any change in the fuel cell temperature influences the quasi-ohmic resistance, which in turn influences both cathode gas flow and the amount of the cathode gas recirculation. Consequently, the recirculation influences the cathode gas composition, which determines the quasi-ohmic resistance. All these parameters are therefore closely related and several manually controlled iterations are needed in order to find the solution for each temperature.

5.4. Results and Discussions

Starting with the overall results, Figure 5.2 shows the overall thermal system efficiency ($\eta_{\text{total LHV}}$) and output distribution based on the energy input. Note that the surfaces in this scale do not represent the ratio of power over heat correctly since we adapted the scale to emphasize different results. The numerical values are also summarized in Table 5.2. Here, we should note that all numbers in the tables are given in at least two digits behind the decimal point, suggesting a high level of precision in our computer simulations. On the other hand, we have used several estimated input values for the performance of heat exchangers and rotating equipments, and consequently the absolute precision in the calculated efficiencies has no practical value. Nevertheless, these numbers are not rounded off in further extend since otherwise the difference in the calculated results will not become apparent. Since all calculations are based on the same system using the same system inputs, the qualitative result remains unaffected by the estimated inputs.

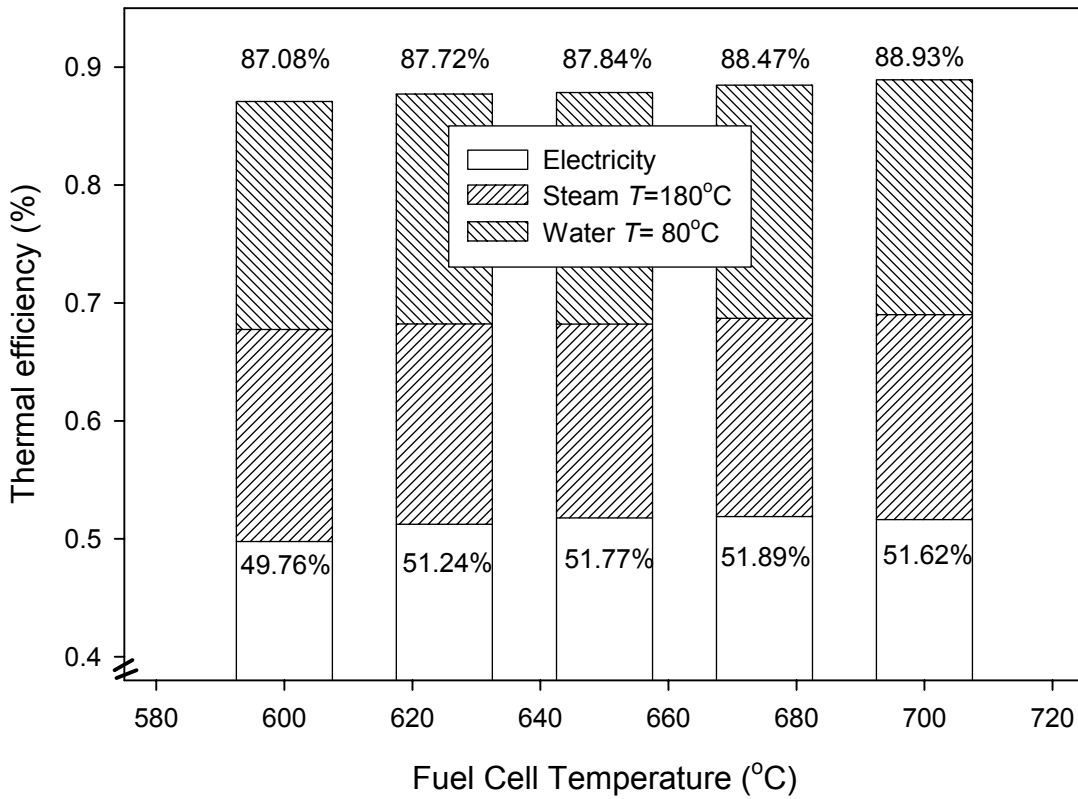


Figure 5.2. Energetic efficiency and distribution as function of temperature.

First, we see that the electrical efficiency ($\eta_{\text{net LHV}}$) of the system increases with operating temperature and reaches a maximum at 675 °C. The difference between the maximum and minimum efficiency is about 2.1 % point. Second, the overall efficiency (i.e. heat and power) increases with operating temperature as well but doesn't reach a peak value in the temperature range investigated. In this range, the difference between the maximum and minimum efficiency is here about 1.9 % point percent. Finally, Table 5.2 shows that the auxiliary power consumption P_{aux} decreases with operating temperature from about 25 % of the gross power production at 600 °C to about 20 % at 700 °C. The auxiliary power is mainly used by the compressor for compressing fresh air for the cathode, and the amount of fresh air is reduced with increasing cell temperature. The rest of the auxiliary power is mainly used by the compressor for air to feed the HER and by the two recycle blowers.

Table 5.2: Summary of energy output.

T_{cell}	600 °C	625 °C	650 °C	675 °C	700 °C
P_{FC} (kW)	297.54	304.20	306.19	305.95	303.86
P_{expander} (kW)	73.86	65.60	60.05	58.64	58.20
$P_{\text{aux.}}$ (kW)	-93.98	-84.08	-77.58	-75.28	-74.22
P_{net} (kW)	277.42	285.72	288.66	289.32	287.84
$(\eta_{\text{net LHV}})$	(49.76 %)	(51.24 %)	(51.77 %)	(51.89 %)	(51.62 %)
P_{steam} (kW)	100.24	94.67	91.59	93.69	96.93
P_{water} (kW)	107.86	108.68	109.49	110.28	111.06
P_{heat} (kW)	208.09	203.35	201.08	203.97	207.99
$(\eta_{\text{heat LHV}})$	(37.32 %)	(36.47 %)	(36.06 %)	(36.58 %)	(37.30 %)
P_{total} (kW)	485.52	489.07	489.74	493.29	495.82
$(\eta_{\text{total LHV}})$	(87.08 %)	(87.72 %)	(87.84 %)	(88.47 %)	(88.93 %)

Next, the causes of the changes in fuel cell power output are discussed in more detail. Figure 5.3 shows the cell resistance and the net power delivered by the fuel cell stack. As expected, the irreversible losses given by the cell resistance decrease with increasing cell temperature. The result is an increase in stack performance and thus an increase in power delivered. On the other hand, the reversible open cell voltage (OCV) given by the Nernst equation decreases linearly with increasing temperature, as described in detail in the previous chapter. The opposite temperature behavior of irreversible losses and OCV result here in a maximum in fuel cell stack power output at $T_{\text{cell}} = 650$ °C. The theoretical study of the previous chapter did not show a maximum in cell performance in this typical range of operating temperature. There, we used a constant gas composition while in this present study the cathode gas composition is mainly determined by the cooling requirement of the stack and by the heat requirement of the cathode gas recirculation subsystem. Therefore, the exact cathode gas composition is here a function of operating temperature and this gas composition influences both the cell resistance as well as the OCV. The difference between the optimum in stack performance of our present results and our previous theoretical result can be attributed to the differences in cathode gas composition.

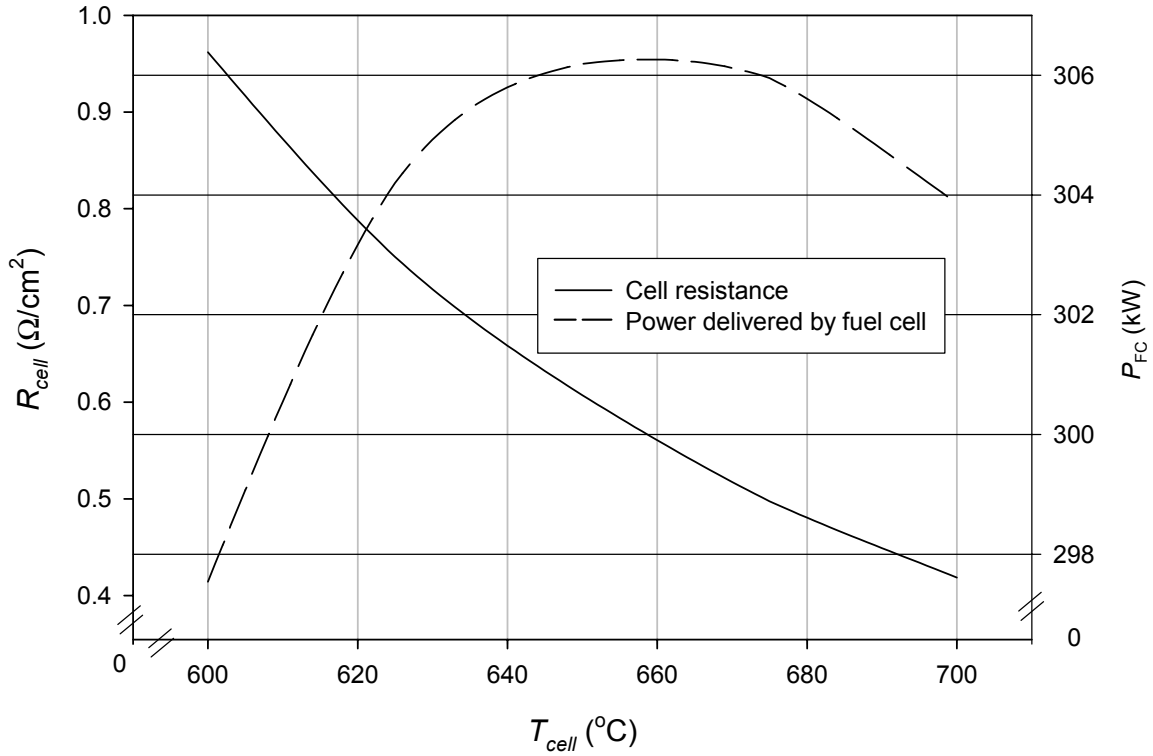


Figure 5.3. Cell resistance and power delivered as function of cell temperature.

The flowsheet calculations show that the overall system has an optimum operating temperature different from the fuel cell stack. This is caused by the net expander output P_{expander} and auxiliary power consumption P_{aux} . We have analyzed this by examining the cell resistance and cathode recirculation data, both given in Table 5.3.

Table 5.3: Summary of quasi-Ohmic resistances and cathode recirculation data.

T_{cell}	600 °C	625 °C	650 °C	675 °C	700 °C
r ($\Omega \text{ cm}^2$)	0.9619	0.7501	0.6072	0.4976	0.4187
%recirculation	72.83	75.02	77.09	78.00	78.84
Φ_{cathode} (kg/s)	1.383	1.304	1.267	1.256	1.262
Φ_{expander} (kg/s)	0.344	0.297	0.264	0.251	0.243

First, we note that the difference in net performance ($\eta_{\text{net LHV}}$), in particular between 650 °C and 700 °C, is very small (a difference of only 0.27 %, see Table 5.1). This result is in accordance with our observation for the whole system as considered in the theoretical study (Chapter 4). First, at low temperature, the net performance is adversely affected by

the high irreversible losses, while it remains constant at high operating temperature. Second, high electrical output by the fuel cell should result in low heat release and consequently little cooling is required. From 600 °C to 650 °C, Table 5.3 shows a decreasing Φ_{cathode} , which is a direct result of the increasing P_{FC} . It's however interesting to note that although the electrical output P_{FC} is highest at 650 °C, the cathode mass flow Φ_{cathode} and cooling requirement is lowest at 675 °C. This seems to contradict what is expected from theory. The cause of this contradiction can be ascribed to the difference in gas composition in the anode outlet caused by the difference in equilibrium of the hydrogen-shift reaction. At 650 °C the average enthalpy of the anode outlet is 33.31 kJ/mol (LHV) while at 675 °C it is 33.42 kJ/mol (LHV). Since the anode mass flow is constant for all calculations, the enthalpy release by anode outlet is slightly higher 675 °C. The higher enthalpy release reduces the cooling requirement of the fuel cell and hence lower cathode mass flow. The difference in cathode mass flow turns the optimum temperature for the system to 675 °C from the optimum temperature of 650 °C for the stack. Finally, this study also shows that operating at elevated temperature requires increase in cathode recycling due to the higher inlet temperature of the fuel cell. This is shown in Table 5.3 where the recirculation percentage of the cathode gas $\%_{\text{recirculation}}$, cathode massflow Φ_{cathode} and expander massflow Φ_{expander} are given. The increase in $\%_{\text{recirculation}}$ reduces expander power output and the overall auxiliary power consumption. The latter is due to the lower air input and less work required for the compression of air.

Table 5.2 gives the overall results and it lists the amount of useful heat produced by the system that is consumed by external users. The production of hot water at 80 °C increases monotone with operating temperature while the steam production at 180 °C shows a minimum at 650 °C. The change of the latter dominates the overall heat production resulting in a minimum total heat production (P_{heat}) of 201.08 kW at 650 °C. The overall efficiency η_{total} (i.e. combined electricity and heat) increases monotone with operating temperature. We should note that the main purpose of the fuel cell plant is the production of electricity while the production of heat is of minor importance. This is more apparent when we evaluate this system based on exergy. Figure 5.4 shows the exergy efficiency and exergy output distribution of the system (note the scale of this figure). The numerical values are summarized in Table 5.4. It's clear that the exergy represented by the heat production is relatively small. Based on exergy, the system efficiency η_{Ex} shows a

maximum at 675 °C. The difference in overall exergy efficiency between the highest and lowest value is here 1.7 %. Again, the change in exergy efficiency in the temperature range within 650 °C and 700 °C is small.

Table 5.4: Summary of exergy output (with $T_0 = 25^\circ\text{C}$).

T_{cell}	600 °C	625 °C	650 °C	675 °C	700 °C
Ex_{net} (kW)	277.42	285.72	288.66	289.32	287.84
Ex_{steam} (kW)	36.48	34.46	33.34	34.10	35.28
Ex_{water} (kW)	17.27	17.41	17.54	17.66	17.79
η_{Ex} (%)	57.02	58.12	58.46	58.72	58.69

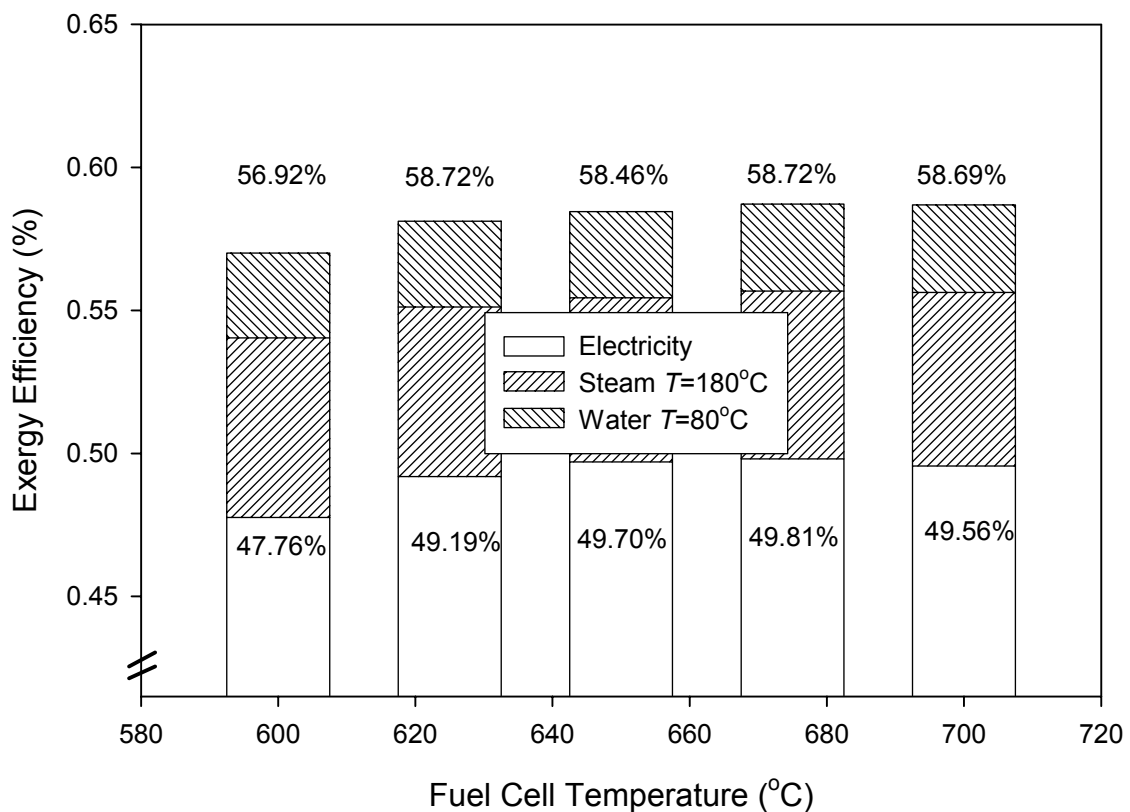


Figure 5.4. Exergy efficiency and distribution as function of temperature.

Furthermore, we have analyzed the exergy loss of the subsystems and their temperature dependency and this is shown by Figure 5.5.

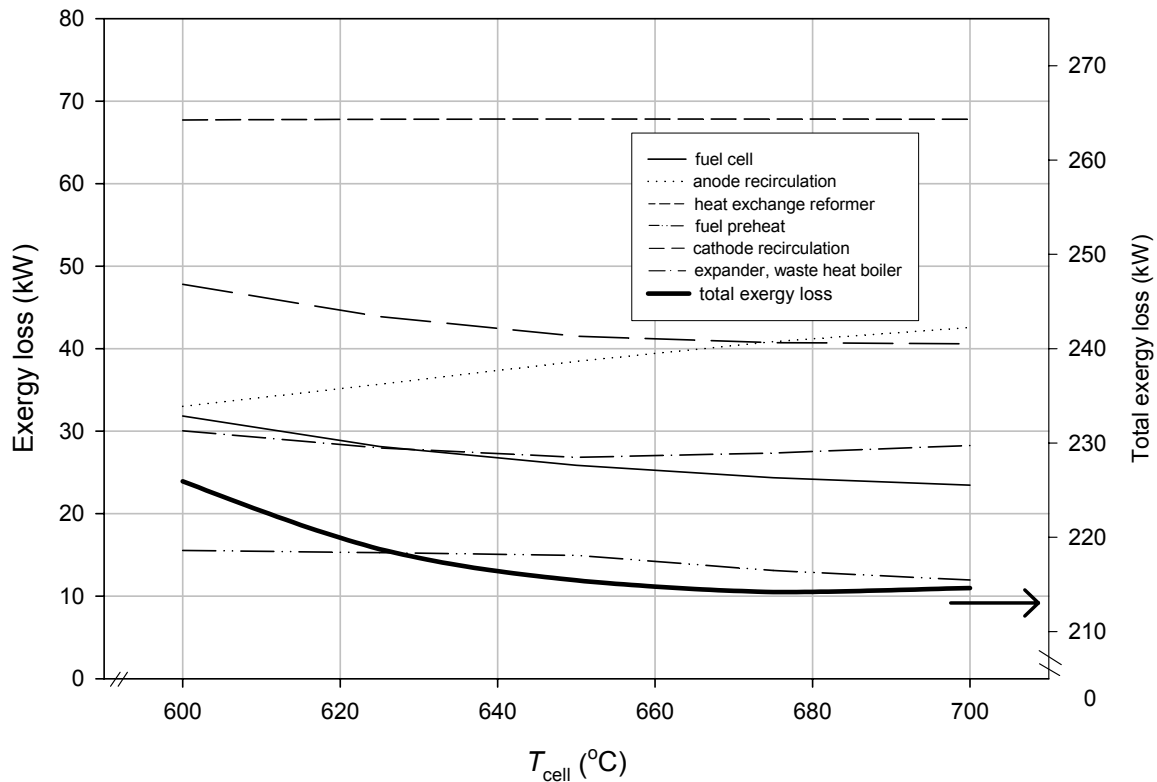


Figure 5.5. Exergy loss of subsystems as function of temperature.

This figure shows that the exergy loss of the subsystems HER, fuel preheat and expander, waste heat boiler are little temperature dependant. The exergy loss of the fuel cell and cathode recycling decreases while the anode recycling increases with operating temperature. The overall result is a minimum of exergy loss at 675 °C and thus an optimum in overall exergy efficiency.

Finally, Figure 5.6 shows the exergy loss distribution at the typical operating temperature of $T_{cell} = 650$ °C. It shows that the HER contributes most to the total exergy loss. The combustion process of the HER is the main cause of the exergy loss of the HER (about 65 %) while the contribution from the reforming reaction is relatively small (the remaining 35 %). Improvement in system efficiency is therefore expected when changing this external reforming configuration to internal reforming. This off course will involve different MCFC stack technology and eventually will affect the system layout.

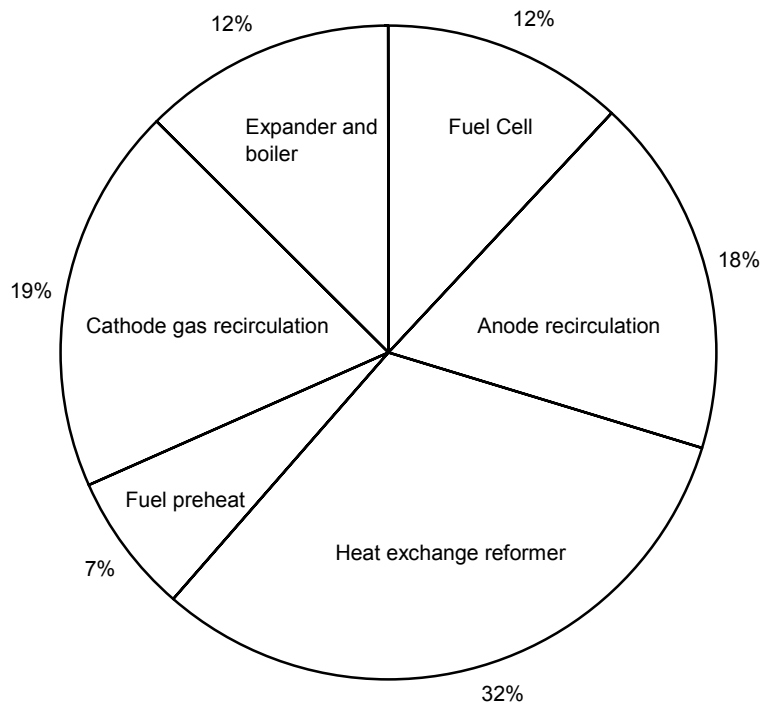


Figure 5.6. Exergy loss distribution at the typical operating temperature of 650 °C.

5.5. Conclusions

The influence of the operating temperature of the fuel cell on the overall system efficiency is small in the operating range within 650 °C and 700 °C. This result is in accordance with the results of chapter 4. This fuel cell system performs best at 675 °C with a net electrical efficiency of 51.89 % point (based on LHV). This is the main conclusion since the production of electricity is the objective while the production of heat is of minor importance. Production of heat plays a role when this system is integrated to industrial processes together with district heating system. Exergy conservation is then an additional requirement for a sustainable society. The exergetic efficiency of this system is at maximum as well at 675 °C with a value of 58.72 %. The overall energetic CHP efficiency based on LHV increases with operating temperature and the highest value is achieved at the highest temperature considered. The exergy loss contributed by the heat exchange reformer is the highest of all subsystems and this should be tackled in case of further system optimization.

The conclusions regarding the efficiencies as function of operating temperature as presented here are restricted to this specific plant design. Nevertheless, the present study has shown the complexity of a fuel cell system. The refinement by detail flowsheet analysis as presented here has revealed interactions between the subsystems of the plant that cannot be seen otherwise. Examples are the different optimum temperature for the fuel cell stack and the overall system, and the mismatch between the optimum stack temperature and the minimum stack-cooling requirement. Furthermore, we have shown the complex interactions between the different processes in a system. We have seen here that changes in cell temperature involve the following changes: 1) reversible heat production and irreversible losses of the fuel cell, 2) cooling requirement of the cell and consequently the auxiliary power consumption, and 3) changes in recirculation mass flows due to the changes in fuel cell inlet temperature. Their relations can only be made visible by flowsheet calculations. This study has therefore shown the importance of flowsheet calculation during the evaluation of the complete fuel cell plant when changing important process parameters. Simple theoretical calculations can show first order trends but detailed flowsheet calculations are required due to the complex behavior and intricate interactions in a fuel cell plant.

Reference

- [1] J.H. Hirschenhofer, D.B. Stauffer, R.R. Engleman, *Fuel Cells- A Handbook (Revision 3)*, prepared by Gilbert/Commonwealth for the U.S. Department of Energy under contract no. DE-AC01-88FE61684, (1994).
- [2] K. Ota, K. Toda, S. Mitsushima, N. Kamiya, *Accerated corrosion of stainless steels with presence of molten carbonate below 923K*, Bulletin of the Electrochemical Society of Japan, p.877-881, (2002)
- [3] C.G. Lee, Y. Kohta, T Nishina, I Uchida, *In situ NiO dissolution behavior in (Li +Na)CO₃ melts under pressurized oxidant gas atmospheres*, p.145-147, Journal of Power Sources **62**, (1996)
- [4] F.R.A.M. Standaert, *Analytical fuel cell modeling and exergy analysis of fuel cells*, PhD thesis Delft University of Technology, (1998)
- [5] E. Arato, B. Bosio, . Massa, F. Parodi, *Optimisation of cell shape for industrial MCFC stacks*, p.302-308, Journal of Power Sources **86** (2000)

- [6] F. Yoshiba, N. Ono, Y. Izaki, T. Watanabe and T. Abe, *Numerical analyses of the internal condition of a molten carbonate fuel cell stack: comparison of stack performances for various gas flow types*, p.328-336, *Journal of Power Sources* **71**. (1998).
- [7] F. Standaert, K. Hemmes, N. Woudstra, *Nernst Loss and Multistage Oxidation in Fuel Cells*, p. 92-95, *Proceedings of the Fuel Cell Seminar*, November 16-19, 1998, Palm Spring, California, USA (1998)
- [8] B. S. Kang, J.H. Koh, H.C. Lim, *Effect of system configuration and operating condition on MCFC system efficiency*, p.232-238, *Journal of Power Sources* **108** (2002)
- [9] S.F. Au, K. Hemmes, N. Woudstra, *The Influence of Operating Temperature on the Efficiency of Combined Fuel Cell and Power Cycle system*, p.A879-A885, *Journal of the Electrochemical Society* **149** (7), (2002).
- [10] S.F. Au, K. Hemmes, N. Woudstra, in *Meeting Abstracts of the 200th Meeting of the Electrochemical Society*, number 0455, September 2001.
- [11] Cycle-Tempo version 4.42, Delft University of Technology, Section Thermal Power Engineering; TNO Environment, Energy and Process Innovation, (2000).
<http://www-pe.wbmt.tudelft.nl/ev/cycle/cycle.html>
- [12] P.C. van der Laag, T.W. Verbrugge, in: *Proceedings of the 1994 Fuel Cell Seminar-Program and Abstracts*, November/December 1994, p.152-155
- [13] S.F. Au, N. Woudstra, K. Hemmes and I. Uchida, *Verification of a Simple Numerical model in a Flowsheeting program by performance testing at a 110cm² Molten Carbonate Fuel Cell*, accepted for publication by *Energy Conversion and Management*, (2002).
- [14] Y. Mugikura, H. Morita, M. Yoshikawa and T. Watanabe, *Modification of cathode performance equation and reaction mechanism of MCFC*, *Proceeding of the 7th FCDIC Fuel Cell Symposium*, Tokyo (JP) (2000).
- [15] S.F. Au, W.H.A. Peelen, F.R.A.M. Standaert, K. Hemmes and I. Uchida, *Verification of Analytical Fuel Cell Models by Performance Testing at a 110cm² Molten Carbonate Fuel Cell*. p.A1051-A1057, *Journal of the Electrochemical Society*, **148** (10), (2001).

Chapter 6: Fuel Cell system optimization (part III)

Multistage Oxidation by serial connection of stacks.

This chapter is submitted for publication to the Journal of Power Sources as: STUDY OF MULTISTAGE OXIDATION BY FLOWSHEET CALCULATIONS ON A COMBINED HEAT AND POWER MOLTEN CARBONATE FUEL CELL PLANT, by S.F. Au, N. Woudstra, and K. Hemmes, (2002).

Abstract

The multistage oxidation configuration consists of a set of serially connected fuel cell stacks. By connecting the stacks serially, more homogenous current distribution over the cell surface can be achieved resulting in lower irreversible losses.

This chapter presents a detailed assessment of multistage oxidation by flowsheet calculations in which the influence of operating temperature and gas composition on the fuel cell performance is incorporated. A 250 kW MCFC combined-heat-and-power (CHP) plant is used as reference and the fuel cell stack unit is substituted by two serially connected units ($N = 2$). Two multistage configurations are examined: A: both anode and cathode flows are serially connected, and B: only the anode flow is serially connected while the cathode flow is parallel connected. For all systems, the total cell active area, cell current density, overall fuel utilization and gas temperature at the inlet and outlet of the fuel cell array are kept constant. Fuel cell performances at the operating conditions are calculated using a numerical fuel cell model of the flowsheeting program. Influences of operating temperature and gas composition on the cell performance are incorporated using empirical relations that describe the irreversible losses of the cell as function of these parameters. System performances are compared in order to assess the benefits of the multistage oxidation configurations. Differences in performance between the two multistage oxidation configurations are studied by analyzing the difference in exergy loss

of stacks, stack power output, cooling requirement and cathode gas massflow and composition.

Detailed flowsheet calculations show that the improvement in efficiency is about 0.6 % for configuration A, and 0.8 % for configuration B. Improvements are obtained by the enhanced fuel cell power output while the expander power output is slightly reduced. Heat output is slightly reduced due to the improved fuel cell conversion. Analysis of stack output revealed an intricate interaction between stack and the rest of the fuel cell system. Their mutual influences are examined and the results explain differences in results between configuration A and B.

6.1. Introduction

In Chapter 2, a one-dimensional fuel cell model is introduced that is based on the equivalent circuit given in Figure 2.1 (see also reference [1]). In this model, we assume that inside the cell the difference between the local Nernst voltage $V_{eq}(x)$ and the uniform cell voltage V_{cell} is the driving force to overcome all irreversible losses (i.e. ionic/electronic conductance and activation/diffusion polarization), lumped into the uniform quasi-Ohmic resistance r . Conversion of gaseous reactants inside the cell causes a gas composition gradient between the fuel cell gas inlet and outlet, and a similar gradient in the $V_{eq}(x)$ exists between the gas inlet and outlet. The quasi-Ohmic resistance r is by definition uniform over the cell, therefore this gradient in $V_{eq}(x)$ results in an inhomogeneous conversion and current density inside the cell (see Figure 6.1). Conversion of the gaseous reactant is high at the fuel cell gas inlet where $V_{rev}(x)$ is high, while the conversion rate is lower at the gas outlet where $V_{rev}(x)$ is low. This inhomogeneous conversion rate is equivalent to an inhomogeneous current distribution and this adversely affects the fuel cells performance (see reference [2] for more details).

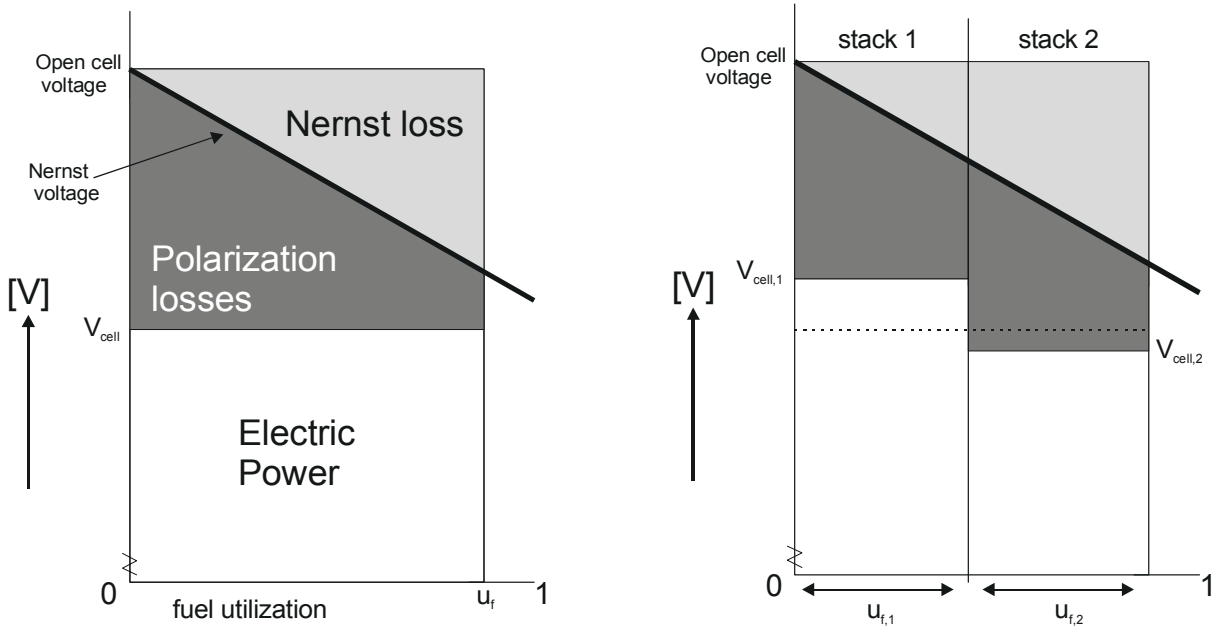


Figure 6.1. Schematic representation of the polarization losses of the stack before and after splitting it into two segments, taken from reference [2].

The multistage oxidation configuration consists of a set of serially connected fuel cell stacks. By connecting the stacks in series, more homogenous current distribution over the cell surface can be achieved resulting in lower polarization losses (see Figure 6.1). Standaert [2, 3] has previously analytically examined the thermodynamic principle of multistage oxidation and he found an analytical expression for the gain in power density w [W/cm^2] as function of the number of segments N (see reference [3])

$$w(N) = \frac{1}{12} \frac{(\alpha u_f)^2}{r} \left(1 - \frac{1}{N^2} \right) \quad (6.1)$$

with r [Ω/cm^2] the quasi-Ohmic resistance, α [V] the slope of the linearized Nernst equation and u_f [-] the fuel utilization.

For the Molten Carbonate Fuel Cell (MCFC), it is shown that an improvement in electric efficiency of about 1 % can be achieved by splitting the cell area up into $N = 2$ segments [3]. This conclusion was based on both analytical mathematical modeling and simplified flowsheet calculations. Liebhafsky [4] and Selimovic [5] both have also considered the use of multistage oxidation, but then for the Solid Oxide Fuel Cell (SOFC). They showed that

an improvement in power output of about 5 % point can be obtained for their systems. In the above-mentioned studies, the influence of temperature and gas composition on the polarization losses was previously neglected. Recent studies show that the cell resistance depends strongly on the operating temperature of the stack [6, 7]. Another study (reference [8], Chapter 4 of this thesis) has shown that the complex interactions between fuel cell stack and auxiliary equipments additionally complicate system evaluations. More realistic and detailed flowsheet calculations are therefore required to further assess the benefit of multistage oxidation in system performance in practice. Selimovic [5] recently presented a flowsheet study in which they investigated the implementation of multistage oxidation on a SOFC gas-turbine hybrid system. They found an 18 % increase in fuel cell power output and 5% increase in total system efficiency. These results are obtained by changing the cell configuration from one-stage to multi-stage oxidation, and by simultaneously increasing the total fuel utilization u_f of the fuel cells. Since u_f is an important parameter for the fuel cell performance, the final result cannot be solely ascribed to the change in cell configuration, and additional studies are required.

6.2. System calculations

The MCFC-CHP reference system selected for this study has the following main features:

- 250 kW class MCFC stack
- Heat production at two temperature levels
(saturated steam at 180 °C and hot water at 80 °C)
- natural gas as primary fuel (equivalent to 557.57 kW LHV)
- fuel gas is externally reformed
- pressurized system operating at 4 bar

This system is used in Chapter 5 in which we investigated the influence of the fuel cell operating temperature on the system efficiency. The flowsheet of this system is given in Figure 5.1. A detailed description of this system and input parameters are given in Section 5.2. For the fuel cell stack, the standard average operating temperature of 650 °C is used as a reference. Table 6.1 gives the operating parameters of the MCFC stacks. The cell

resistance r is calculated using the empirical relations [6, 7] determined by CRIEPI¹⁾ (equation 4.25). The empirical relations and the fitting values are given in Paragraph 4.4.1. The cell resistance is determined by the average cell temperature T_{cell} , operating pressure p , and the average gas composition at both the anode and cathode (by means of average partial pressures p_i and mol fractions m_i). The cell resistance of the reference stack is given in Table 6.1. Other input parameters represent the operating condition and characteristics of state of the art MCFC stacks at full load. The MCFC stack performance (characterized by the cell voltage V_{cell}) is calculated by the numerical fuel cell model of the flowsheeting program Cycle Tempo [9]. A detailed description and assessment of accuracy of the fuel cell model is given in Chapter 3 and in reference [10]. The overall performance of the MCFC-CHP plant is calculated by the program Cycle-Tempo using the flowsheet given in Figure 5.1.

Table 6.1. Input parameters of the fuel cell stack of the reference stack and sub-stacks of multistage oxidation systems.

	Reference	Multistage A		Multistage B	
	FC stack	1 st sub-stack A1	2 nd sub-stack A2	1 st sub-stack B1	2 nd sub-stack B2
T_{cell}	650 °C	calculated	calculated	650 °C	650 °C
p	4 bar	4 bar	4 bar	4 bar	4 bar
u_f	70 %	35 %	53.85 %	35 %	53.85 %
A_{cell}	250 m ²	125 m ²	125 m ²	125 m ²	125 m ²
i_{cell}	1500 A/m ²	1500 A/m ²	1500 A/m ²	1500 A/m ²	1500 A/m ²
r	0.6072 Ωcm ²	calculated	calculated	calculated	calculated
$T_{out}-T_{in}$	100 K	calculated	calculated	100 K	100 K
Δp_{anode}	0.05 bar	0.025 bar	0.025 bar	0.025 bar	0.025 bar
$\Delta p_{cathode}$	0.10 bar	0.05 bar	0.05 bar	0.10 bar	0.10 bar
η_{DC-AC}	96 %	96 %	96 %	96 %	96 %

The fuel cell stack of the reference system is here split into two equal segments, which anode flows are connected in series (see Figure 6.2). These two serially connected sub-stacks represent multistage oxidation with $N = 2$. Each sub-stack has an active cell area that is half of the reference stack. The active cell area, pressure losses and current density are the same for both sub-stacks. The cumulative fuel utilization u_f of the complete stack unit

¹⁾ Central Research Institute of Electric Power Industry (Japan)

of the reference system is shared equally by the two sub-stacks. The fuel utilization u_f is defined according to the fuel input at the cell inlet. Since the second stack is fed with leaner fuel than the first stack, u_f of each sub-stack is therefore different by definition. The fuel utilization of the reference stack is 70 %, therefore the fuel utilization of the first sub-stack of the multistage system is 35 %, while according to the definition, the second sub-stack is operating at a fuel utilization of 53.85 %²⁾, relative to the inlet of the second sub-stack. With these stack operating-parameters, the anode mass flow and the overall fuel utilization of two sub-stacks together are kept the same as for the stack of the reference system. Note that the fuel utilization of this reference system is relatively low and that the gain in power density by multistage oxidation is proportioned to the fuel utilization (see equation (6.1)). It is however not possible to increase the fuel utilization without significantly modifying the reference system, hence the fuel utilization is kept at 70 %.

Two configuration of multistage oxidation are examined (see Figure 6.2):

- Multistage A: cathode flows of the two sub-stacks are connected *serially*
- Multistage B: cathode flows of the two sub-stacks are connected in *parallel*

Multistage A resembles the original fuel cell stack simply devised into two sub-stacks. Multistage B on the other hand is also devised but may need some additional changes in the cathode pipe arrangement. It's important to note that the sub-stacks in both configurations are electrically disconnected allowing both stacks to have different stack voltages and power densities according to their operating conditions. Having the anode massflow connected serially, both configurations represent multistage oxidation and only the cathode flows are different.

²⁾ the ratio of $0.35 / (1-0.35)$

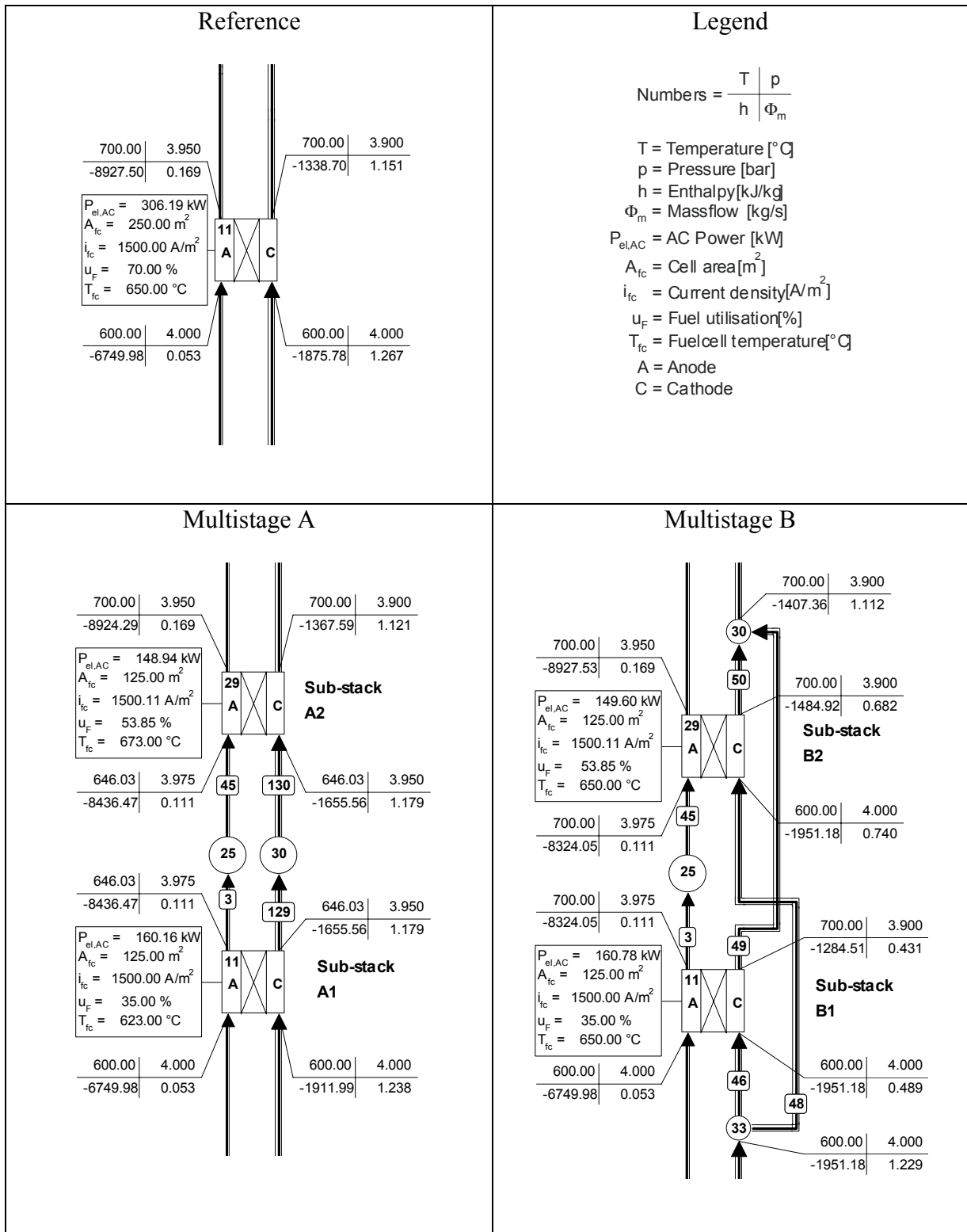


Figure 6.2. The reference single stack unit and the two Multistage configurations.

Other difference between multistage A and multistage B is the operating temperatures of the stack. This difference is the result of a combination of boundary conditions and the cooling principle of the stacks. In order to solely assess the effect of multistage oxidation,

it is crucial to keep the rest of the system the same as much as possible. The inlet and outlet temperatures of the stack unit should therefore be kept the same in all case. The inlet temperature of the first sub-stack in both Multistage A and B is therefore set at 600 °C and the outlet temperature of the second sub-stack is set at 700 °C. This boundary condition results in a difference in the mean average temperature of the sub-stacks between the two multistage configurations. All stacks are cooled by the cathode massflow resulting in a temperature difference between the inlet and outlet. Since the cathode flows of Multistage A are serially connected, the intermediate temperature between the two sub-stack is somewhere between 600 °C and 700 °C, and the operating temperature³⁾ of each sub-stacks is therefore different. Multistage B does not have the cathode flow connected serially but instead they are both joint together forming the stack unit's outlet. The outlet temperatures of the cathode of the sub-stacks can therefore be set the same as the reference stack. For the anode flow, it is assumed that it is heated up only at the first sub-stack, while it is kept constant in the second sub-stack. Since the anode flow is relatively low compared to the cathode flow, it is assumed that the stack operating temperature is solely determined by the average temperature of the cathode gas. Hence, both sub-stacks are assumed to operate at the same temperature as the reference stack. Figure 6.2 shows the differences in stack configurations and cathode outlet temperatures.

The flowsheet calculation of the Multistage B system is analogous to that of the reference system, and the calculation is described in details in Chapter 5. The calculation of the flowsheet of Multistage A is some what different, since the operating temperature of the sub-stacks are calculated instead of defined. For this, we need to calculate the intermediate temperature between the first and the second sub-stack. This intermediate temperature is calculated by the flowsheeting program by solving the energy and mass balances of the stacks using the numerical solving routine of the program. The numerical solving routine allows two options for the user to fulfill the energy and mass balances. The first option is that the temperature-increase of the flows through the cell is specified, resulting in the calculation of the cathode mass flow⁴⁾. The second option is that the cathode mass flow is

³⁾ The mean average temperature between the stack inlet and outlet is assumed as the operating temperature of the stack.

⁴⁾ Both fuel utilization and anode mass flow should be given. This is compulsory in Cycle-Tempo, thus the cathode massflow is determined by the cooling of the stack.

specified, resulting in the calculation of the temperature increase ($T_{out}-T_{in}$). The combination of both options solves the energy and mass balances of the stack-unit and determines the operating temperatures of the sub-stacks. The first option is used for the second sub-stack; this determines the cathode mass flow of both sub-stacks. The second option is used for the first sub-stack; this determines the outlet temperature of the stack, which in turn is the inlet temperature of the second stack. The combination of both options enables the program to iteratively determine the intermediate temperature between the two stacks. As in the reference system, the operating temperatures of the (sub) stacks are set as the mean average of the gas in and outlet.

The operating temperatures of the stacks are determined using the calculations by the program. However, the fuel cell model of the program requires the input of both cell temperature and cell resistance for calculating the performance of the sub-stacks. Both inputs should be given prior to each flowsheet iteration. It is obvious that the stack performance determines the cooling requirement of the stack, and for system A, it also determines the operating temperature through the intermediate temperature between the two sub-stacks. In other words, intermediate temperature, stack operating temperatures, cell resistances⁵⁾ and stack performance are all coupled, and the stack operating temperatures and cell resistances can only be determined by iterative steps until conversion is reached. Since these iterative steps were not programmed in the flowsheeting program, numerous manual iterations are required before the solution is found that satisfies both the flowsheet results and the separately calculated cell resistances.

The input parameters of the reference and multistage oxidation fuel cell stacks are summarized in Table 6.1.

6.3. Results and Discussions

6.3.1. Net power efficiencies

Table 6.2 gives the energy and exergy outputs and efficiencies of the systems. For the multistage configurations, the improvements in efficiencies over the reference system are

⁵⁾ The cell resistances are calculated using a spreadsheet program with the CRIEPI empirical relations given in Section 4.4.1.

given between brackets. Again, the numbers in the tables are given in two digits behind the decimal point. These numbers are not round off since here we are only interested in the difference in the calculated results, which will not become apparent otherwise (see also the comments in Paragraph 5.4).

Table 6.2. Energy output and efficiencies of the reference and multistage systems.

	Reference	Multistage A	Multistage B
FC stack output (kW)	306.19	A1: 160.16 A2: 148.94 total: 309.10	B1: 160.78 B2: 149.60 total: 310.38
Expander (kW)	60.05	58.71	58.09
Auxiliary (kW)	-77.58	-75.97	-75.20
Net power (kW)	288.66	291.84	293.27
η_{th} (%)	51.77	52.34 (+0.57)	52.60 (+0.83)
η_{Ex} (%)	49.70	50.25 (+0.55)	50.49 (+0.79)
Heat $T=180C$ (kW)	91.59	89.66	88.84
Heat $T=80C$ (kW)	109.49	110.22	109.49
Total output (kW)	489.74	491.72	491.59
η_{th} (%)	87.84	88.19 (+0.35)	88.17 (+0.33)
η_{Ex} (%)	58.46	58.90 (+0.44)	59.08 (+0.62)

Table 6.2 shows that both multistage oxidation systems perform better than the reference system and that system B is the best performing system of the three. By splitting up the fuel cell stack, the stack output increases with 2.9 kW for system A, and 4.2 kW for system B (see the differences in Table 6.2). Simultaneously, the auxiliary power consumption decreases with 1.7 kW for system A, and 1.9 kW for system B. However, the expander power output decreases with 1.3 kW for system A, and 2.0 kW for system B. Hence we see here a leveling effect in the overall system efficiencies: An increase in stack power output results in a decrease in heat release by the stack thus a lower power output by the heat recovery expander. Overall, the improvement in both thermal efficiency η_{th} and exergy efficiency η_{EX} is here in the order of 0.6 point % for system A, and 0.8 point % for system B. The improvements in system efficiencies are clearly less than the improvements in stack outputs.

A similar leveling effect has also occurred in the fuel cell stacks and we have analyzed this effect by examining the data of the stacks.

6.3.2. Improvements by Multistage Oxidation

Starting with Multistage A, the intermediate temperature for the two sub-stacks of Multistage A is calculated as 648 °C (see Figure 6.2). With this, the operating temperatures for the sub-stacks are determined as 623 °C, and 673 °C, for the first and the second sub-stacks respectively (see footnote 3, page 92). The irreversible losses of the cell depend strongly on the operating temperatures and they are represented by the differences in cell resistance r (see Table 6.3.). Sub-stack A1 is operating at a relatively low temperature resulting in a high r . Vice versa, Sub-stack A2 is operating at a relatively high temperature resulting in a low r . Comparing to the reference stack, the cell resistance r of A1 is about 33 % higher than the reference stack. This means an increase in irreversible losses, which adversely affects the stack performance. Nevertheless, the net power density \tilde{P}_{cell} of this sub-stack is about 5 % higher than the reference stack (1.281 kW/m² vs. 1.225 kW/m², see Table 6.3). This paradox is a direct result of the multistage oxidation concept, and it is caused by the lower Nernst loss of this stack (see Figure 6.1, and reference [2] for more details). A similar paradox holds for the second stack. The cell resistance of A2 stack is about 14% lower than the reference stack, but the power density of this stack is about 3 % lower compared to the reference stack. Here, the difference is caused by the leaner fuel. The net power output of both stacks combined is 2.91 kW (or 0.52 % point η_{th}) higher than the reference stack. Additional chemical energy is therefore converted into electric power and less heat is produced. This enhanced conversion reduces the cooling requirement of the stack, hence lowering the cathode mass flow $\Phi_{cathode}$ (see Table 6.3). Combined with the lower input of air that can be seen from the lower expander mass flow $\Phi_{expander}$ given in Table 6.3, the result is a decrease in auxiliary power consumption of 1.61 kW (see Table 6.2). On the other hand, the reduced expander mass flow results in a reduction of power output by the generator with the amount of 1.34 kW. The overall result is an increase of 3.18 kW to the total net power production, which amounts to a relative increase of 1.1 % with respect to the reference system. Based on the input of fuel, this results in an increase of net efficiency of 0.57 % point and 0.55 % based on η_{th} and η_{ex} respectively. Hence, Multistage A performs slightly better than the reference system.

Table 6.3. Stack data, and cathode recycling data and gas composition.

	Reference	Multistage A	Multistage B
T_{cell} (°C)	650	A1: 623 A2: 673	B1: 650 B2: 650
r (Ω cm ²)	0.6072	A1: 0.8082 A2: 0.5246	A1: 0.6224 A2: 0.6212
Ex_{loss} (kW)	25.86	A1: 14.15 A2: 10.80 total: 24.95	A1: 12.29 A2: 12.05 total: 24.34
\tilde{P}_{cell} (kW/m ²)	1.225	A1: 1.281 A2: 1.192	A1: 1.286 A2: 1.197
$\Phi_{cathode}$ (kg/s)	1.267	1.238	A1: 0.489 A2: 0.740 total: 1.229
$\Phi_{expander}$ (kg/s)	0.264	0.258	0.255
$\%o_{recycling}$ (%)	77.09	77.01	77.10
\bar{p}_{O_2} (bar)	0.228	A1: 0.237 A2: 0.198	B1: 0.197 B2: 0.216
\bar{p}_{CO_2} (bar)	0.385	A1: 0.435 A2: 0.355	B1: 0.375 B2: 0.412
\bar{m}_{H_2O} (-)	0.119	A1: 0.117 A2: 0.122	B1: 0.124 B2: 0.122

The increase in net performance by Multistage B is even more than Multistage A. Here, the increase in power output of both sub-stacks combined is 4.19 kW (or 0.75 % point η_{th}) vs. reference, and 1.28 kW (or 0.23 % point η_{th}) vs. Multistage A (see Table 6.2). We have analyzed the differences using the stack data given in Table 6.3, and have looked, in particular, at the difference between Multistage A and Multistage B. For Multistage B, we have used the typical 650 °C for the operating temperature of both sub-stacks. Since the operating temperature of both stacks is the same as the reference, the cell resistances of both stacks are of the same order as the reference (see Table 6.3). This results in a more even distribution of exergy losses over the two stacks compared to Multistage A. Hence the total exergy loss for Multistage B is lower than Multistage A (see Table 6.3). The cell resistances for both sub-stacks of Multistage B are still slightly higher than the reference stack. The differences are caused by the differences in the cathode gas composition⁶⁾ and in particular the lower \bar{p}_{O_2} . The cathode gas compositions are given in Table 6.3 and they are calculated by the program. The situation here is very complicated since the cathode gas

⁶⁾ The contribution of the anode to the total cell resistance is relatively small.

composition is influenced by the cooling requirement of the stack (given by Φ_{cathode}) and by the heat requirement of the fresh air (given here by $\%_{\text{recycling}}$). The complex interactions between the stack performance, cooling requirement and heat requirement, and their results cannot be predicted by theory. What we observed here is an increase in fuel cell stack irreversibility (higher $r!$) due to increase in stack power output! Hence, this system shows a leveling effect in the increase of stack power output. It is an excellent example of the complex interactions within a fuel cell system.

6.3.3. Overall CHP efficiencies

Table 6.2 also summarizes the heat outputs of the systems. The multistage systems produce less heat, in the form of super heated steam at $T = 180\text{ }^{\circ}\text{C}$, than the reference system. This follows directly from the improved efficiency of the fuel cell stacks. Since the increase in stack output is more for Multistage B than Multistage A, thus less super heated steam is produced by B than by A. Heat output in the form of steam is about the same. For Multistage A, the slightly increased output of hot water (at $T = 80\text{ }^{\circ}\text{C}$) is caused by the differences in gas composition at the outlet of the anode. This difference results from the higher operating temperature of the 2nd sub-stack compared to the other systems ($675\text{ }^{\circ}\text{C}$ for A2 while the others operate at $650\text{ }^{\circ}\text{C}$). This increase in operating temperature alters the chemical equilibrium of the shift-reaction and therefore the outlet gas composition. The resulting difference in water vapor content of the anode off gas explains the small difference in hot water output of both systems.

Overall, the net CHP performances of the multistage oxidation systems are higher than the reference system. For Multistage A, the increases in efficiencies are 0.35 % point and 0.44 % point for η_{th} and η_{ex} respectively. For Multistage B, the increases in efficiencies are 0.33 % point and 0.62 % point for η_{th} and η_{ex} respectively.

6.3.4. Comparison with previous works and discussions

The present multistage oxidation systems are different from the system used previously by Standaert [3], and a direct comparison of results is hence not possible. For example, Standaert's reference system has a net electrical efficiency of 47 % point vs. 52 % point

here (both based on η_{th}). Nevertheless, when comparing the improvement of multi-stage oxidation, our present results are lower than Standaert's results (see reference [3]). His calculations suggest an improvement of about 1% in net efficiency for Multistage A configuration, while our present detailed calculations show that about 0.6 % improvement in net power output is more realistic. The relatively low fuel utilization of our present system may have contributed in the lower system improvement.

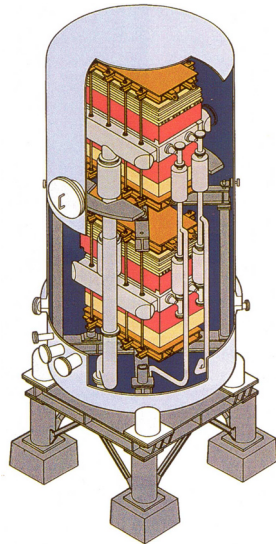
Our present results are also less optimistic compared to Selimovic's result (see reference [5]). Moreover, this study shows an additional gain in overall net efficiency by parallel cathode flow, as done here with Multistage B. The latter contradicts Selimovic's results. However, we should note that Selimovic's results were obtained by changing simultaneously both system layout and fuel cell operating parameters. Especially the changes in fuel utilization u_f and current density i_{cell} have significant impact on the fuel cell stack performance. Therefore again, our present results cannot be directly compared with the results from the previous study (reference [5]).

Finally, we will make some remarks regarding the application of multistage oxidation in practice. Splitting up the fuel cell stack seems to involve significant changes in the design and manufacturing of fuel cell stacks. In practice, it's more likely that the multistage oxidation as presented here only involves a rearrangement of piping. State-of-the-art MCFC stack-modules that are currently used in pilot plants consist of two small size sub-stacks that are fed parallel. An example is the IHI⁷⁾ 250 kW MCFC stack unit shown in Figure 6.3. Two units were built for the 1MW MCFC pilot plant in Kawagoe, Japan (see Figure 6.4). Multistage oxidation configuration can be obtained by simply connecting the sub-stacks in series instead of parallel (see Figure 6.5). Since the power plant itself often consists of several stack units, these units can also be placed in series providing another alternative for multistage oxidation. In the Multistage A configuration, the temperature difference between the gas inlets and outlets of each sub-stack is also reduced, which may improve endurance and reduction of production cost.

Lastly, multistage oxidation configuration allows additional implementation of intermediate cooling and fuel injection between the two sub-stacks, as proposed in reference [11]. These features require significant changes in system layout making the

⁷⁾ Ishikawajima-Harima Heavy Industries Co., Ltd.

assessment on the effect of multistage oxidation less transparent. These system changes are hence here omitted and the possible improvements by these two changes should be addressed in the future.



Specifications:

Rated Power	:250 kW
Operating pressure:	pressurized
Electrode area	:1.0 m ²
Number of stacks	:2
Number of cell of each stack:	140

Figure 6.3. Conceptual drawing and specifications of the 250 kW manufactured by IHI, (figure taken from reference [12])

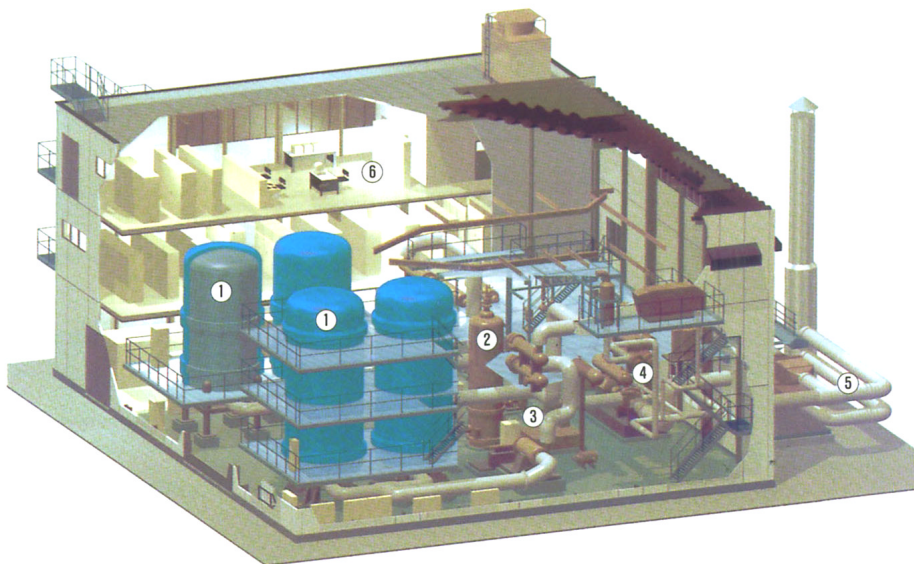


Figure 6.4. Artist impression of the 1 MW MCFC pilot plant built in Kawagoe, Japan, (figure taken from reference [13]).

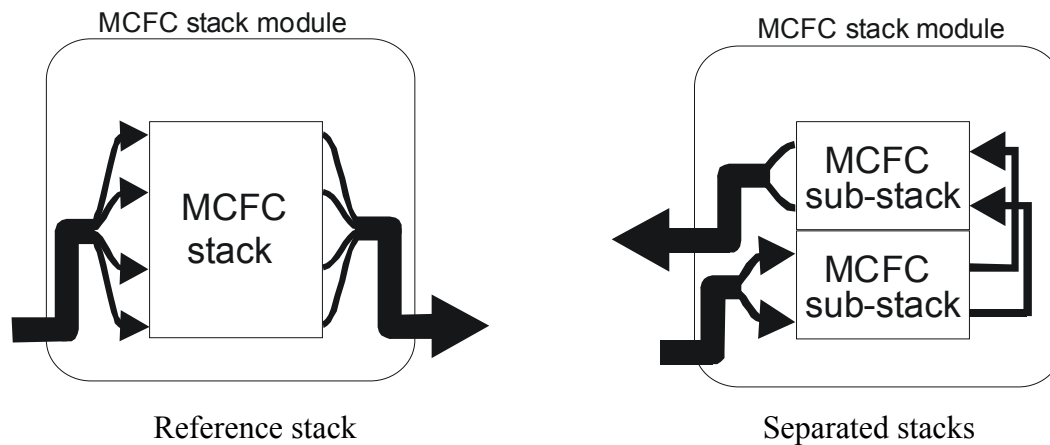


Figure 6.5. Separating stack to multistage oxidation with $N = 2$

6.4. Conclusions

A gain in performance is achieved by implementing multistage oxidation instead of parallel connection of stacks. Detailed flowsheet calculations show that the improvement in net efficiency is about 0.6 % when both anode and cathode flows are placed in series. Additional 0.3 % point improvement can be obtained by placing solely the anode flow in series while keeping the cathode flow parallel. Both configurations increase fuel cell power output and reduce slightly the expander power output. They also reduce slightly the heat output. Overall, the net power efficiency (based on LHV, thermal) of this 250 kW class CHP MCFC plant is increased from 51.8 % to 52.3 %, by placing both anode and cathode flows in series, and to 52.6%, by placing solely the anode flow in series. Based on exergy, the net efficiency increases from 49.7 % to 50.3 %, for both flows in series, and to 50.5 %, for solely the anode flow in series. The increase in total CHP efficiency (net power and heat combined) is slightly lower. Based on exergy, the CHP efficiency increases from 58.5 % to 58.9 % for both flows in series, and to 59.1 % for solely the anode flow in series. These improvements can simply be obtained by rearranging piping in state-of-the-art modular fuel cell systems, which are currently being tested in pilot plants.

This study has again shown the complicated interactions between the fuel cell stack and the rest of the system. Improvement in fuel cell conversion not only increases the fuel cell stack output, but it also reduces the auxiliary power consumption by reduced cooling requirement. Less cooling translates to lower cathode mass flow, which increases oxidant

utilization and hinders reaction kinetics. The latter results to increase in irreversible losses and thus decrease in cell performance. Hence, it is not possible to translate improvement in stack performance directly to absolute improvement in overall system performance. The results in these complex situations can only be revealed by detailed flowsheet calculations as presented by this study.

References

- [1] S.F. Au, W.H.A. Peelen, F.R.A.M. Standaert, K. Hemmes and I. Uchida, *Verification of Analytical Fuel Cell Models by Performance Testing at a 110cm² Molten Carbonate Fuel Cell*. p. A1051-A1057, Journal of Electrochemical Society, Pennington, **148** (10), NJ, USA, (2000).
- [2] F. Standaert, K. Hemmes, N. Woudstra, *Nernst Loss and Multistage Oxidation in Fuel Cells*, Proceedings of the Fuel Cell Seminar, November 16-19, 1998, Palm Spring, California, USA, pp. 92-95
- [3] F. Standaert, *Analytical Fuel Cell Modelling and Exergy Analysis of Fuel Cells*, Ph. D. Thesis, Delft University of Technology, (1998)
- [4] H.A. Liebhafsky, E.J. Cairns, *Fuel Cells and Fuel Batteries*, Wiley, New York, (1968)
- [5] A. Selimovic, J. Palsson, *Networked solid oxide fuel cell stacks combined with a gas turbine cycle*, pp 76-82, Journal of Power Sources 106 (2002)
- [6] F. Yoshida, N. Ono, Y. Izaki, T. Watanabe and T. Abe, *Numerical analyses of the internal condition of a molten carbonate fuel cell stack: comparison of stack performances for various gas flow types*, pp328-336, Journal of Power Sources 71. (1998).
- [7] Y. Mugikura, H. Morita, M. Yoshikawa and T. Watanabe, *Modification of cathode performance equation and reaction mechanism of MCFC*, Proceeding of the 7th FCDIC Fuel Cell Symposium, Tokyo (JP) (2000).
- [8] S.F. Au, S.J. McPhail, N. Woudstra, K. Hemmes, *The Influence of Operating Temperature on the Efficiency of a Combined Heat and Power Fuel Cell plant*, Submitted to the Journal of Power Sources, (2002).
- [9] Cycle-Tempo version 4.42, Delft University of Technology, Section Thermal Power Engineering; TNO Environment, Energy and Process Innovation, (2000).
<http://www-pe.wbmt.tudelft.nl/ev/cycle/cycle.html>

- [10] S.F. Au, N. Woudstra, K. Hemmes and I. Uchida, Verification of a Simple Numerical model in a Flowsheeting program by performance testing at a 110cm² Molten Carbonate Fuel Cell, submitted to Energy Conversion and Management, (2002).
- [11] J.G. Wimer, M.C. Williams, *Molten Carbonate Fuel Cell Networks: Principles, Analysis, and Performance*, Springfield, NTIS (1993)
- [12] T. Ogawa, A. Matsunaga, T. Matsuyama, H. Kasai and K. Miyazawa, *Evaluation of 250 kW MCFC stack for 1,000 kW MCFC Power plant*, Abstracts of the Fuel Cell Seminar, (2000)
- [13] Y. Izaki and H. Yasue, *Demonstration of the first 1000 kW MCFC power plant in Japan*, Abstracts of the Fuel Cell Seminar, (2000)

Chapter 7: Innovative Fuel Cell Concepts (part I)

The MCFC with a separate CO₂ channel

This chapter is submitted for publication to the Journal of Power Sources as: FLOWSHEET CALCULATION OF A COMBINED HEAT AND POWER FUEL CELL PLANT WITH A CONCEPTUAL MOLTEN CARBONATE FUEL CELL WITH SEPARATE CO₂ SUPPLY, by S.F. Au, K. Hemmes and N. Woudstra, (2002).

Abstract

A new type of molten carbonate fuel cell (MCFC) with a separate CO₂ supply (improved or i-MCFC) is previously presented, which has the potential for reducing NiO cathode dissolution and system enhancement by CO₂ removal from fuel gas. This chapter presents the first flowsheet calculations of an i-MCFC system that utilizes the potential of reducing NiO dissolution. A sub-model that simulates energy and mass flows of the i-MCFC is created using standard flowsheeting components. The performance of the i-MCFC is assumed to be equal to the MCFC and differences in Nernst potentials and irreversible losses are neglected. To compare the differences in concept, a MCFC combined-heat-and-power (CHP) system flowsheet is modified and the MCFC model substituted by the i-MCFC sub-model. The overall efficiencies of both fuel cell systems are calculated using a flowsheeting program. The calculated results are compared and the differences analyzed. The overall system performance of this i-MCFC CHP system is slightly lower than the MCFC CHP reference system (about 0.1 % point in average). The difference in performance is ascribed to the change in gas composition and heat capacity of the cathode gas. The change in heat capacity increases the total massflow through the i-MCFC resulting to an increase in overall auxiliary power consumption. The low CO₂ content of the cathode gas should reduce the NiO cathode dissolution to a negligible level.

7.1. Introduction

The improved molten carbonate fuel cell or i-MCFC is a new fuel cell design that is developed at the Faculty of Applied Science of Delft University of Technology (see reference [1]). In contrast to conventional fuel cells that features two gas inlets and outlets, the i-MCFC features three separate gas inlets and outlets, which is shown by Figure 7.1.

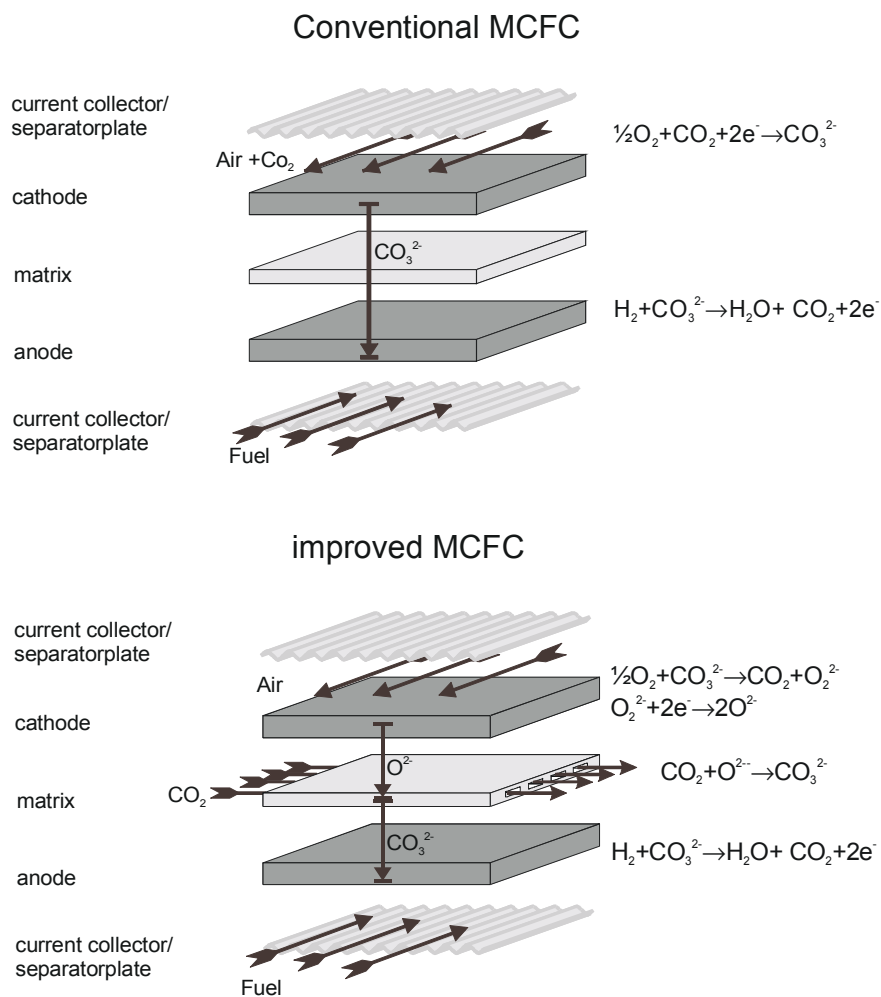


Figure 7.1. Schematic representations of the conventional MCFC and the improved MCFC.

Although this new concept has only been demonstrated on laboratory scale, it is worthwhile studying the benefits first by flowsheet simulations before starting an expensive development program on the i-MCFC. This paper presents the first study of

system concept by flowsheet calculations in which the i-MCFC is implemented. Using standard flowsheeting components, a sub-model is created that simulates the energy and mass balance of the i-MCFC. This sub-model is implemented in a 250 kW class conventional MCFC combined-heat-and-power (CHP) plant by modifying the fuel cell's inputs and outputs to match the requirements of the i-MCFC's. The CO₂ that is needed for the electrochemical reaction of the cathode is here supplied solely by the matrix flow. The cathode is fed with air that has low CO₂ content (about 0.03 mol%). This low CO₂ content should sufficiently suppress NiO cathode dissolution that at present severely limits endurance of the MCFC. The change in the overall system performance is assessed by flowsheet calculations using the flowsheeting program Cycle-Tempo [2] that has been developed by the Delft University of Technology.

7.2. Theory

7.2.1. Principles

At the MCFC's cathode, O₂ molecules react electrochemically with CO₂ molecules to form CO₃²⁻ ions



There is a general agreement that this reaction can be divided into three sequential reaction steps. Using the peroxide mechanism¹⁾ as an example (see reference [3]), we can distinguish these following steps (see Figure 7.2).

¹⁾ The peroxide mechanism is named to the peroxide ion, which is assumed to be an intermediate specie.

Others propose the superoxide as the other possible intermediate specie. Many years of study on the reaction mechanism has not led to a generally accepted mechanism but the principle of i-MCFC is valid for both species.

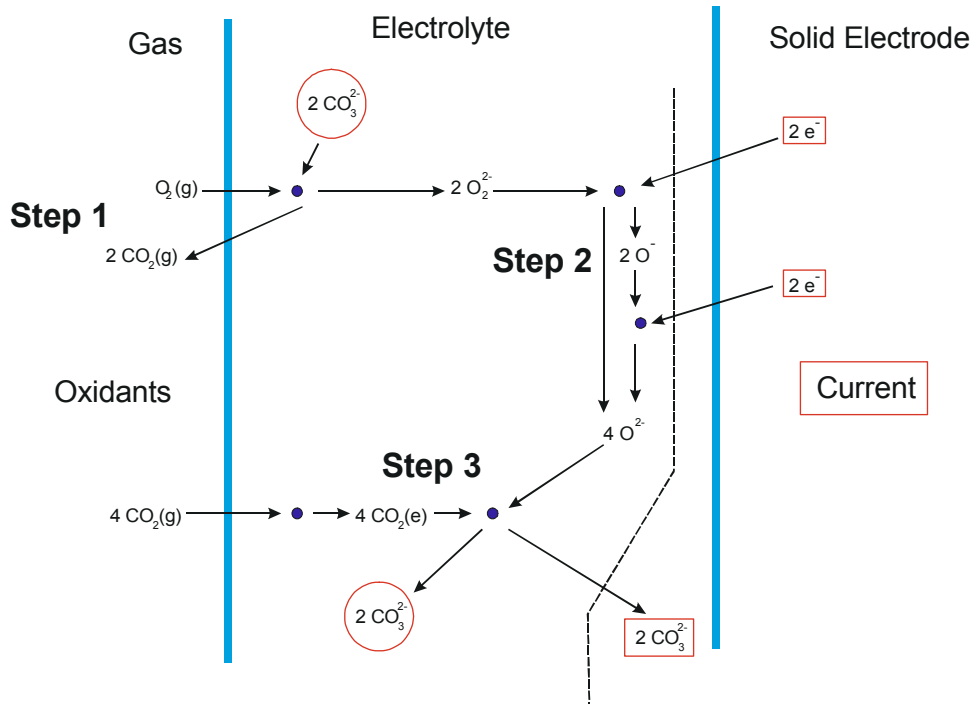


Figure 7.2. MCFC peroxide cathode mechanism.

Step 1: Chemical dissolution of O_2 molecules



Step 2: Reduction of O_2^{2-} peroxide ion



Step 3: Recombination reaction



The first step releases CO_2 while the third step consumes CO_2 . From that, we can see that Step 1 is favored by a low partial pressure of CO_2 (p_{CO_2}) of the cathode gas or oxidant while Step 3 is favored by a high p_{CO_2} of the cathode gas. These two conflicting demands

can be satisfied if Steps 1 and 3 can take place at different locations. The principle of the i-MCFC is based on the assumption that Steps 1 and 3 will take place at different locations inside the cell, if the O₂ and CO₂ are supplied separately at different locations. Both reaction steps can be enhanced then by choosing the p_{CO_2} accordingly.

In the i-MCFC, the O₂ is supplied with the cathode gas and Step 1 can take place at the gas electrolyte interface. CO₂ is supplied by an additional channel that is made in the matrix support tile that contains the molten carbonate electrolyte (see Figure 7.1). Step 3 can take place anywhere between this additional matrix channel and the cathode where the oxide ions are produced. Both gasses are now supplied separately and their concentration can be chosen individually to meet the conflicting demands of p_{CO_2} .

7.2.2. Advantages and disadvantages of the i-MCFC

Starting with the disadvantages, we note that making a gas channel in the matrix tile is very difficult. Present MCFC already suffers from a low mechanical stability of the matrix. In addition, increased effects of diffusion polarization are expected due to the diffusion distance that the O²⁻ and CO₂ need to overcome.

The advantages of the i-MCFC are based on the extra degree of freedom in the choice of gas compositions of the cathode gas. Since CO₂ is supplied separately, the typical restriction in a minimum of CO₂ concentration of the cathode gas is no longer required. Intricate connections between the anode output and cathode input can be omitted giving additional degrees of freedom in system design.

Removing the CO₂ restriction opens a unique opportunity to bring down the dissolution of the porous NiO cathode electrode, used in present MCFC. The NiO cathode dissolution severely limits the endurance of the MCFC (see reference [4]), and this problem needs to be solved in order to make the MCFC competitive to other fuel cell types and to other power production technologies (see reference [5]). The importance of this problem can be seen from the numerous research projects that are carried out at present (see references [6 - 11]). These research projects focus on finding alternative materials or material enhancements for the MCFC cathode. The i-MCFC concept creates a new unique opportunity to lower the NiO- cathode dissolution by changing cathode gas composition. The NiO dissolution process depends strongly on the p_{CO_2} and it shows a minimum at p_{CO_2} of around 10⁻² to 10⁻³ bar, with a rapid increase with increasing p_{CO_2} (see references

[12 - 14]. It is not possible to operate the MCFC at this minimum due to the electrochemical cathode reaction that requires CO_2 . Hence, alternative cathode material is needed in order to improve endurance of the MCFC (references [6 - 11]). On the other hand, the i-MCFC with its separate CO_2 supply does not require CO_2 in the cathode gas. Hence in the i-MCFC, NiO cathode dissolution can be reduced to a negligible level when low CO_2 containing cathode gas (e.g. air) is used. Therefore, the i-MCFC creates a unique possibility to reduce this NiO cathode dissolution to enhance endurance and thus reducing operating costs of the MCFC power plants.

Next to these opportunities in enhancing endurance, the extra degree of freedom in the choice of gas compositions creates opportunities in reducing cathode polarization, which is the main cause of irreversible losses of the MCFC. For example, heated air can be fed directly to the cathode, and its high O_2 and low CO_2 concentration enhances Step 1 of the cathode reaction mechanism. Concentrated CO_2 gas can be supplied to the matrix thus enhancing Step 3 of the reaction mechanism.

Another opportunity for the i-MCFC is to utilize the active CO_2 separation process of the matrix gas stream. This feature can be used in new system designs: e.g. removing CO_2 from low caloric fuel gas (e.g. landfill gas or biogas) thus enriching the fuel gas prior feeding it to the anode. For this option, the fuel gas should contain sufficient CO_2 , since each mol of H_2 that is converted in the anode requires the transport of one mol of CO_2 from the matrix stream. Landfill gas and biogas should be suited for this option since they both contain relatively large amount of CO_2 . Reformed natural gas (containing mostly methane) on the other hand is not suited due to its low CO_2 content relatively to the H_2 content. Reforming methane produces ideally three H_2 molecules together with only one CO_2 molecule hence the H_2/CO_2 ratio is too high and therefore methane is not suited as fuel for this specific system concept.

7.2.3. Modeling the i-MCFC

Studying the influence of the i-MCFC concept on system level requires models that fully describe the performance and energy and mass flows. They can be distinguished by two sub-models:

- 1) A sub-model that describes the cell voltage of the i-MCFC at various load conditions (see Paragraph 2.2.1 and Figure 2.1)
- 2) A sub-model that calculates the energy and mass balance of the i-MCFC (see Figure 7.3)

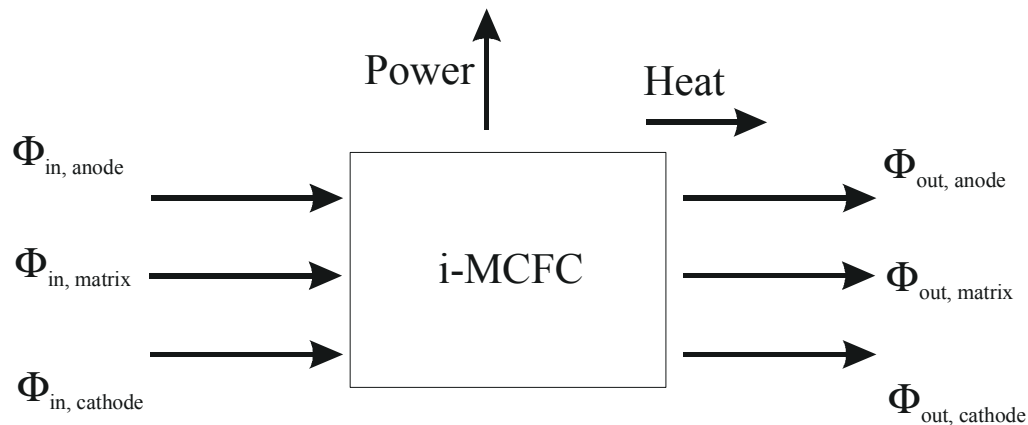


Figure 7.3. Mass flows and energy flows of the i-MCFC

At present, we are still investigating the i-MCFC mechanism in detail but already the basic thermodynamics felt short in defining the Nernst voltage of the cell (V_{eq}). With the present knowledge, it is not possible yet to create a model that calculates the cell performance at load condition. We therefore need to rely on experimental results in order to estimate the cell performance of the i-MCFC. Peelen et al [15] have shown that the performance of the i-MCFC is comparable to the conventional MCFC. Hence, the present study assumes the same performance for both the i-MCFC and the MCFC in order to study this new concept. This means that the cell voltage of a MCFC operating under similar condition is used here as the cell voltage of the i-MCFC. In other words, the design point of an MCFC operating under similar operating conditions is used for the i-MCFC. The differences between the two types of cells in open cell voltage (OCV), Nernst loss and irreversible losses are therefore neglected. All possible differences in system performances are direct results of differences in system layout.

Once the performance of the i-MCFC is determined, this data is used as input values for the sub-model that calculates the energy and mass balance of the i-MCFC, as required for

the flowsheet calculations. This sub-model is created with the standard components of the flowsheeting program Cycle-Tempo [2]. This sub-model simulates process and energy flows of the i-MCFC. These process and energy flows are given by Figure 7.3. The following three reactions take place inside the i-MCFC

At the anode, the normal MCFC anode reaction takes place



In the matrix, CO₂ dissolves into the electrolyte and reacts with O²⁻ ions:



At the cathode, oxygen is reduced to O²⁻ ions:



The overall reaction is exactly the same as that of the MCFC: H₂ from the anode inlet mass flow $\Phi_{in,anode}$ reacts with O₂ from the cathode inlet mass flow $\Phi_{in,cathode}$ to form H₂O that is released by the anode outlet mass flow $\Phi_{out,anode}$, and CO₂ is transported from the cathode to the anode.



The energy that is released by this reaction is partly released as electric power and partly as heat that is used for heating up the three mass flows. The unique feature of the i-MCFC is that CO₂ is introduced by the matrix inlet mass flow $\Phi_{in,matrix}$, and part of this CO₂ is transported to the anode and released by the anode outlet mass flow $\Phi_{out,anode}$.

This summarizes the process and energy flows of the i-MCFC, given by Figure 7.3.

A sub-model is created that simulates the flows inside the i-MCFC (see Figure 7.4). This model features:

- matrix gas flow with CO₂ separation that is transferred to the anode
- O²⁻-ion conducting high temperature fuel cell simulated by the Cycle-Tempo model for the solid oxide fuel cell (SOFC) but operated at 650°C with additional heat bypass to matrix stream
- Some heat from the fuel cell is transferred to the matrix gas flow.

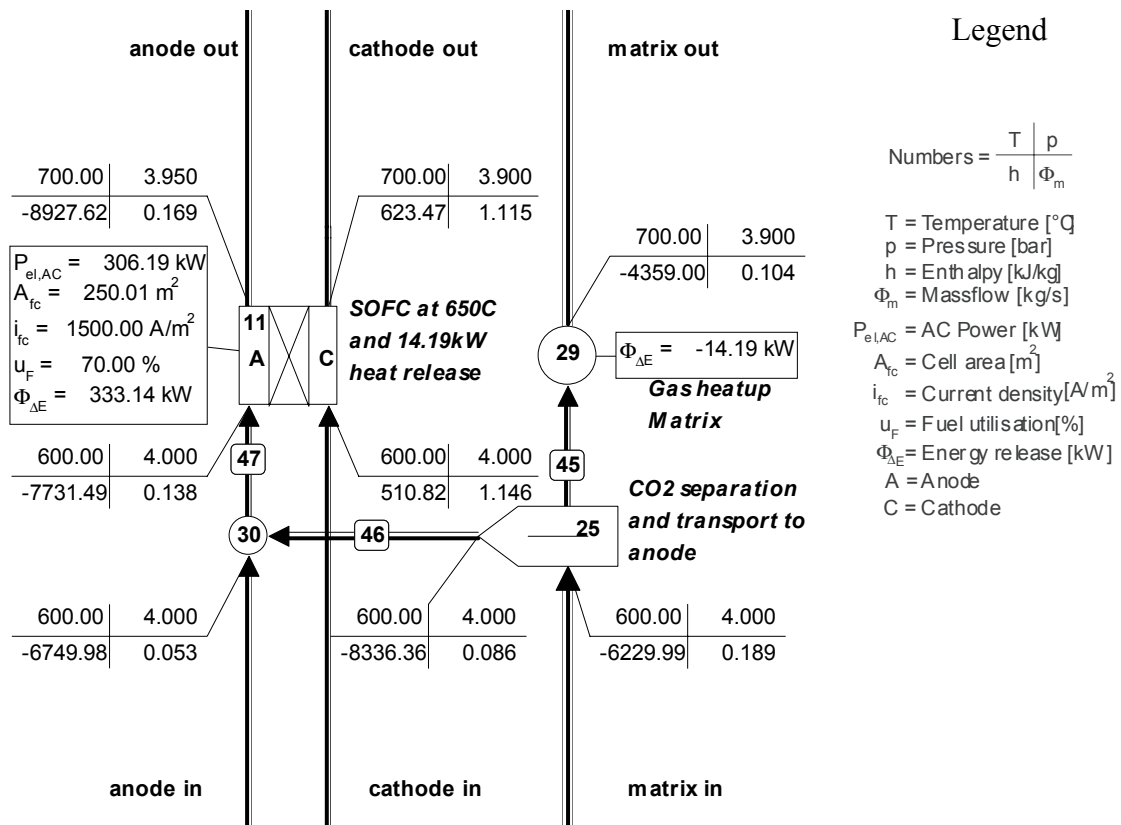


Figure 7.4. i-MCFC energy and mass flow model in Cycle-Tempo

In this simulation of the i-MCFC, CO₂ is separated from the matrix inlet mass flow and added to the anode inlet mass flow (Figure 7.4, apparatus #25, pipe #46 and node #30).



This separation process partly fulfills reaction (7.6) and the release of CO₂ in the anode as given by reaction (7.5). The electrochemical reaction from H₂ with ½O₂ to H₂O and the transport processes are simulated by the SOFC model (apparatus #11).



It's clear that the i-MCFC overall reaction (reaction (7.8)) is obtained by combining reactions (7.9) and reaction (7.10).

The SOFC model calculates the enthalpy change of the mass flows, and with the pre defined power release, it calculates the heat release that determines the cooling requirement of the cell. Part of the heat release is subtracted and transferred to the matrix mass flow in order to heat it up to the fuel cell outlet temperature. This heat up process is simulated here by means of a heat source (apparatus #7 of Figure 7.4) by defining an outlet temperature of 700 °C. This standard flowsheeting apparatus calculates the amount of heat that is required for this heating process and this amount of heat is used as additional cooling or energy release defined for the fuel cell. In addition, apparatus 7 has the function of imposing pressure loss to the matrix channels, and this pressure loss is here set the same as the cathode pressure loss.

The molar flow of CO₂ (Φ_{CO_2}) from the matrix channel to the anode is given by Faraday's law

$$\Phi_{CO_2} = \frac{A_{cell} i_{cell}}{nF} \quad (7.11)$$

With A_{cell} the total cell area, i_{cell} the current density, n number of charge (here $n = 2$) and F Faraday's number

Exactly this molar flow of CO₂ is separated from the matrix mass flow and sent to the anode inlet.

Note here that the CO₂ is fed to the anode inlet massflow prior to feeding it to the cell. This significantly changes the inlet gas composition, which in theory will alter the Nernst

voltage and thus the performance of the cell. Nevertheless, this change of the inlet gas composition has no influence on the overall results in the way the i-MCFC is modeled here, since the performance of the cell (i.e. power output) is here an external given input and not calculated by means of the Nernst equation.

The purpose of feeding the CO₂ to the inlet is to obtain chemical equilibrium at the outlet for the shift reaction equilibrium



At high temperature, the equilibrium of this fast chemical reaction is assumed and this reaction is considered by the MCFC model of the references system. Changes in gas composition by this equilibrium influences the energy balance and cooling requirement of the fuel cell. By feeding the CO₂ at the anode inlet of the fuel cell, the SOFC model also considers the shift equilibrium and compensates changes in the anode gas composition. It therefore adjusts the cooling requirement for the cell, as done by the MCFC model of the reference system

In this way, all characteristics of the i-MCFC are simulated by the subsystem given by Figure 7.4 enabling the calculation system performed. Note again, that only the energy and mass flows of the i-MCFC are simulated while the power output of the i-MCFC is defined based on currently available knowledge.

7.3. System Calculations

7.3.1. Reference system and adjustments to match the i-MCFC

The same MCFC combined-heat-and-power (CHP) system, as used in Chapter 5, is selected as a benchmark for this study of concept. In summary, this system has the following main features:

- 250 kW class fuel cell stack operating at 650 °C
- Waste heat utilization at two levels (steam at $T = 180\text{ }^{\circ}\text{C}$ and hot water at $T = 80\text{ }^{\circ}\text{C}$)
- natural gas as primary fuel (equivalent to 557.57 kW LHV)
- fuel gas is externally reformed
- pressurized system operating at 4 bar

Figure 5.1 shows the flowsheet of the reference system that is implemented in Cycle-Tempo. A detailed description of this system is given in Paragraphs 5.2 and 5.3.

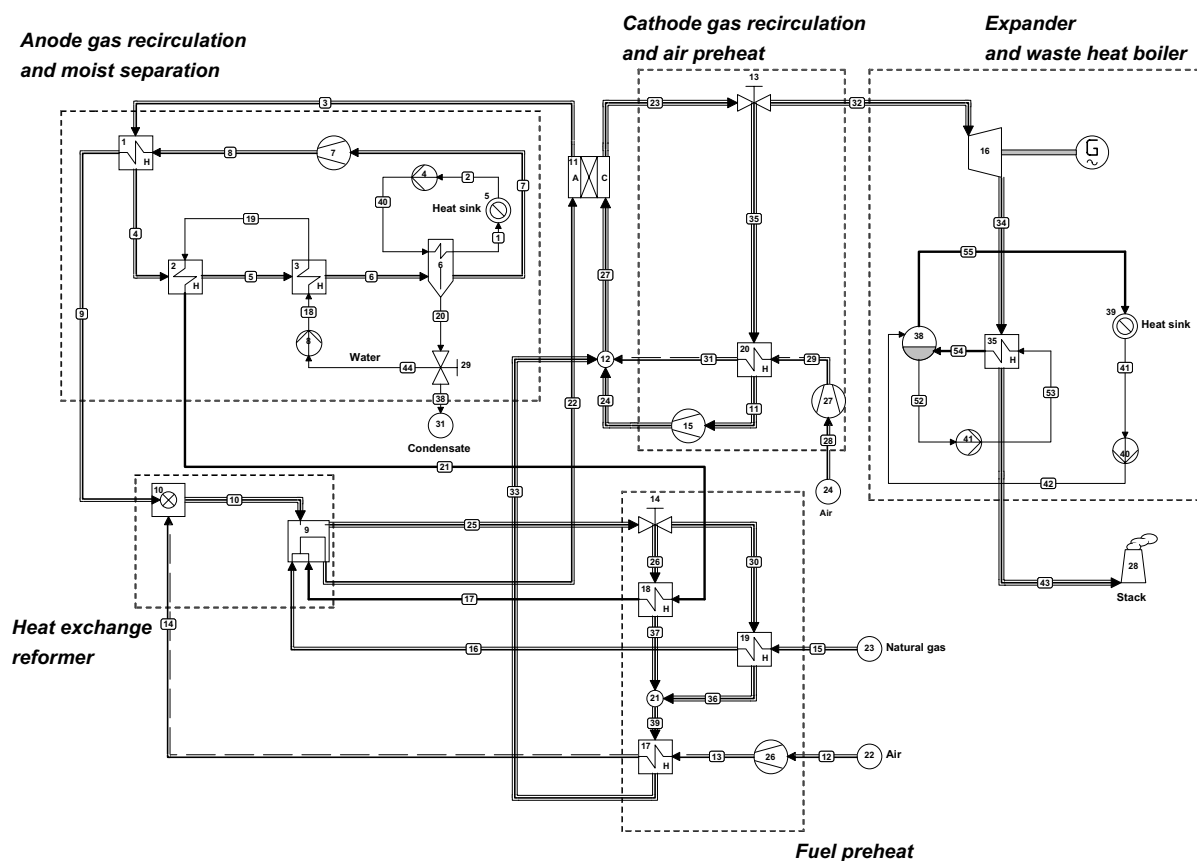


Figure 5.1. Flowsheet of the 250kW-class MCFC CHP plant (see Chapter 5)

Using this system as reference, the MCFC stack is substituted by an i-MCFC sub-model as shown by Figure 7.5.

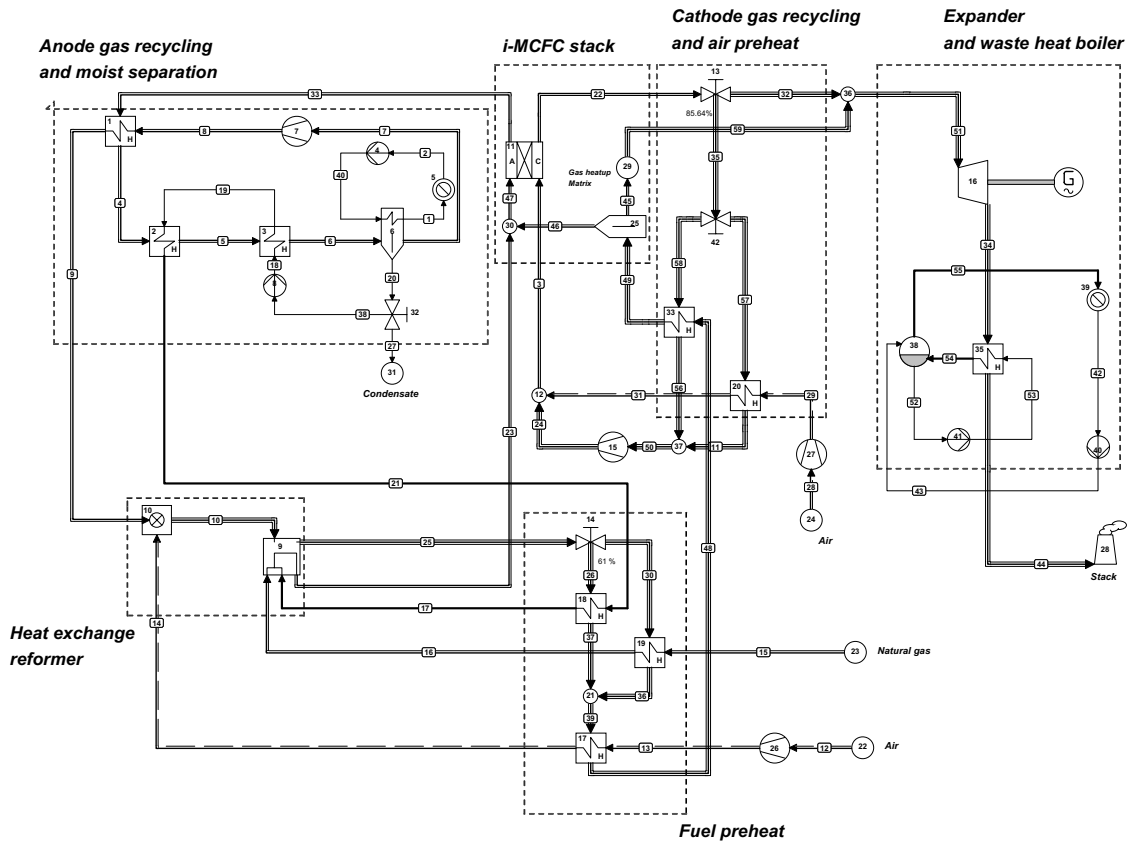


Figure 7.5. Flowsheet of the 250kW-class i-MCFC CHP plant

In the reference system, the required CO₂ for the cathode reaction is supplied by the flue gas of the heat exchange reformer (HER). This flue gas has the highest CO₂ concentration and therefore it is used here for feeding the matrix channel. Removing the connection to the cathode gas recycling results in a low CO₂ content of the cathode gas. This should bring down the NiO cathode dissolution to a negligible level (see references [12 - 14]). Before entering the matrix channel, the flue gas first goes to the fuel preheating stage (see Figure 7.5), and the heat of the flue gas is used for preheating fuel and air for the HER. As a result, the flue gas is cooled to a temperature of about 430°C and it needs to be heated again to the fuel cell entry temperature of 600°C. The existing heat exchanger that is used for preheating air for the cathode is therefore extended to incorporate a heating stage for the matrix gas. This heat exchanger is modeled by two parallel-connected heat exchangers. In practice, both heat exchangers can be integrated into a single unit, thus reducing investment costs. The matrix outlet is connected to the inlet of the expander and the exergy of this flue gas, and part of gas from the cathode outlet, is partly recovered by the expander and waste heat boiler.

7.3.2. Input parameters for the i-MCFC

The same input parameters of the reference MCFC stack are used here for the i-MCFC stack. The cell area (A_{cell}), fuel utilization (u_f) and current density i_{cell} are set the same as the reference MCFC stack. Temperature difference between the inlets and outlets ($T_{out}-T_{in}$) are also set equal to the reference. Following the experimental results of Peelen et al. [15], the cell performance of the reference MCFC stack is used for the i-MCFC as well. In this flowsheeting program, this is done by defining the total power output ($P_{el,AC}$) and cell voltage (V_{cell}). With the current density as the other required input, the program calculates the required cell area, which of course is here the same as the reference stack. Inverter efficiency (η_{DC-AC}) and pressure losses (Δp_i) are also set according to the reference system. Gas compositions and mass flows are calculated by the program.

Three input parameters that are specific for this i-MCFC model are the CO₂ molar flow from matrix to anode (Φ_{CO_2}), heating the matrix stream (Q_{matrix}) and pressure loss in the matrix channel (Δp_{matrix}). The CO₂ flow (Φ_{CO_2}) from the matrix flow to the anode inlet is calculated separately using equation (7.11) and set at the separator (apparatus 25, Figure 7.4). After the calculations, the accuracy of this flow is checked by comparing the gas compositions and mass flows of the anode outlet of the i-MCFC with the reference. Both must be the same. Q_{matrix} is calculated by the program and this is set at the fuel cell as heat dissipation. The pressure drop Δp_{matrix} is set at the same heat source that transfers heat to the matrix flow.

Table 7.1 summarizes the input parameters of the i-MCFC. The input parameters of the rest of the i-MCFC system are the same as the reference system described in Chapter 5. A detailed list of the input parameters is given in Table 5.1.

Table 7.1. Operating conditions and input parameters of the i-MCFC

Cell temperature T_{cell}	650 °C
Operating pressure p	4 bar
Fuel utilization u_f	70 %
Current density i_{cell}	1500 A/m ²
Cell voltage V_{cell}	0.8505 V
Cell Power output P_{cell}	306.19 kW
Inverter efficiency η_{DC-AC}	96 %
Temperature raise $T_{out}-T_{in}$	100 °C
Anode pressure loss Δp_{anode}	0.05 bar
Cathode pressure loss $\Delta p_{cathode}$	0.1 bar
Matrix pressure loss Δp_{matrix}	0.1 bar
CO ₂ molar flow Φ_{CO_2}	1.9433 mol/s
Heat transfer to matrix Q_{matrix}	14.19 kW

7.4. Results and discussions

Table 7.2 gives the resulting CO₂ and O₂ partial pressures and mass flow at the cathode inlet.

Table 7.2. p_{CO_2} and p_{O_2} of the cathode or matrix, and mass flows through the fuel cell.

	Reference	i-MCFC
p_{CO_2} (bar)	0.468 (cathode)	0.001(cathode) 1.890 (matrix)
p_{O_2} (bar)	0.262 (cathode)	0.378 (cathode)
$\Phi_{expander}$ (kg/s)	0.261	0.262
$\Phi_{cathode}$ (kg/s)	1.257	1.146
Φ_{anode} (kg/s)	0.053	0.053
Φ_{matrix} (kg/s)	-	<u>0.189</u>
Φ_{total} (kg/s)	1.310	1.388

It shows that the i-MCFC system concept has a much lower p_{CO_2} (0.001 bar) in the cathode and high p_{CO_2} (1.89 bar) in the matrix. The i-MCFC should operate under these gas compositions. With a p_{CO_2} in the cathode of 10^{-3} bar, the NiO cathode dissolution should reduce to a negligible level (see references [12 – 14]).

Table 7.3. Energy output and efficiencies of the reference and i-MCFC systems.

	Reference	i-MCFC
P_{FC} (kW)	306.19	306.19
$P_{expander}$ (kW)	60.05	60.34
P_{aux} (kW)	-77.58	-78.66
P_{net} (kW)	288.66	287.87
$(\eta_{net\ LHV})$	(51.77 %)	(51.63 %)
$(\eta_{net\ Ex})$	(49.70 %)	(49.56 %)
P_{steam} (kW)	91.59	91.98
P_{water} (kW)	109.49	109.49
P_{total} (kW)	489.74	489.34
$(\eta_{total\ LHV})$	(87.84 %)	(87.76 %)
$(\eta_{total\ Ex})$	(58.46 %)	(58.34 %)

Table 7.3 gives the energy output and efficiencies of the two systems. It shows that the overall efficiency η_{total} of this i-MCFC system is slightly lower than the MCFC. This is caused by the increased auxiliary power consumption. The cathode mass flow of the i-MCFC is lower but nevertheless, the total mass flow Φ_{total} (see Table 7.2) that is going through the cell is slightly higher than for the MCFC. This results in an increase of auxiliary power consumption. In theory, similar power output for both stacks should result in the same cooling requirements, and the total massflow through the stacks should be about the same. The difference in total massflow can be ascribed to the difference in gas composition and thus heat capacity of the cathode gas. CO₂ has a high heat capacity, and in the reference system, part of the CO₂ in the flue gas from the HER is recycled by the cathode recycling (Figure 5.1). In the i-MCFC system, this CO₂ is not recycled in any way but leaves the system via the expander. Therefore, the relative cooling capacity of the gas

flow through the i-MCFC is lower than the reference system, thus the total gas flow is here higher than the reference in order to meet the same cooling requirement.

The flowsheet calculation shows that the air input of the i-MCFC system is slightly higher than the reference resulting in a higher expander mass flow (Φ_{expander} , see Table 7.2). This increases the power consumption by the compressor, but part of this power is recovered by the expander. Finally, the i-MCFC system suffers from additional pressure loss from an extra heating stage that is required for heating up the matrix gas to fuel cell entrance temperature. This gas is driven by the anode recycle blower, and the additional pressure loss results in an increase in power consumption by this blower. The heat output of the i-MCFC system is slightly higher than the MCFC reference system. Production of hot water ($T = 80\text{ }^{\circ}\text{C}$) is the same but the amount of steam ($T = 180\text{ }^{\circ}\text{C}$) is slightly more (0.4 kW).

All together, the i-MCFC system performance is slightly lower than the reference system as shown by Table 7.3. The net power output is about 0.8 kW lower than the reference system resulting in a decrease of 0.14 %, point based on LHV, and a decrease of 0.10 % point, based on exergy. Due to the slightly higher steam output of the i-MCFC system, the decrease in overall CHP efficiency is only 0.08 % point, based on LHV, and 0.12 % point, based on exergy.

7.5. Conclusions

This present study shows that the i-MCFC concept with its unique three mass flows feature can be implemented in a MCFC system layout with just minor modifications to the reference system. When keeping the fuel cell performance the same, the overall system performance does not suffer significantly when the MCFC stack is substituted by an i-MCFC stack. The net power efficiency (η_{net}) of the system is about 0.15 % and 0.14 % lower than the reference MCFC system, based on the lower heating value and the exergy of the fuel input respectively. The decrease in overall CHP efficiency (η_{total}) is just 0.08 % and 0.11 % based on LHV and exergy respectively. An advantage of this system as implemented here is the elimination of the lifetime limiting NiO cathode dissolution. This is achieved by utilizing the unique feature of the i-MCFC of separating the CO₂ supply for the cell from the cathode gas. The p_{CO_2} of the cathode gas is here reduced from 0.468 bar

for the reference MCFC system to 0.012 bar for this i-MCFC system. This should sufficiently suppress the cathode dissolution.

Finally, it should be mentioned that the i-MCFC system that is presented here does not utilize the unique feature of active CO₂ separation from fuel gas by the matrix channel. This option promises enhanced system performance. The reference MCFC system we used does not allow this option without major system modification, which makes a proper comparison impossible. Other system studies are required in order to assess the possible improvement in system efficiency that fully exploits the features of the i-MCFC. Especially systems that are fueled by biogas and landfill gas are promising due to the low caloric value and high CO₂ content of these gasses.

References

- [1] K. Hemmes, W.H.A. Peelen, J.H.W. de Wit, *Molten carbonate fuel cell with separate CO₂ gas supply*, *Electrochemical and Solid State Letters*, **2** (3) pp.103-106 (1999)
- [2] Cycle-Tempo version 5.0, Delft University of Technology, Section Thermal Power Engineering; TNO Environment, Energy and Process Innovation, (2002).
<http://www-pe.wbmt.tudelft.nl/ev/cycle/cycle.html>
- [3] J.D. Fehribach, J.A. Prins-Jansen, K. Hemmes, J.H.W. de Wit, F.W. Call, *On modelling molten carbonate fuel-cell cathodes by electrochemical potentials*, *J Appl Electrochem*, **30** (9), pp.1015-1021, (2000)
- [4] J.P.P. Huijsmans, G.J. Kraaij, R.C. Makkus, G. Rietveld, E.F. Sitters, H. Th. J. Reijers, *An analysis of endurance issues of MCFC*, *J. Power Sources*, **86**, pp.117-121 (2000)
- [5] G. Cacciola, V. Antonucci, S. Freni, *Technology up date and new strategies in fuel cells*, *J. Power Sources*, **100**, pp.67-79 (2001)
- [6] R.C. Makkus, K. Hemmes, J.H.W. de Wit, *A comparative-study of NiO(Li), LiFeO₂, and LiCoO₂ porous cathode for molten-carbonate fuel-cells*, *J. Electrochem. Soc*, **141** (12), pp.3429-3438, (1994)
- [7] M. Mohamedi, Y. Hisamitsu, K. Kihara, T. Kudo, T. Itoh, I Uchida, *Ni-Al alloy as alternative cathode for molten carbonate fuel cells*, *J. Alloys and Compounds*, **315**, pp.224-233, (2001)
- [8] A. Lundblad, S. Schawantz, B. Bergman, *Effect of sintering procedures in development of LiCoO₂-cathode for the molten carbonate fuel cell*, *J. Power Sources*, **90**, pp.224-230, (2000)

- [9] B. Fang, H. Chen, *A new candidate material for molten carbonate fuel cell cathodes*, J. Electroanalytical Chemistry, **501**, pp.128-131, (2001)
- [10] A. Duairajan, H. Colon-Mercado, B. Haran, R. White, B. Popov, *Electrochemical characterization of cobalt-encapsulated nickel as cathode for MCFC*, J. Power Sources, **104**, pp.157-168, (2002)
- [11] M.J. Escudero, X.R. Nóvoa, T. Rodrigo, L. Daza, *Influence of lanthanum oxidized as quality promotor on cathodes for MCFC*, J. Power Sources, **106**, pp. 196-205, (2002)
- [12] J.D. Doyon, T. Gilbert, and G. Davies, *NiO Solubility in Mixed Alkali/Alkaline Earth Carbonate*. J. Electrochem. Soc., **134**, pp3035-3038 (1987)
- [13] M. L. Orfield and D. A. Shores, J. Electrochem. Soc., **136**, 2862 (1989).
- [14] K. Ota, S. Mitsushima, S. Kato, S. Asano, H. Yoshitake, and N. Kamiya, *Solubilities of Nickel Oxide in Molten Carbonate*, J. Electrochem. Soc., **139**, pp.667-671 (1992).
- [15] W.H.A. Peelen, K. Hemmes, G.P.J. Dijkema, *MCFC with separate CO₂ channel, a feasibility study on a type of fuel cell*, Delft University of Technology, (1998)
- [16] S.F. Au, N. Woudstra, K. Hemmes, *Assessment of Multistage Oxidation by Flowsheet Calculations on a Combined Heat and Power Molten Carbonate Fuel Cell plant*, Submitted to the Journal of Power Sources, (2002).

Chapter 8: Innovative Fuel Cell Concepts (part II)

Electrochemical conversion of solid fuel

Part of this chapter is published in the conference proceeding of the 3rd International Fuel Cell Conference, titled: FUEL CELLS THE NEXT STEP; ENERGY AND EXERGY ANALYSIS OF PARTIAL OXIDATION, DIRECT CARBON FUEL CELL AND INTERNAL DIRECT-OXIDATION CARBON FUEL CELL, By S.F. Au, W.H.A. Peelen, K. Hemmes and N. Woudstra, (1999).

Abstract

Reversible heat production is inevitable for hydrogen fuel cells. This chapter presents alternative fuel cell concepts that in theory do not produce reversible heat. The decrease of entropy associated with the decrease in gas molecules causes the reversible heat production. Several innovative fuel cell concepts are presented that do not reduce the amount of gas molecules hence in theory eliminates the reversible heat production. Two fuel cell concepts are introduced that absorb heat and convert this heat into work: the Direct Carbon Fuel Cell (DCFC) and the Internal Direct-Oxidation Carbon Fuel Cell (IDOCFC). Both innovative fuel cell concepts are electrochemical gasification processes that produce valuable chemical feedstock next to electricity making them attractive alternative concepts. This chapter continues with the analyses of energy and exergy balances of these two concepts. The exergy efficiencies are calculated and compared with their conventional counter parts under ideal conditions. By defining these systems ideally, the theoretical ultimate performance limit can be identified which helps setting goals and directions where large advantages over conventional systems may be achieved. The exergy analyses show that electrochemical conversion is indeed a preferable process. The hypothetical DCFC absorbs heat and converts it into power. The IDOCFC almost completely maintains the thermodynamic advantages of the DCFC. Moreover, the

IDOCFC may practically be more convenient to realize since it is based on present technologies and a gaseous reactant (CO) is here converted electrochemically instead of a solid (C).

8.1. Introduction

After two centuries in which electrochemical energy conversion has had a chance to develop, we have entered the next century and millennium in which electrochemical energy conversion is expected to play an essential role [1]. Electrochemical processes are in theory capable of converting energy without exergy loss, hence fuel cells promise improved conversions efficiency over conventional combustion techniques. Although fuel cells can be operated reversibly, they still produce reversible heat due to the second law of thermodynamics. Hence part of the enthalpy of the fuel is released as heat and not as electric work, even when is the fuel cell is operated reversibly!

This chapter discusses the cause of reversible heat production and presents alternative fuel cells concepts that in theory do not produce reversible heat. Two interesting fuel cell concept are further examined by evaluating the exergy balances of these concepts. The two fuel cell concepts are:

1. Direct Carbon Fuel Cell (DCFC)
2. Internal Direct-Oxidation Carbon Fuel Cell (IDOCFC).

Both concepts produces valuable chemical feedstock next to electricity and in theory they absorb heat and convert this heat fully into work (see references [2, 3]). The theoretical limits of these processes are compared with the theoretical limits of conventional processes by defining these systems ideally. Identifying the theoretical ultimate limits of processes can help setting goals and directions where we may achieve large advantages over conventional systems including current state of the art fuel cell systems.

8.2. Theory

In general, fuel cells are electrochemical devices that convert the Gibbs energy Δg of hydrogen oxidation reaction into electricity.



In chapter 4, it is discussed that when the hydrogen fuel cell is operated reversibly, part of the enthalpy Δh is converted into electricity while the amount of $T\Delta s$ is released as reversible heat. The cause of this reversible heat production is that the amount of gas molecules is reduced from one and a half gas molecules to one (see equation (8.1)). Hence the entropy associated with the amount of gas molecules is reduced. The amount of $T\Delta s$ ¹⁾ of reversible heat is produced to fulfill the requirement of zero entropy production of a reversible process. This reversible heat production is inevitable for the hydrogen oxidation process and it increases linearly with the operating temperature. At elevated temperature, the reversible heat production results in the need for a bottoming cycle to recover the exergy of this heat (see paragraph 4.3).

A possibility to circumvent the need for a bottoming recovery cycle is to operate the hydrogen fuel cell at ambient temperature. Operating at ambient temperature reduces the reversible heat production but it requires the use of costly catalyst materials (platinum for example) for the electrode due to the poor kinetics. Moreover, the heat produced by irreversible losses represents little exergy and the irreversible heat losses are of little use.

An alternative in reducing the reversible heat production is using other fuel with electrochemical oxidation processes in which the amount of gas molecules is not reduced. We can distinguish two categories of processes:

1. Process that produces an equal amount of gas molecules, hence with a reversible heat production $T\Delta s = 0$.
2. Processes that increase the amount of gas molecules, hence with a reversible heat absorption $T\Delta s > 0$ ²⁾.

¹⁾ In a fuel cell, the gas partial pressures in the anode and cathode also play a role in the reversible heat production, as can be seen from the Nernst equation for the Open Cell Voltage (OCV). The effect of gas partial pressure is here neglected.

²⁾ The sign convention is that $Q > 0$ when heat is absorbed and $Q < 0$ when heat is released.

8.2.1. Fuel cell processes with zero reversible heat production

Electrochemical oxidation of methane (CH₄) and carbon (C) are examples of processes that in theory do not produce reversible heat. The oxidation reactions are:



Methane is considered as the ideal fuel for fuel cells due to its availability. Direct electrochemical conversion is however not possible due to the slow electrode kinetics hence steam reforming to hydrogen is required. High temperature fuel cell can be designed to have the reforming process take place near the anode hence partly maintaining the thermodynamic advantage. An example of an internal reforming high temperature fuel cell is the Direct FuelCell© of Fuel Cell Energy Inc. [4].

The principle of electrochemical oxidation of carbon is already mentioned by Becquerel [5] a century ago. Technical problems and lack of interest had stopped this conversion process to mature. Several attempts in using carbon as fuel for fuel cells have been published recently [6-10], and in particular Cooper et al [10] of the Lawrence Livermore National Laboratory (LLNL) have made great progress. Cooper introduced the Direct Carbon Conversion Cell (DCCC) that electrochemically converts crystallographic disordered carbon particles to CO₂ (see Figure 8.1).

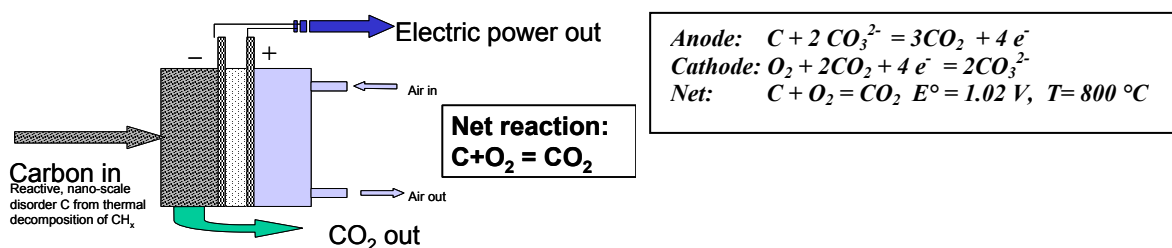


Figure 8.1. Schematic representation of the Direct Carbon Conversion Cell of the Lawrence Livermore National Laboratory, (figure taken from reference [10]).

The high reactivity of the disordered carbon solves some of the technical problems encountered in the past. The DCCC is derived from the MCFC and it shares the same electrolyte, electrolyte support matrix and cathode. The anode consists of carbon particles that serve both as fuel and as electrode. Carbon fuel is fed pneumatically into the cell using CO_2 as a carrier gas. Since CO_2 is the only product leaving the anode exhaust, it can be easily recycled for the pneumatic transport and the off-gas can be stored with little effort to meet future stringent emission requirement [10]. In principle, the cell operates at 100% fuel utilization with zero Nernst loss. The operation of the DCCC has been proven on small laboratory and the measured performance of the lab scale DCCC is given in Figure 8.2.

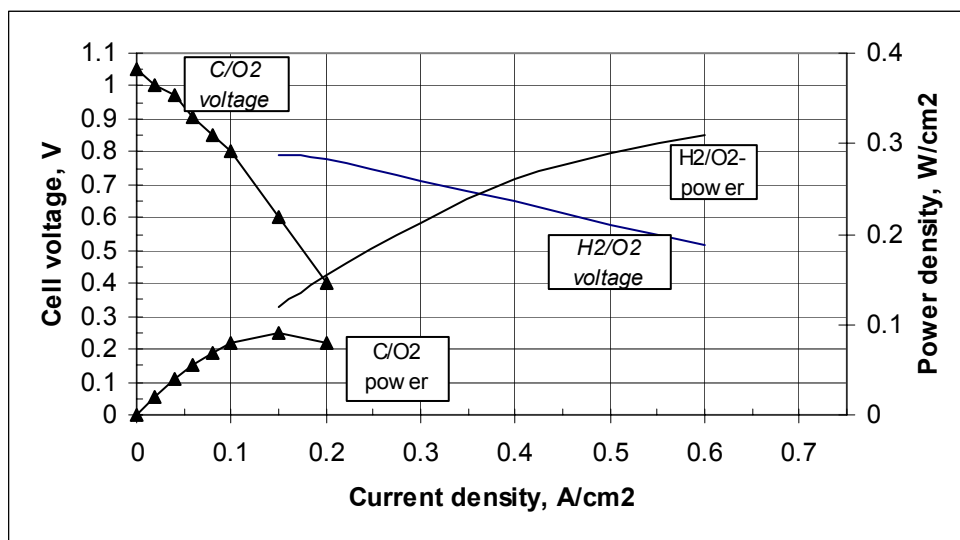


Figure 8.2. Polarization curve and power density of the lab scale DCCF (C/O_2) and a comparison with the SOFC (H_2/O_2), (figure taken from reference [10]).

An engineering concept is made to study the cost of the DCCC (see Figure 8.3) and it has resulted in an estimate of operating costs of 473 US\$ / kW [10].

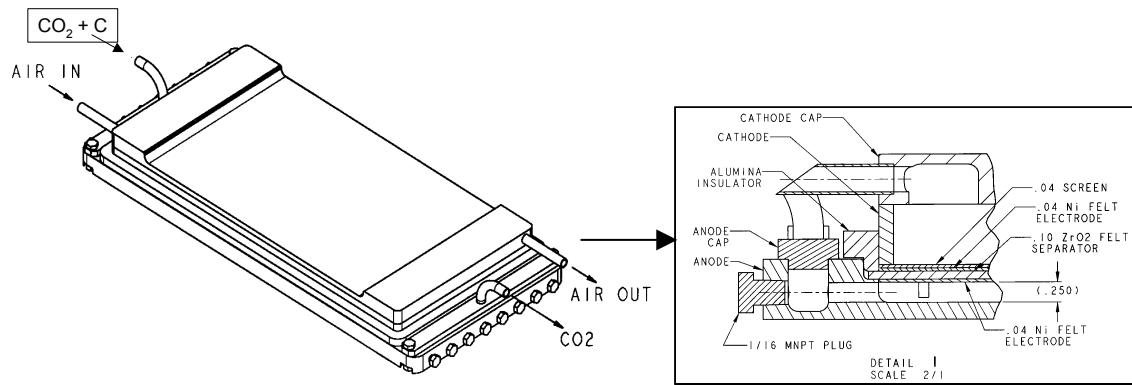


Figure 8.3. Engineering design of a 100 W DCCC by Lawrence Livermore National Laboratory, (figure taken from reference [10]).

8.2.2. Fuel cell concepts with reversible heat absorption

In theory, any electrochemical oxidation process that produces less gas molecules than it uses will absorb reversible heat. Liquid or solid fuels are excellent candidates for these fuel cell concepts due to their low entropy compared to gaseous fuels. Most available liquid fuels however are less electrochemical reactive, or they have lower boiling point than the main product water. The latter means that fuel needs to be evaporated or the main product of the fuel cell is liquid water, depending on the operating temperature. Hence, in both cases, the overall entropy associated with the reactants and product is reduced resulting in reversible heat production.

Solid carbon is an interesting fuel for heat absorbing fuel cells and Hemmes [1] previously introduced the Direct Carbon Fuel Cell (DCFC) concept that electrochemically oxidizes solid carbon. In contrast to the Direct Carbon Conversion Cell, discussed in previous paragraph, the DCFC partially oxidizes C to CO resulting in an increase of gas molecules:



This partial oxidation process is thermodynamically³⁾ favored over the combustion process (reaction (8.3)) at high temperature (see Section 8.3.4). The carbon fuel can be made from biomass or coal similar to that of the DCCC. Although the product CO is toxic to human

³⁾ Kinetically however, CO₂ is more often observed as product even at temperature as high as 1000°C [11].

and animals, it is also a valuable feedstock for the chemical industry. Hence, the DCFC combines the production of chemical feedstock and the production of electricity and can be considered as *electrochemical gasification*. Chemical feedstock is now made from oil and the DCFC may help reducing the load on world's oil resources by changing the fuel from oil to biomass or coal.

The dual-purpose DCFC seems to be very attractive. The next paragraph presents a comparison of exergy balances of the DCFC with several conventional techniques in power generation and gasification to study their theoretical limits under ideal conditions.

8.3. Exergy balances of idealized power generation and gasification processes

8.3.1. Standard exergy values for several species

The exergy of several species are calculated using available thermodynamical data from reference [12]. Exergy values are calculated for the temperature of 1200 K and are given in Table 8.1. The method used for calculating the exergy is given in Appendix A. The process temperature is chosen at 1200 K since the formation of CO is thermodynamically favored over that of CO₂ at high temperature. This temperature is still moderate hence avoiding costly construction materials. The reference conditions, under which the exergy of O₂ and CO₂ are assumed to be zero are given in Table 8.2.

Table 8.1. Exergy of C, CO, CO₂, H₂, H₂O and O₂ at 1200K.

$Ex^{C(s)}$	419.1 kJ/mol
$Ex^{CO(g)}$	290.9 kJ/mol
$Ex^{CO_2(g)}$	45.0 kJ/mol
$Ex^{H_2(g)}$	249.7 kJ/mol
$Ex^{H_2O(g)}$	27.7 kJ/mol
$Ex^{O_2(g)}$	20.4 kJ/mol

Table 8.2. Reference conditions.

T_0	298 K
$p_0^{H_2O}$	0.0312 bar
$p_0^{O_2}$	0.203 bar
$p_0^{CO_2}$	0.0003 bar

The exergy efficiency η_{EX} of a process is defined as the ratio of the total exergy output Ex_{out} over the total exergy input Ex_{in} :

$$\eta_{EX} = \frac{Ex_{out}}{Ex_{in}} \quad (8.5)$$

Note that throughout this chapter, the absolute temperature T [K] is used and p^i symbolize the partial pressure of the specie i .

8.3.2. Combustion process for power generation

In conventional power generation processes, fuel is combusted and the amount of heat of the exothermic reaction is further converted into work. The combustion of hydrogen is taken here as an example.

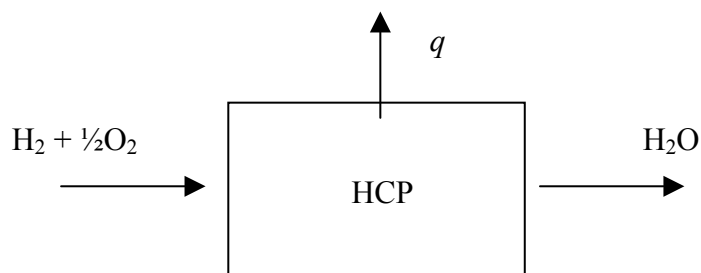


Figure 8.4. Schematic representation of a Hydrogen Combustion Process (HCP)

This process chemically converts H_2 and O_2 into H_2O . The overall reaction is



The change in enthalpy is released as heat $q = 249$ kJ/mol.

The exergy input and output of the HCP are

$$\sum Ex_{in} = 1 * Ex^{H_2} + 0.5Ex^{O_2} = 260 \text{ kJ/mol} \quad (8.7)$$

$$\sum Ex_{out} = 1 * Ex^{H_2O} + q \left(1 - \frac{T_0}{T} \right) = 215 \text{ kJ/mol} \quad (8.8)$$

The exergy efficiency of the HCP is then

$$\eta_{Ex}^{HCP} = 0.826$$

This is the efficiency we can get when the entire exergy of heat can be utilized and therefore represent the theoretical maximum. Even then, it shows that about 17 % of the exergy is lost simply by combustion. Better alternatives are therefore desired.

8.3.3. Hydrogen Fuel Cell for power generation

The fuel cell type commonly presented is the hydrogen fuel cell. This type of fuel cell is schematically depicted in Figure 8.5.

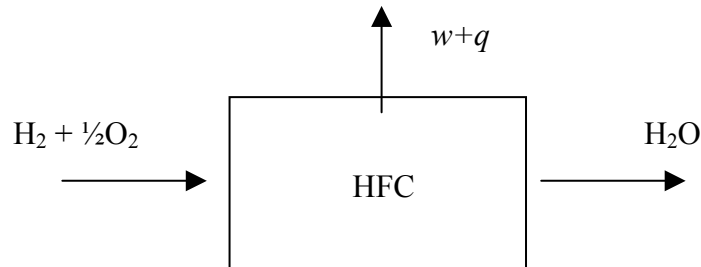


Figure 8.5. Schematic representation of a Hydrogen Fuel Cell (HFC)

These devices electrochemically convert H_2 and O_2 into H_2O . The overall reaction is



The change in Gibbs energy is converted into electrical work

$$w = \Delta g = \Delta h - T\Delta s \quad (8.10)$$

The amount of heat $q = T\Delta s$ is dissipated as to fulfill the overall $\Delta s = 0$, as required for a reversible process.

Assuming $p^{H_2} = 1$, $p^{O_2} = 0.203$ (i.e. air) and $p^{H_2O} = 1$ the changes in Δg and thus amount of work is calculated to be: $w = 173$ kJ/mol. Since work is released here as electricity, the resulting exergy released is equal to this work. The amount of heat dissipated is equal to $q = T\Delta s = 75$ kJ/mol.

The exergy input and output of the HFC are

$$\sum Ex_{in} = 1 * Ex^{H_2} + 0.5 Ex^{O_2} = 260 \text{ kJ/mol} \quad (8.11)$$

$$\sum Ex_{out} = 1 * Ex^{H_2O} + w + q \left(1 - \frac{T_0}{T} \right) = 258 \text{ kJ/mol} \quad (8.12)$$

The exergy efficiency of the HFC is then

$$\eta_{Ex}^{HFC} \approx 1$$

This result shows that this conversion takes place with no exergy loss, which is consistent with the assumption that the electrochemical process is reversible. Deviation from unity is probably due to the uncertainty in the thermodynamic data given by reference [12].

Note that HFC system discussed here is equivalent to a combination fuel cell-power cycle system driven both reversibly (see paragraph 4.3.1). These systems are often evaluated using the definition of thermal efficiency, i.e

$$\eta_{th} = \frac{w}{\Delta_f h^0} \quad (8.13)$$

Using this definition the efficiency of the HFC is 94 % (see Paragraph 4.3.1). The evaluation by thermal efficiency is in some way misleading since it stresses that 6 % of the enthalpy is lost by this conversion process. Hence, it gives the impression that it may be possible to improve the efficiency of this process by a couple of percent. The exergy evaluation given here shows that the thermodynamic ultimate is achieved, hence excluding any possible way of improvement for this conversion. Therefore in this and similar situations where energy is converted into work, evaluations based on exergy analysis are more suitable than evaluations based on energy analysis.

8.3.4. Gasification by Partial Oxidation

This partial oxidation process gasifies carbon into CO (and some CO₂), shown in Figure 8.6.

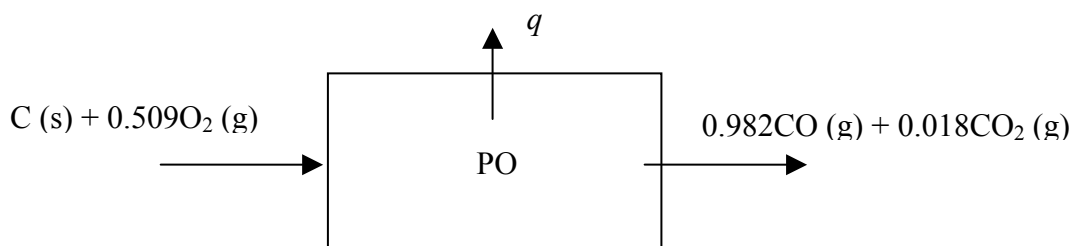


Figure 8.6. Schematic representation of the P.O.

Carbon and oxygen react chemically into an equilibrium mixture of CO and CO₂. This overall reaction is an exothermal reaction so heat is released, represented by q . Figure 8.6 shows also the molar flows of this process.

We assume: 1) reactions are in equilibrium, 2) carbon is in excess available and 3) both CO and CO₂ are produced. This leads to a combination of these chemical reactions

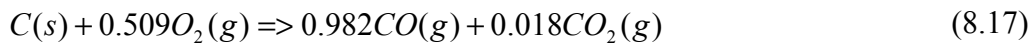


The equilibrium constants at 1200 K of these reactions are respectively: $K = 3.032E+09$ and $K = 1.74E+17$, which indicates that all the oxygen will react with carbon into both CO and CO₂.

Next, the fraction CO and CO₂ is calculated using the Boudouard equilibrium, given by



Using the $\Delta_f h^0$ of CO and CO₂ at 1200 K we can calculate the fractions CO and CO₂ at equilibrium, which are: $p_{CO} = 0.982$; $p_{CO_2} = 0.018$. Using these results, we derive the molar balance of the P.O., shown by Figure 8.6.



Calculation of the energy balance of reaction (8.17) using $\Delta_f h^0$ of CO and CO₂ at 1200K shows that this reaction is an exothermic reaction and the amount of heat released by this reaction is: $q = \sum \Delta_f h^0 = -118 \text{ kJ/mol}$

From the input and the output given by Figure 8.6, we can calculate the total amounts of exergy going in and out of the system

$$\sum Ex_{in} = 1 * Ex^C + 0.509Ex^{O_2} = 429 \text{ kJ/mol} \quad (8.18)$$

$$\sum Ex_{out} = 0.982 * Ex^{CO} + 0.018 Ex^{CO_2} + q \left(1 - \frac{T_0}{T} \right) = 375 \text{ kJ/mol} \quad (8.19)$$

The exergy efficiency of this P.O process is then calculated as

$$\eta_{Ex}^{PO} = 0.873$$

This result shows that in ideal situation about 13% of exergy is lost due to the irreversibility of this chemical reaction. Having this process take place at higher temperature may reduce this loss due to the exergy of q (i.e. larger part of the heat q can be converted into work).

8.3.5. Direct Carbon Fuel Cell for power generation and gasification

The DCFC is briefly described in paragraph 8.2.2 and it is still a hypothetical concept. The mass and energy flows of the DCFC is schematically depicted in Figure 8.7.

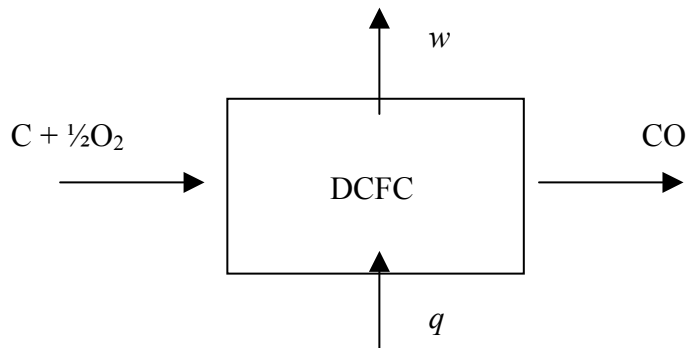


Figure 8.7. Schematic representation of the DCFC

Carbon and oxygen are assumed to be electrochemically converted into CO at 1200K and 1 bar.



Similar to the hydrogen fuel cell, the changes in Gibbs energy are converted into electrical

work (8.10). Since reversibility is assumed, the DCFC necessarily also converts addition heat $q = T\Delta s$ into work.

Assuming $p^{CO} = 1$ and $p^{O_2} = 0.203$ (i.e. air) the changes in Δg and thus amount of work is calculated to be: $w = 210$ kJ/mol. Since work is released here as electricity, the resulting exergy released is equal to this work. The total enthalpy change is: $\Delta_f h^0 (T=1200K) = -130$ kJ/mol, which results into an amount of heat absorbed equals to: $q = w + \Delta_f h^0 = 96$ kJ/mol.

The exergy input and output of the DCFC are

$$\sum Ex_{in} = 1 * Ex^C + 0.5 Ex^{O_2} + q \left(1 - \frac{T_0}{T} \right) = 502 \text{ kJ/mol} \quad (8.20)$$

$$\sum Ex_{out} = 1 * Ex^{CO} + w = 501 \text{ kJ/mol} \quad (8.21)$$

The exergy efficiency of this DCFC process is calculated as

$$\eta_{Ex}^{DCFC} \approx 1$$

This result shows that this conversion takes place with no exergy loss, which again is consistent with the assumption that the electrochemical process is reversible. In addition, the small deviation from unity is probably due to the uncertainty in the thermodynamic data given by reference [12]. Since the whole amount of q and not $q(1-T_0/T)$ is transferred into work, heat can electrochemically be transferred fully into work and the Carnot limitations seems to be circumvented. However, this is off course only one part of the system. The exergy efficiency shows that this can only be achieved in close combination with another process, which in its turn introduces exergy loss (or entropy production) resulting in a system, which does obey the second law of thermodynamics i.e. $\Delta s \geq 0$ or equivalently $\eta_{Ex} \leq 1$.

In the previous calculation we have assumed that the heat needed for the DCFC was already available at $T = 1200$ K. A possible source of heat is the sun, which provides heat for a solar oven. In this case, we assume that the temperature of the sun is 6000 K [13] and the overall exergy efficiency therefore becomes

$$\eta_{Ex}^{DCFC*} = 0.961$$

Here we see that this highly idealized system exhibits an exergy loss of about 4%.

In the cases where no external heat source is available, heat can be provided by direct combustion of carbon into CO_2 or partial oxidation into CO :



The change of enthalpy by these reaction is $\Delta_f h^0$ is -395 kJ/mol and -113 kJ/mol for reaction (8.22) and (8.23) respectively. Using $q = 96$ kJ/mol necessary for the DCFC, the total process changes into processes shown by respectively Figure 8.8 and Figure 8.9

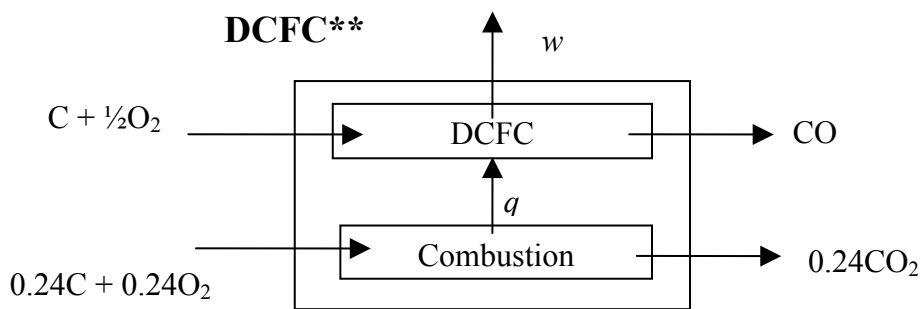


Figure 8.8. Schematic representation of the DCFC** with no external heat-source but direct combustion of carbon to CO_2 .

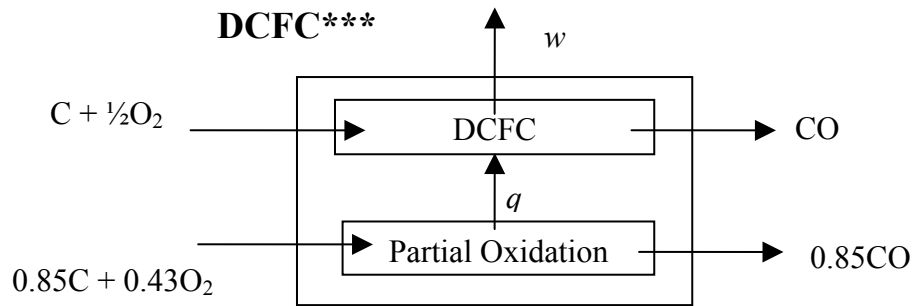


Figure 8.9. Schematic representation of the DCFC*** with no external heat-source but partial oxidation of carbon to CO.

Both processes can be evaluated with the DCFC by calculating their exergy efficiencies.

The exergy input and output of the DCFC** are

$$\sum Ex_{in} = 1.24 * Ex^C + 0.74Ex^{O_2} = 536 \text{ kJ/mol} \quad (8.24)$$

$$\sum Ex_{out} = 1 * Ex^{CO} + 0.24 * Ex^{CO_2} + w = 512 \text{ kJ/mol} \quad (8.25)$$

The exergy efficiency of this DCFC** process is calculated as

$$\eta_{Ex}^{DCFC^{**}} = 0.955$$

The exergy input and output of the DCFC*** are

$$\sum Ex_{in} = 1.24 * Ex^C + 0.74Ex^{O_2} = 797 \text{ kJ/mol} \quad (8.26)$$

$$\sum Ex_{out} = 1 * Ex^{CO} + 0.24 * Ex^{CO_2} + w = 749 \text{ kJ/mol} \quad (8.27)$$

The exergy efficiency of this DCFC** process is calculated as

$$\eta_{Ex}^{DCFC^{**}} = 0.940$$

We see that in both cases, the conversions are no longer perfect and exergy is lost. The exergy lost is entirely caused by the irreversibility of the combustion processes. Since the dissipated heat from this combustion process is assumed to be directly converted into power by the DCFC, the exergy loss is still fairly small, especially compared with the Partial Oxidation process (paragraph 8.2.3).

8.3.6. Internal Direct-Oxidation Carbon Fuel Cell

The Internal Direct-Oxidation Carbon Fuel Cell (IDOCFC) process is introduced by Nakagawa [7] and it is shown by Figure 8.10.

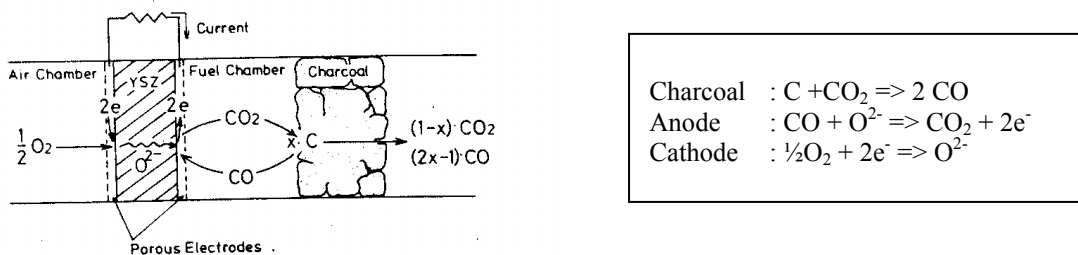


Figure 8.10. Internal Direct-Oxidation Carbon Fuel Cell (IDOCFC) presented by Nakagawa, taken from reference [7].

In the IDOCFC, carbon in the charcoal is gasified to CO by the Boudouard reaction. The CO is electrochemically converted to CO₂ by a SOFC and electrical work is delivered.

An alternative to this concept was presented by Peelen et al [9] that uses molten carbonate as molten salt gasifier combined with the tubular SOFC as manufactured by Siemens-Westinghouse [14]. High temperature heat is supplied externally by solar ovens using the molten carbonate of the gasifier as heat carrier.

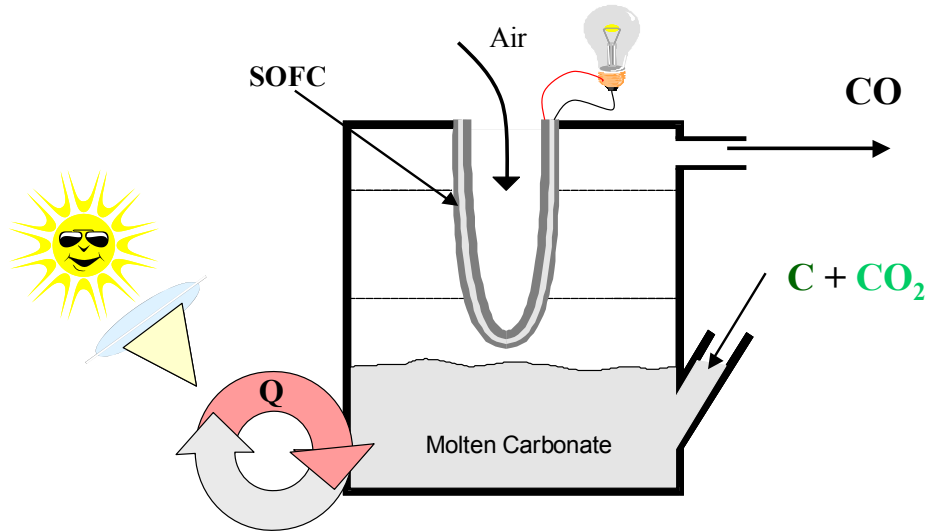


Figure 8.11. Alternative concept for the IDOCFC presented by Peelen et al [9].

Figure 8.12 gives a schematic representation of mass and energy flows the IDOCFC. Note that the IDOCFC has the same input and output as the DCFC

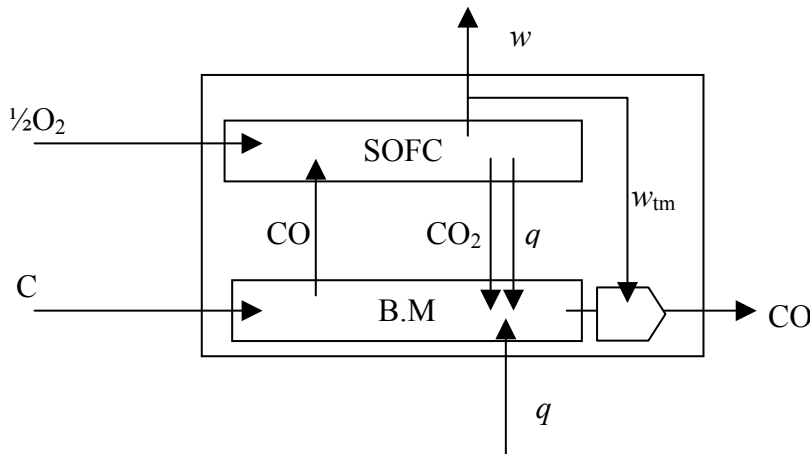


Figure 8.12 Mass and energy flows of the IDOCFC.

This process is a combination of a hypothetical Boudouard machine (B.M.) and a solid oxide fuel cell (SOFC). The B.M. reversibly converts carbon into CO given by reaction (8.16). This Boudouard reaction is an endothermic reaction with an enthalpy change of $\Delta h = +169 \text{ kJ/mol}$. Part of this heat is provided by the exothermic reaction of the SOFC and it is assumed here to be transferred ideally.

Overall, the SOFC converts CO and O₂ electrochemically into CO₂



The SOFC's anode is fed directly by the B.M. Assuming equilibrium, the anode gas composition is given by Boudouard reaction, i.e. $p_{CO} = 0.982$; $p_{CO_2} = 0.018$ ($T = 1200$ K). The work delivered by the SOFC is equal to the total change in Δg . By assuming the cathode is fed with air (i.e. $p_{CO_2} = 0.203$), the amount of work is calculated to be: $w = -\Delta g = 210$ kJ/mol. This work is released as electricity and the resulting exergy released thus equal that amount. The heat released by the SOFC reaction is the difference between the changes in the enthalpy and the Gibbs free energy: $q_{SOFC} = \Delta h - \Delta g = -71$ kJ/mol. Combined with the heat needed for the Boudouard reaction, the heat absorbed by the total IDOCFC is: $q = \Delta h_{bm} - q_{sofc} = +97$ kJ/mol.

Combination of reaction (8.16) and (8.28) shows more CO is produced by the B.M. than converted by the SOFC. We here assume that only CO is released from the IDOCFC by first compressing it into $p_{CO} = 1$ and than selectively releasing it using an ideal membrane. The thermo-mechanical work needed for the compressing CO from 0.982 to 1 bar equals to $w_{tm} = 0.18$ kJ/mol.

The exergy input and output of the IDOCFC are

$$\sum Ex_{in} = 1 * Ex^C + 0.5 Ex^{O_2} + q \left(1 - \frac{T_0}{T} \right) = 502 \text{ kJ/mol} \quad (8.29)$$

$$\sum Ex_{out} = 1 * Ex^{CO} + w - w_{tm} = 500 \text{ kJ/mol} \quad (8.30)$$

For the IDOCFC, these results show an exergy efficiency of

$$\eta_{Ex}^{IDOCFC} \approx 1$$

This is the same as the efficiency of a DCFC, which is no surprise a thermodynamical

point of view. Both processes have same input and output and the processes take place inside the system are assumed to be reversible. Therefore, the exergy efficiency of the overall processes will always be 100 %, as verified by the calculations

Since DCFC and IDOCFC are thermodynamically equivalent, the exergy efficiency of the IDOCFC-derivatives with heat provided by solar-oven or carbon combustion will therefore also be the same.

As an alternative to the proposed SOFC used inside the IDOCFC, a MCFC can also be used for the electrochemical conversion as shown by Figure 8.13. Both forms of IDOCFC are thermo dynamical equivalent and show therefore the same thermo dynamical advantages.

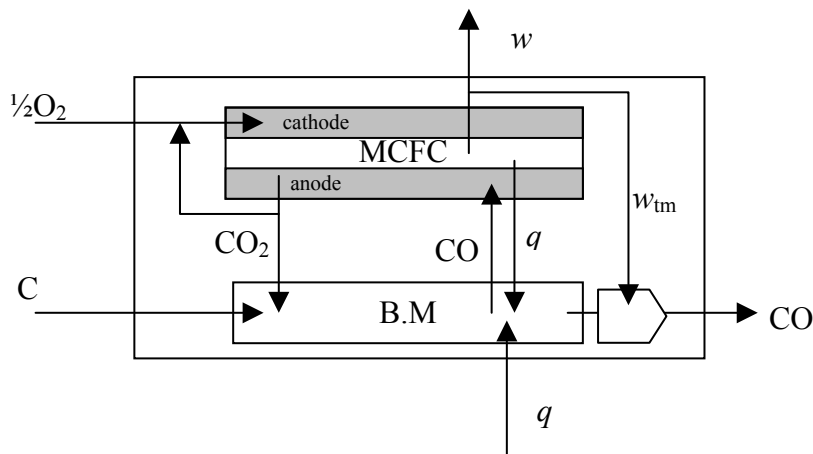


Figure 8.13. IDOCFC with an MCFC for the electrochemical conversion.

8.4. Conclusions

Not surprisingly, the exergy analyses show that electrochemical conversion is indeed a preferable process in order to fully utilize the exergy of fuel. Both the Direct Carbon Fuel Cell (DCFC) and the Internal Direct-Oxidation Carbon Fuel Cell (IDOCFC) concepts have shown to be attractive alternatives in electricity and chemical feedstock productions. The IDOCFC may be more convenient to realize in practice since a gaseous reactant (CO) is converted here electrochemically instead of solid (C) as for the DCFC. Furthermore, this

IDOCFC is based on technologies already available today, which reduces the technological investment in the development.

So far non of the irreversible losses were taken into account. In practice of course, these losses will occur due to kinetic limitation (e.g. in the Fuel Cell and in the Boudouard machine), diffusion, ohmic losses, heat transfer etc. At this point, both the DCFC and IDOCFC can have a definite advantage above “conventional” Fuel Cells (MCFC, SOFC, PAFC, PEMFC etc.). Having heat as input rather than output means that part or all of these internal irreversible losses in the form of heat “dissipation”, can theoretically also be converted into work. This may result in exergy efficiencies not much lower than the theoretical ultimate suggesting possible large advantages over conventional systems, including state of the art fuel cell systems. Therefore both the DCFC and the IDOCFC are promising fuel cell concepts.

References

- [1] K. Hemmes, *The role of electrochemistry in the energy supply of the 21st Century*. In Proc. of the 50th ISE meeting, Pavia (Italy), (1999)
- [2] A.J. Appleby and F.R. Foulkes, in *Fuel Cell Handbook*, Van Nostrand Reinhold, New York, (1989).
- [3] K. Hemmes, in Proc. of the 6th Int. Symp. On MCFC Technology. Eds. K. Hemmes, Lindbergh, S.R. Narayanan, J.R. Selman, D. A. Shores, and I. Uchida, *The Electrochemical Softbound Proc. Series*, Pennington, NJ, (1999).
- [4] Fuel Cell Energy, Inc. USA; <http://www.fce.com>
- [5] A.C. Becquerel, *Traité d'Electricité*, I, Paris, (1855)
- [6] D.G. Vutetakis, D.R. Sidmore, H.J. Byker, *Electrochemical oxidation of molten salt carbonate-coal slurries*, p. 3037-3035, *Journal of the Electrochemical Society*, Pennington, **134** (12), NJ, USA, (1987)
- [7] N. Nakagawa and M. Ishida, *Performance of an Internal Direct Oxidation Carbon Fuel Cell and its Evaluation by Graphic Exergy Analysis*. *Ind. Eng. Chem. Res.* **27**, 1181-1185, (1988)
- [8] W.H.A. Peelen, M. Olivry, S.F. Au, J.D. Fehribach and K. Hemmes, *Electrochemical oxidation of Carbon in a 62/38 mol% Li/K Carbonate Melt*, p. 1389-1395, *Journal of Applied Electrochemistry*, **30**, Kluwer Academic Publisher, (2000).
- [9] W.H.A. Peelen, K. Hemmes and J.H.W. de Wit, *Carbon a major energy*

carrier for the future? Direct carbon fuel cells and molten salt coal/biomass gasification. High Temp. Mater. P.-US 2: (4), pp471-482 (1998)

- [10] J.F. Cooper, N. Cherepy, R. Upadhye, A. Pasternak, M. Steinberg, *Direct carbon conversion: Review of production and electrochemical conversion of reactive carbons, economics and potential impact on the carbon cycle.* US Department of Energy & Lawrence Livermore National Laboratory, UCRL-ID-141818, (2000).
- [11] J.F. Cooper, private communication.
- [12] D.R. Lide, Handbook of Chemistry and Physics 76th edition, CRC-Press, (1995).
- [13] Encarta 97 Encyclopaedia, Microsoft, (1996).
- [14] <http://www.siemenswestinghouse.com/en/fuelcells/sofc/index.cfm>

Chapter 9

Conclusions and Discussions

The objective of this thesis is to obtain profound knowledge in the overall fuel cell process and the interactions in a fuel cell system. The results of this study have shown two important aspects:

1. The usefulness of simplified approach for complex systems and the general understanding of the thermodynamic basis.
2. Detailed flowsheet calculations and analyses brought out important effects that are concealed otherwise.

9.1. Simplified approaches

The processes that take place inside a fuel cell are very complex. Transport of species, heat transfer, chemical and electrochemical reactions are just some of the processes that take place inside the fuel cell. The influence of all these processes on the operating condition of a fuel cell can be combined into a single experimental parameter r and Standeart has made further simplification that resulted in two analytical models. These models are named the Simple Model and the Extended Model and they are introduced in Paragraph 2.2.2 of this thesis. The Simple Model describes a simple bi-linear relation of the cell performance while the Extended Model is non-linear and contains corrections terms to the Simple Model. Both models are verified with experiments on a Molten Carbonate Fuel Cell (MCFC) and the results are described in Section 2.4. Although the processes that take place inside a fuel cell are highly non-linear, the experimental results for an MCFC can be perfectly described by a bi-linear function. The simple approach is therefore sufficient in describing the operating characteristic of the MCFC. This Simple Model has the advantages in the transparency in which reversible and irreversible processes can be distinguished. This advantage is used in Chapter 4 when the influence of fuel cell operating

temperature on the system efficiency of a fuel cell-power cycle hybrid system is studied in theory. After studying the ideal situation, the effects of Nernst loss and irreversible losses were studied using this Simple Model. From this, it is clear that the MCFC produces most of its heat by the reversible electrochemical process while the contribution from irreversible losses is relatively small. Heat recovery as done in a hybrid system is then the solution when high electrical efficiency is required. A simple theoretical analysis furthermore shows that the operating temperature of the fuel cell has small influence on the efficiency of these hybrid systems. Therefore, the efforts in optimization can be focussed on fuel cell endurance and heat recovering power cycle efficiency. Combining fuel cells and power cycles will surely result in relatively complex systems that need more detailed analyses.

From a thermodynamic point of view, the studies in Chapter 8 show that the electrochemical gasification of solid fuel is a very promising concept. This concept is used in the Direct Carbon Fuel Cell (DCFC) and the Internal Direct-Oxidation Carbon Fuel Cell (IDOCFC), both simultaneously produce electricity and CO, which can be used as feedstock in chemical plants. The simple theoretical calculations using exergy balances helps evaluate different processing techniques by showing their theoretical ultimate limits. These limits are the upper bounds in later optimization processes and they are very useful during the stage of process evaluation. It is clear that the process with the highest ultimate limit is preferred over the process with the lower limit. Hence, the electrochemical gasification process should be studied in more detailed. This will initiate a new direction in the field of solid fuel conversion, potentially leading to much better efficiencies than present systems using conventional gasification.

9.2. Detailed flowsheet calculations

The complexity of a fuel cell system requires analysis of detailed flowsheet calculations to reveal effects that otherwise remain concealed. These flowsheet calculations should be accurate and reliable. In Chapter 3, it was shown that the simple numerical fuel cell model in the flowsheeting program Cycle-Tempo is indeed accurate. The power of detailed flowsheet calculations is shown in the Chapters 5 thru 7. Chapter 5 first confirms the

results of Chapter 4: the influence of fuel cell operating temperature on the overall system efficiency is small. Furthermore, the flowsheet calculations show the complex interaction between the fuel cell and the rest of the system. These complex interactions cannot be derived in advance from theory and can only be understood from the results from detailed flowsheet calculations. In addition, flowsheeting software is an excellent tool for pinpointing losses and bottlenecks. Finding further improvements has then become much easier. For the studied system, the Heat Exchange Reformer (HER), and in particular the combustion process, is the main cause of exergy loss. This result suggests that this system can be improved by using internal reforming MCFC. Furthermore, exergy loss due to combustion should be reduced to a minimum and this suggests using the highest fuel utilisation as possible. Alternatives for combustion of non-utilized fuel from the anode outlet are required for further improvements in efficiency.

Chapter 6 has shown for a more practical situation that the gain in efficiency by multi-stage oxidation is much lower than suggested by theory. Here, the complex interactions between fuel cell and the rest of the system have introduced several factors that have adversely affected the overall efficiency. The flowsheet calculations show a small gain in efficiency, which is factor 10 lower than theory (0.5% instead of 5%). Further improvement is possible by changing system configuration, which is also shown by another flowsheet calculation. As small as the differences are, detailed flowsheet calculations are here indispensable to pinpoint the differences.

Another application of flowsheet calculations is shown in Chapter 7, which considers a new concept of MCFC with separate CO₂ supply that opens new ways to improve endurance of the MCFC. Detailed flowsheet calculations are required here since it can handle many details needed to investigate the interaction of the fuel cell with the rest of the system. It is shown that this concept can be applied to a conventional MCFC plant with just minor adjustments and with a minimal loss in efficiency (about 0.1% point). It is noted however that the extra advantages of having an active CO₂ separation channel has not been utilised yet in this design study. Utilising the active CO₂ separation opens new ways of improving overall system efficiency. Future work should focus on examining this promising concept in detailed level. The same holds for the concept of direct electrochemical conversion of solid fuel as presented in Chapter 8. This concept has only

been evaluated theoretically and the results are very promising. Future detailed flowsheet calculations should further study this concept. By applying this concept in a more realistic situation, results that are more convincing can be obtained that gives new directions for future researches.

Appendix A

Exergy and the calculations of chemical exergy

The first law of thermodynamics states that the total amount of energy is conserved during any energy transformation. Still energy comes in different qualities. For example, you can cook a whole meal with 100 kWh of electricity while that same amount of energy in the form of water at ambient temperature is of little use. The concept of exergy is introduced to express the differences in quality of energy. Exergy is defined as the maximum accessible work. For a given amount Q of heat at temperature T , the amount of exergy is defined as

$$Ex_Q = Q \left(1 - \frac{T_0}{T} \right) \quad (\text{A.1})$$

This relation is known as the Carnot limitation with $1 - T_0/T$ as the Carnot factor.

For thermal combustion processes, the enthalpy Δh of the fuel is converted into heat Q , hence the lower the temperature of combustion the higher the exergy loss. Reversibility is only obtained in theory when the combustion takes place at infinitely high temperature.

For a chemical component, the exergy is defined as the maximum accessible work when transforming this component into the most stable component at ambient condition (i.e. component of our environment at 298 K). This can be shown with an imaginary process given by Figure A.1

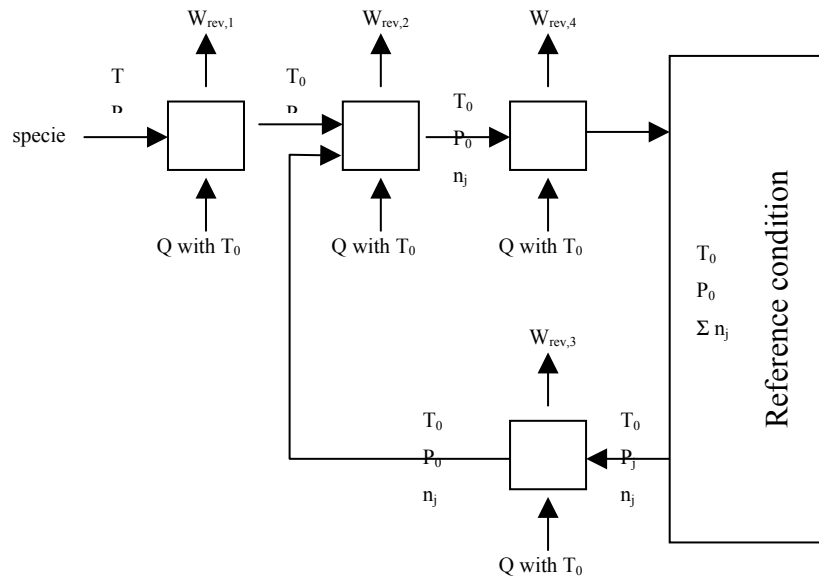


Figure A.1. Scheme to calculate the exergy of specie (see text).

As an example we will show how this is done for carbon at 1200 K. The reference conditions are given in Table A.1.

Table A.1. Ambient reference conditions.

T_0	298 K
$p_0^{H_2O}$	0.0312 bar
$p_0^{O_2}$	0.203 bar
$p_0^{CO_2}$	0.0003 bar

The exergy of carbon is calculated by the combustion of C into CO_2 at reference condition.



The first process is the isobaric cooling of the carbon from 1200 K to 298 K, followed by the adiabatic expansion from p to p_0 . The amount of work released here is

$$w_{rev,1} = h_{1200K}^C - h_{298K}^C - T_0 (s_{298K}^C - s_{1200K}^C) - RT \ln \left(\frac{p}{p_0} \right) \quad (A.3)$$

The second process is the conversion into environmental species at reference condition, i.e. chemical reaction (A.2)

$$w_{rev,2} = -\sum \Delta_f g^0 \quad (A.4)$$

The oxygen needed for reaction (A.2) is supplied by the environment. This oxygen needs first to be compressed to the standard condition defined for $\Delta_f g^0$. The work for this compression is given by

$$w_{rev,3} = -RT \ln p_0^{O_2} \quad (A.5)$$

After reaction (A.2) the CO₂ can be expanded into reference condition. The amount of work that is released is

$$w_{rev,4} = -RT \ln \left(\frac{1}{p_0^{CO_2}} \right) \quad (A.6)$$

The exergy of carbon is the sum of all work

$$EX_{1200K,p}^{CO_2} = \sum w_{rev,i} \quad (A.7)$$

Using this and similar processes we can calculate the exergy of carbon and the other involved species in our system. From available thermodynamic data [1], the calculated exergy of C (s), CO (g), CO₂ (g), H₂(g), H₂O(g) and O₂(g) at 1200 K are given in Table A.2.

Appendix A

Table A.2. Exergy of C, CO, CO₂, H₂, H₂O and O₂ at 1200 K.

$Ex^{C(s)}$	419.1 kJ/mol
$Ex^{CO(g)}$	290.9 kJ/mol
$Ex^{CO_2(g)}$	45.0 kJ/mol
$Ex^{H_2(g)}$	249.7 kJ/mol
$Ex^{H_2O(g)}$	27.7 kJ/mol
$Ex^{O_2(g)}$	20.4 kJ/mol

These exergy-values are used in Chapter 8 to evaluate different processes by examining the exergy efficiency.

Reference

- [1] D.R. Lide, Handbook of Chemistry and Physics 76th edition, CRC-Press, (1995).

Appendix B

Performance measurements on a MCFC bench-cell

The experimental work used for verifying the analytical fuel cell models (Chapter 2) and numerical fuel cell model (Chapter 3) were performed in the end of 1997 as a collaborative work between Delft University of Technology, The Netherlands, and Tohoku University, Sendai, Japan. At Tohoku University, the Applied Electrochemistry group of Professor Uchida had a collaboration with IHI and they had made a 110 cm² benchmarking class MCFC available for scientific research.

The experimental set-up used for verifying the models is shown by Figure B1.



Figure B1: MCFC bench cell setup at Tohoku University. MCFC manufactured by IHI.

The setup at Tohoku University can be distinguished in three groups of equipments:

1. The Fuel Cell setup, consisting of the MCFC, thermal insulation, heaters and temperature controllers.
2. Gas supply and gas testing equipment, consisting of cylinders of various purified gas, massflow controllers, humidifiers and a gas chromatograph.
3. Performance measurement equipments, consisting of a potentiostat, a galvanostat, a mercury switch, an oscilloscope and a frequency response analyzer.

Only some of the equipments are shown in Figure A2 and they are schematically depicted in Figure B2. The piston above the MCFC is used solely to ensure perfect contact between the electrodes, the matrix and the current collectors of the MCFC.

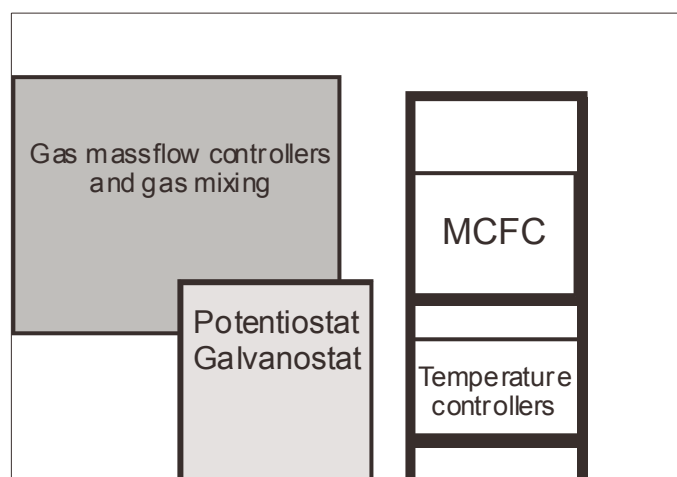


Figure B2: Schematical representation of the equipments shown in Figure B1.

This typical MCFC setup allows a limited number of control variables:

- Fuel Cell temperature (through the temperature controllers).
- Gas composition and massflows of the anode and cathode.
- The total current output or the cell or the cell voltage (through a galvanostat respectively a potentiostat).

Gas utilization is varied by fixing the mass flow (and gas composition) and by varying the current output.

It is obvious that only macroscopic measurements are possible (V_{cell} and I_{cell}). In addition, the bench cell is relatively small and sandwiched between electric heaters. Hence, it is reasonable to assume that the bench-cell is operating under isothermal conditions.

Typical performance measurements are done by measuring the $I_{\text{cell}} - V_{\text{cell}}$ characteristic of the cell. Other performance measurements are measuring the cell voltage V_{cell} at a typical full load condition (e.g. $u_f = 0.8$ and $i_{\text{cell}} = 150 \text{ mA/cm}^2$), or measuring the current density i_{cell} at a typical cell voltages (e.g. $u_f = 0.8$ and $V_{\text{cell}} = 0.7\text{V}$). Optionally, the mercury switch and oscilloscope enables transient response measurements, and the frequency response analyzer connected to the potentiostat/galvanostat enables impedance measurements.

Summary

The world's energy consumption is growing extremely rapidly. Fuel cell systems are of interest by researchers and industry as the more efficient alternative to conventional thermal systems for power generation. The principle of fuel cell conversion does not involve thermal combustion and hence in theory fuel cell systems can be far more efficient than thermal power systems. This advantage is only partly utilized in present fuel cell pilot plants and additional optimization is needed. The complexity of fuel cell systems makes the optimization process anything but simple.

This thesis presents the results of studies to understand the complex interactions between the different segments of a fuel cell system, and it presents additional insights into the fundamental aspects of the fuel cell conversions. Theories are presented and tested in practical situations with the objective of generating innovative ideas for future high temperature fuel cell systems.

After a short introduction (Chapter 1), this thesis presents a verification of two analytical fuel cell models by comparing modeled results with experimental results (Chapter 2). The analytical models are the so-called Simple Model and the Extended Model. Both models describe the operating characteristics of fuel cells using two thermodynamic parameters (determined by gas composition, operating pressure and temperature), two operating parameters (set by the fuel cell operator), and one performance characterizing parameter (cell resistance) that needs to be determined experimentally. The transparency of these analytical models is crucial to gain understanding of the complex nature of fuel cell systems, and the verification of these models with experimental results is essential. The operating characteristics of a molten carbonate fuel cell (MCFC) bench cell are measured and the result is used for the verification of the models. Two methods of determining the cell resistance are used: measurement of the macroscopically cell resistance R and calculation of the fitted quasi-Ohmic resistance r . The accuracies of both methods are evaluated. This study has shown that both analytical models can be used to model the

operating characteristics of the MCFC bench cell from low load to typical full-load condition. The relative errors in the modeled results are within 5% and 1% for the Simple Model and the Extended Model respectively.

Flowsheet calculations are very valuable in providing an insight into complex process flows. The study of fuel cell system processes will become much easier when accurate fuel cell models are created and included in flowsheeting software. Cycle-Tempo is an example of flowsheeting software that has a fuel cell model incorporated as a standard component. Chapter 3 presents an introduction to this fuel cell model and it presents a verification of the model using the same experimental results given in Chapter 2. Again, two different methods for determining the cell resistance are used (R and r), and the modeled cell operating characteristics using the two values for the cell resistance are compared with the experimentally measured characteristics. The comparisons show that the operating characteristics of the bench cell are accurately described by the fuel cell model of Cycle-Tempo. The relative error in the modeled cell voltage is highest at full load condition but the error stays within 3% using the measured R and within 1.7% using the fitted r .

After verifying the validity of the models, this thesis continues with the optimization studies of fuel cell systems. Chapter 4 presents a theoretical optimization study of the system efficiency by varying the fuel cell operating temperature. The fuel cell system considered in this chapter is a hybrid fuel cell-power cycle and the optimization study starts with the calculation of the theoretical reversible limits. Next, a simple temperature independent-function for the irreversible losses is introduced. This study shows that the reversible limit of the system is independent of the fuel cell operating temperature. Introducing temperature independent-irreversible losses results in an optimum in the system efficiency but the fuel cell operating temperature has only a small influence on the efficiency around this optimum. Finally, the highly temperature-dependent irreversible losses of an MCFC are introduced into this theoretical evaluation. Even then, the influence of the operating temperature on the system efficiency around the optimum is small. This is due to the heat recovery power cycle that partly recovers the dissipated irreversible heat from the fuel cell. Hence, in conclusion, the hybrid fuel cell-power cycle is an interesting concept that allows optimization of the fuel cell operating temperature for other important requirements (e.g. endurance) with little loss in system efficiency.

This study is continued by looking at a more complex fuel cell power plant. Chapter 5 presents a similar temperature study by flowsheet calculations. A 250 kW class cogeneration MCFC plant is considered in this study and the fuel cell operating temperature is varied from 600 °C to 700 °C while keeping the rest of the system the same as much as possible. At the typical operating temperature of 650 °C, the exergy efficiency of this fuel cell power plant is calculated as 58.5 %. This study shows that over the investigated temperature range, the exergy efficiency varies over a range of only 1.7%, with the maximum exergy efficiency at 675 °C. Between 650°C and 700 °C, the variation is only 0.3%. The flowsheet calculations have revealed a complex interaction between the fuel cell and the rest of the system. However, the flowsheeting results are in accordance with the results from the theoretical study presented in Chapter 4.

Chapter 6 continues with the flowsheet calculations, assessing the improvement in the exergy efficiency when multistage oxidation is introduced. The multistage oxidation configuration can reduce the irreversible losses caused by inhomogeneous current distribution in the fuel cell, and this chapter assesses the behavior of a complete fuel cell plant. The same scheme of a 250 kW MCFC plant as in the previous chapter is used. Here however, the fuel cell stack is split up into two segments while keeping the total cell area, fuel utilization and current density the same. By placing both the anode as well as the cathode flows in series, the exergy efficiency of the fuel cell plant increases by 0.4%. Placing solely the anode flow in series while keeping the cathode flows parallel results in an increase in exergy efficiency of 0.6%.

Chapter 7 presents the first flowsheet calculation of a system incorporating a new type of MCFC with a separate CO₂ supply (improved or i-MCFC). A sub-model is created that simulates the energy and massflows of the i-MCFC. Again, the same scheme of a 250 kW MCFC plant is used for the flowsheet calculation. The system is adapted to the unique three massflows configuration of the i-MCFC. The cathode operating condition in this new i-MCFC system is such that the lifetime limiting problem of NiO cathode dissolution is solved. Only minor modification to the existing system was needed and the exergy efficiency of this i-MCFC system is only 0.2 % lower than the reference MCFC system.

Finally, Chapter 8 discusses future research directions in electrochemical conversion. Reversible heat production is inevitable for hydrogen fuel cells and this chapter starts by presenting the source of the reversible heat production. Then, some innovative fuel cell

concepts that in theory do not suffer from this heat production are discussed. Two fuel cell concepts are introduced that in theory absorb heat, converting it into work: the Direct Carbon Fuel Cell (DCFC) and the Internal Direct-Oxidation Carbon Fuel Cell (IDOCFC). Both innovative fuel cell concepts are electrochemical gasification processes that produce valuable chemical feedstock (Syngas) in cogeneration with electricity. This chapter continues with the analyses of energy and exergy balances of these two concepts. The exergy efficiencies are calculated and compared with their conventional counterparts under ideal conditions. By defining these systems ideally, the theoretical ultimate performance limit can be identified, which is useful in setting goals and directions where large advantages over conventional systems may be achieved. The exergy analyses show that electrochemical conversion is indeed a preferable method. In particular, the IDOCFC is a promising concept since it is based on present technology without suffering from the exergy loss in thermal combustion, nor from the reversible heat production in hydrogen operated fuel cells.

Samenvatting

De wereld energie consumptie is sterk groeiende. Brandstofcelssystemen met hogere omzettingsrendementen worden gepresenteerd als alternatief voor thermische centrales. De brandstofcel maakt gebruik van elektrochemische energie omzetting waarbij in principe geen thermische verbranding plaats vindt. Hierdoor kunnen brandstofcelssystemen in theorie veel efficiënter werken dan thermische systemen. Bij de huidige brandstofcel-(test)opstellingen wordt dit voordeel maar ten dele benut en een verdere optimalisatie op dit gebied moet nog plaatsvinden. Brandstofcelssystemen zijn vanwege de noodzakelijke hulpsystemen zeer uitgebreid en complex wat het optimalisatieproces niet eenvoudiger op maakt.

Dit proefschrift geeft een overzicht van de resultaten van een onderzoek naar meer inzicht in de complexe interacties die plaatsvinden tussen verschillende onderdelen van een brandstofcelstelsel. Daarnaast heeft dit onderzoek ook geleid tot een extra verdieping in het inzicht van de basisprincipes van brandstofcelomzettingen. Het heeft onder meer geleid tot enkele nieuwe concepten voor elektrochemische omzetting. Nieuwe en bestaande theorieën worden gepresenteerd en getoetst aan de praktijk met als doel het uitwerken en ontwikkelen van innovatieve ideeën voor toekomstige hoge temperatuur brandstofcelssystemen.

Na een korte inleiding gegeven in hoofdstuk 1 geeft dit proefschrift een verificatie van twee analytische brandstofcelmodellen door middel van een vergelijkvernis van de modelverwachtingen met gemeten resultaten. Deze twee analytische modellen zijn het “Simple Model” and het “Extended Model”. Beide modellen beschrijven de stroomspanningskarakteristiek van een brandstofcel waarbij gebruik gemaakt wordt van twee thermodynamische parameters (bepaald door gassenstelling, druk en temperatuur van de cel), twee bedrijfsvoeringsparameters (voor de gebruiker vrij te kiezen) en één prestatie karakteriserende parameter die experimenteel bepaald dient te worden, namelijk de celweerstand. De overzichtelijkheid van deze beide analytische modellen is van

onschatbare waarde voor het begrijpen van complexe brandstofcelssystemen. Deze modellen zijn aan waarnemingen uit de praktijk getoetst. Verschillende stroomspanningskarakteristieken van een gesmolten carbonaat testcel bij verschillende groottes van gasstromen zijn gemeten. De modelresultaten zijn aan deze meetresultaten getoetst. Hiervoor zijn twee methodes gebruikt om een waarde voor de celweerstand te bepalen: een macroscopische gemeten weerstand R en een gefitte quasi-Ohmse weerstand r . De nauwkeurigheden van de modelresultaten met deze twee waardes zijn bekeken. Deze studie laat zien dat beide analytische modellen de stroom-spanningskarakteristieken goed beschrijven. De relatieve foutmarges waarbinnen de modelresultaten vallen zijn 5% voor het “Simple Model” en 1% voor het “Extended Model” dat een aantal verfijningen bevat ten opzichte van het “Simple Model”.

Systeemberekeningen zijn waardevol voor het verkrijgen van inzicht in de interactie tussen de verschillende processen in een systeem. De studie naar brandstofcelssystemen kan sterk worden vereenvoudigd door betrouwbare brandstofcelmodellen op te nemen in rekenprogramma's voor de berekening van energiesystemen. Het rekenprogramma Cycle-Tempo beschikt standaard over een brandstofcelmodel. Hoofdstuk 3 geeft na een beschrijving ervan de verificatie van dit brandstofcelmodel. De verificatie maakt gebruik van de in Hoofdstuk 2 beschreven metingen, en ook hier worden de modelresultaten met de twee verschillende methoden voor het bepalen van de celweerstand vergeleken. Uit de toetsing blijkt dat het brandstofcelmodel van Cycle-Tempo de experimentele stroomspanningskarakteristieken goed beschrijft. De relatieve fout tussen de gemodelleerde en de gemeten waarde is het hoogst onder volle celbelasting. De fout blijft hierbij binnen 3% wanneer de gemeten celweerstand R wordt gebruikt, en binnen 1,7% wanneer de gefitte celweerstand r wordt gebruikt.

Na de verificatie van de modellen worden verschillende optimalisatiestudies van brandstofcelssystemen beschreven. Hoofdstuk 4 beschrijft een theoretische optimalisatie van de brandstofceltemperatuur. Het systeem bestaat uit een hybride van een brandstofcel en een Carnot kringproces dat dient voor de productie van arbeid uit de door de brandstofcel afgegeven warmte. Eerst wordt de theoretische bovenlimiet bepaald die onafhankelijk blijkt van de brandstofceltemperatuur. De studie wordt vervolgd met berekeningen van systeemrendementen met aannames van verschillende temperatuur-onafhankelijke verliesfactoren. Onder deze aannames worden verschillende maxima in het

systeemrendement gevonden. Rond deze maxima heeft de celtemperatuur echter een relatief geringe invloed op het systeem rendement. Ten slotte worden de gegevens van de sterk temperatuur-afhankelijke irreversibele verliezen van de gesmolten carbonaat brandstofcel (MCFC) toegepast. Zelfs dan blijkt dat rond deze nieuwe maxima de celtemperatuur maar relatief weinig invloed heeft op het systeemrendement. Concluderend mag worden aangenomen dat het hybride systeem van brandstofcel-kringproces een interessant concept is. De brandstofceltemperatuur kan binnen ruime grenzen worden afgestemd op andere belangrijke factoren (bijvoorbeeld de levensduur) met behoud van een hoog systeemrendement.

Vervolgens zijn complete en dus complexe brandstofcelsystemen gesimuleerd. Hoofdstuk 5 beschrijft een vergelijkbare optimalisatiestudie aan de hand van gedetailleerde systeemberekeningen. Een 250 kW klasse warmte-kracht MCFC-systeem is voor deze studie gebruikt waarbij de gemiddelde brandstofcel temperatuur gevarieerd wordt tussen 600 °C en 700 °C. Veranderingen aan parameters van de rest van het systeem worden hierbij zo veel mogelijk vermeden. Het is gebruikelijk om de MCFC te bedienen op 650 °, het systeem heeft dan een exergierendement van 58,5%. Deze studie laat zien dat over een temperatuurtraject van 100 K het verschil tussen de hoogste en laagste waarde van het exergie rendement 1,7% bedraagt. Het exergetisch maximum ligt op 675 °C maar het verschil tussen 650 °C en 700 °C is maar 0,3%. De systeemberekeningen laten een complexe wisselwerking zien tussen de brandstofcel en de rest van het systeem. Het uiteindelijke resultaat van een relatief geringe invloed van de brandstofceltemperatuur op het systeemrendement komt overeen met de resultaten van hoofdstuk 4.

In hoofdstuk 6 wordt de verbetering in het systeemrendement door meervoudige oxidatie bepaald middels systeemberekeningen. De meervoudige oxidatieconfiguratie reduceert irreversibele verliezen doordat een inhomogenere stroomverdeling binnen in de brandstofcel wordt bereikt. Hetzelfde 250 kW warmte-kracht systeem als in het vorige hoofdstuk wordt hier opnieuw gebruikt. De berekeningen laten zien dat een verbetering van 0,4% in het exergierendement wordt verkregen door de cel in twee gelijke segmenten te delen. Hierbij zijn zowel de anode als de kathode gasstromen in serie geschakeld. Door alleen de anodestroom in serie te zetten en de kathodestroom parallel te houden krijgt men een verbetering in het exergie rendement van 0,6%.

Hoofdstuk 7 beschrijft een eerste systeemberekening van een systeem dat gebruikt maakt van een nieuw type MCFC met een aparte CO₂ (de i-MCFC). Wederom wordt het 250 kW

warmte-kracht systeem als basis gebruikt na aanpassing aan de i-MCFC. Daarbij is er gestreefd naar het oplossen van de NiO kathode in hoge mate te onderdrukken zodat de levensduur van de brandstofcel wordt verlengd. De wijzigingen aan het basissysteem waren gering en het exergierendement van de i-MCFC is slechts 0,2% lager dan van het basissysteem.

Tot slot behandelt hoofdstuk 8 toekomstige onderzoeksrichtingen op het gebied van elektrochemische omzetting. Reversibele warmteproductie is onvermijdelijk voor brandstofcellen die waterstof als brandstof gebruiken en dit hoofdstuk begint met het aangeven van de bron van deze warmteproductie. Dit wordt gevolgd door een beschouwing van alternatieve en innovatieve brandstofcelconcepten waarbij deze warmteproductie in theorie niet plaats vindt. Twee concepten worden met name onder de aandacht gebracht: de “Direct Carbon Fuel Cell” (DCFC) en de “Internal Direct Oxidation Carbon Fuel Cell” (IDOCFC). Deze twee concepten kunnen in theorie warmte opnemen en deze omzetten in elektrische arbeid. Daarnaast produceren beide concepten naast elektriciteit ook koolmonoxide dat een kostbare grondstof is voor de chemische industrie. Beide concepten kunnen daarom ook als elektrochemische vergassingsconcepten worden beschouwd. De energie- en exergiebalansen van deze concepten zijn op basis van globale beschouwingen vergeleken met hun conventionele varianten. Hierbij worden ideale procesomstandigheden aangenomen om zodoende de theoretische omzettingslimieten te berekenen. Deze theoretische limieten kunnen als richtlijn gebruikt worden om potentiële onderzoeksrichtingen te identificeren. De exergieanalyses laten zien dat de voorkeur moet worden gegeven aan elektrochemische omzetting. Met name de IDOCFC is een veelbelovend concept. Dit concept maakt gebruik van bestaande technieken zonder dat de omzetting gepaard gaat met het exergieverlies van thermische verbranding en de reversibele warmteproductie van op waterstof gevoede brandstofcellen.

Acknowledgement

I would like to thank the promoters professor Kouffeld and professor de Wit, who gave me the opportunity to perform the studies presented by this thesis. Special thanks go to the co-promotor Kas Hemmes and to the supervisor Nico Woudstra for their advices and guidance. Willy Peelen is acknowledges for his advices and discussions during my first year as a PhD student. My master's students José Maria Campos, Thien Dao and Stephen McPhail are acknowledged for their graduation work that has contributed to this thesis. Theo Woudstra and Teus van der Stelt are acknowledged for their support with the Cycle-Tempo calculations. Yuk Yee Man is acknowledged for the cover-design. Brian, Chris and Wouter are acknowledged for proofreading parts of this thesis. My colleagues, Barry, Francesco, Gerrit, José, Mae, Paola, Peter, Saskia, and Xiaolong, are thanked for their pleasant conversations during lunch and thee breaks. Special thanks go to Bart and Jeroen for their morning starters with a cup of coffee. My parents, who supported me in all my decisions. And finally my wife Yvonne,

Curriculum Vitae

The author Siu Fai Au was born on March 8th 1972 in Hong Kong. At the age of eight, he and his family immigrated to the Netherlands. He attended secondary school at the Katholiek College Amsterdam-West, where he graduated in 1991 (VWO-Atheneneum). Then he started his study Materials Science and Engineering at Delft University of Technology. As part of this study, he had an internship at the European headquarter of General Electric Plastics in Bergen op Zoom, where he has worked on the vacuum molding of glass fiber reinforced thermoplastic. He completed his study in 1997 with a Master thesis on the corrosion of 304 stainless steel and ceramic coated 304SS in molten carbonate salt. After that, he was appointed as a research associate at Delft University of Technology for a year of which he spent six month at Tohoku University in Sendai Japan where he has performed corrosion measurements of stainless steel in molten carbonate at elevated pressure and the performance measurements on a molten carbonate fuel cell. From 1998-2002, he was appointed as a *promovendus* at Delft University of Technology in a cooperation between the sections Corrosion Technology and Electrochemistry of the Faculty of Applied Science, and Thermal Power Engineering of the Faculty of Design, Engineering and Production. From December 2002, he is appointed as a research scientist at Forschungszentrum Jülich GmbH, where he works on the development of solid oxide fuel cell systems.

List of Publications

International Journals

S.F. Au, K. Hemmes and N. Woudstra, *Flowsheet calculation on a Combined Heat and Power Fuel Cell plant with a conceptual Molten Carbonate Fuel Cell with separate CO₂ supply*, submitted to the Journal of Power Sources, (2002).

S.F. Au, N. Woudstra and K. Hemmes, *Assessment of Multistage Oxidation by Flowsheet Calculations on a Combined Heat and Power Molten Carbonate Fuel Cell Plant*, submitted to the Journal of Power Sources, (2002).

S.F. Au, S.J. McPhail, N. Woudstra and K. Hemmes, *The Influence of Operating Temperature on the Efficiency of a Combined Heat and Power Fuel Cell plant*, submitted to the Journal of Power Sources, (2002).

S.F. Au, N. Woudstra, K. Hemmes and I. Uchida, *Verification of a simple numerical model of a flowsheeting program performance testing at a 110cm² Molten Carbonate Fuel Cell*, accepted for publication in Energy Conversion and Management, (2002).

S.F. Au, K. Hemmes and N. Woudstra, *The Influence of Operating Temperature on the Efficiency of Combined Fuel Cell and Power Cycle System*, p. A879-A885, Journal of Electrochemical Society, **149** (7), Pennington, NJ, USA, (2002).

S.F. Au, W.H.A. Peelen, F.R.A.M. Standaert, K. Hemmes and I. Uchida, *Verification of Analytical Fuel Cell Models by Performance Testing at a 110cm² Molten Carbonate Fuel Cell*. p. A1051-A1057, Journal of Electrochemical Society, **148** (10), Pennington, NJ, USA, (2000).

W.H.A. Peelen, M. Olivry, S.F. Au, J.D. Fehribach and K. Hemmes, *Electrochemical oxidation of carbon in a 62/38 mol% Li/K carbonate melt*, p. 1389-1395, Journal of Applied Electrochemistry, **30**, Kluwer Academic Publisher, (2000)

K. Hemmes, S.F. Au, G. Bart and N. Woudstra, *The Principle of Electrochemistry in the Energy Supply of the 21st Century*, Proceedings of ECOS2000, (2000)

International Conference Proceedings

S.F. Au, K. Hemmes and N. Woudstra, *The Influence of Cell Temperature on the Efficiency of Combined Fuel Cell and Power Cycle system*, Abstracts of the 200th Meeting of the Electrochemical Society (2001)

S.F. Au, W.H.A. Peelen, K. Hemmes and N. Woudstra, *Fuel Cells the Next Step; Energy and Exergy Analysis of Partial Oxidation, Direct Carbon Fuel Cell and Internal Direct-Oxidation Carbon Fuel Cell*, Conference Proceedings of the 3rd International Fuel Cell Conference (1999)

S.F. Au, W.H.A. Peelen, F.R.A.M. Standaert, K. Hemmes and I. Uchida, *Assesment of Two Analytical Fuel Cell Models by Performance Testing at a 110cm² Molten Carbonate Fuel Cell*. p. 90-98, Electrochemical Society Conference Proceeding PV 99-20, The Electrochemical Society, Pennington, NJ, USA (1999), ISBN 1-56677-243-5.

S.F. Au, M. Keijzer, K. Hemmes, P.J.J.M. van der Put, J.H.W. de Wit and J. Schoonman,
Corrosion protection of Stainless Steel in Molten Carbonate by a Ceramic Coating, p. 699-
706, Materials Science Forum, **289-292** (1997), ISBN 0-87849-821-4

List of symbols

<i>Symbol</i>	<i>Description</i>	<i>Units</i>
A_{cell}	Active cell area	(m ²)
C	Fitting constant for quasi-Ohmic resistance	(Ωm ²)
E_{kin}	Kinetic energy	(J)
Ex	Exergy	(kJ/mol)
F	Faraday's constant	(C/mol)
Δg	Change in Gibbs free energy	(J/mol)
d	Electrolyte thickness	(mm)
d_b	Normalization constant for the electrolyte thickness	(mm)
Δh	Change in Enthalpy	(J/mol)
i	Current density	(A/m ²)
i_{in}^f	Equivalent current density of fuel input	(A/m ²)
i_{in}^{ox}	Equivalent current density of oxidant input	(A/m ²)
i_{cell}	Current load density of the unit cell	(A/m ²)
m	Molar fraction	(-)
n	Number of electrons involved in the cell half-reaction	(-)
OCV	Open-circuit voltage, i.e. $V_{cell}(0)$	(V)
P	Power delivered	(kW)
p	Pressure	(bar)
p_i	Partial pressure of gas of specie i	(bar)
p_1	Loss constant for the fuel cell efficiency	(-)
Δp	Pressure loss	(bar)
Q	Heat	(J)
q	Heat	(J/mol)
r	Quasi-Ohmic resistance	(Ωm ²)
R	Universal gas constant	(J/mol K)
R	Macroscopic resistance	(Ωm ²)
R^{EM}	Macroscopic resistance given by the Extended Model	(Ωm ²)
Δs	Change in Entropy	(J/mol K)
T	Temperature	(°C or K)

T_0	Standard ambient temperature	(K)
T_{BE}	Break-even temperature	(K)
T_{max}	Temperature of maximum efficiency	(K)
$T_{\Delta G=0}$	Spontaneous combustion temperature	(K)
$T_{\Delta G=0}^{u_f}$	Nernst loss corrected spontaneous combustion temperature	(K)
ΔT_{high}	High end temperature difference	(K)
ΔT_{low}	Low end temperature difference	(K)
$T_{out}-T_{in}$	Temperature raise over the inlet and outlet	(K)
u	Cumulative fuel conversion or utilization	(-)
u_f	Total fuel utilization	(-)
u_{ox}	Total oxidant utilization	(-)
V_0	Open circuit voltage	(V)
V_{cell}	Cell voltage	(V)
V_{cell}^{EM}	Cell voltages as calculated by the Extended Model	(V)
V_{cell}^{SM}	Cell voltages as calculated by the Simple Model	(V)
V_{irrev}	Irreversible cell voltage	(V)
V_{rev}	Reversible cell voltage	(V)
V_{eq}	Theoretical Nernst potential	(V)
V_{in}	Thermal neutral voltage	(V)
V_u	Slope of the of the linear empirical function	(V)
V_{eq}^*	Lineair fit for V_{eq}	(V)
Z	Dimensionless number	(-)

Greek symbols

α_f	Slope of the linear part of $V_{eq}(u_f)$	(V)
α_{ox}	Slope of the linear part of $V_{eq}(u_{ox})$	(V)
$\alpha_{tot.}$	α calculated with both fuel and oxidant utilization	(V)
β	Proportionality factor	(-)
Φ	Mass flow	(kg/s)
η_c	Carnot efficiency	(-)

η_c^*	Non-ideal Carnot efficiency	(-)
η_{DC-AC}	DC to AC inverter efficiency	(-)
η_{fc}	Fuel cell efficiency	(-)
η_i	Intrinsic efficiency	(-)
η_s	Combined system efficiency	(-)
η_s^*/η_s^{**}	Non-ideal combined system efficiency	(-)

Attachments

a	anode
aux	auxiliary
c	cathode
<i>Ex</i>	exergy
in	input
Ω	ohmic
out	output
react	reaction